



APPENDIX A

Sample Details, Geological Data and Apatite Compositions

A.1 Sample details

This document describes AFTA data in a suite of outcrop and borehole samples from **southern Norway**. Details of all samples, including locations and stratigraphic ages, are summarised in Table A.1. Yields of apatite obtained from each AFTA sample are also listed in Table A.1.

Vitrinite Reflectance (VR) measurements were also carried out on one sample. These analyses were carried out by Paddy Ranasinghe, Principal Organic Petrologist, Energy Resources Consulting Ltd (ex-Keiraville Konsultants), Wollongong, New South Wales. Results of these analyses, together with sample details, are summarised in Table D.2 (Appendix D).

A.2 Stratigraphic details

Details of stratigraphic age assignment for each sample are described in the text. The chronostratic (relative succession) assignment of each sample was converted to a chronometric (numerical) scale using the timescale of Gradstein et al. (2012), with results summarised in Table A.1.

Any slight uncertainty in the estimated chronometric age of the sample is not expected to affect the thermal history interpretation of either the AFTA or VR data to any significant degree.

A.3 Present temperatures

In application of any technique involving estimation of paleotemperatures, it is critical to control the present temperature profile, since estimation of maximum paleotemperatures proceeds from assessing how much of the observed effect could be explained by the magnitude of present temperatures.



For this report, an average surface temperature of 5°C has been adopted to represent the present-day temperature of each outcrop sample. Note that the thermal history solutions derived from the AFTA data in these samples are not influenced to any significant degree by the assumed present-day temperatures.

A.4 Grain morphologies

The apatite grains obtained from samples of igneous and metamorphic rocks analysed for this study were dominated by euhedral forms while those from the single sedimentary rock sample show a variety of forms, with euhedral to sub-euhedral and sub-rounded to rounded morphologies present.

A.5 Apatite compositions

The annealing kinetics of fission tracks in apatite are affected by chemical composition, specifically the Cl content, as explained in more detail in Appendix C. In all samples analysed for this report, Cl contents were measured in all apatite grains analysed (i.e. for both fission track age determination and track length measurement), and the measured compositions in individual grains have been employed in interpreting the AFTA data, using methods outlined in Appendix C.

Chlorine contents were measured using a fully automated Jeol JXA-5A electron microprobe equipped with a computer controlled X-Y-Z stage and three computer controlled wavelength dispersive crystal spectrometers, with an accelerating voltage of 15kV and beam current of 25nA. The beam was defocussed to 20 µm diameter to avoid problems associated with apatite decomposition, which occur under a fully focussed 1 - 2 µm beam. The X-Y co-ordinates of dated grains within the grain mount were transferred from the Autoscan Fission Track Stage to a file suitable for direct input into the electron microprobe. The identification of each grain was verified optically prior to analysis. Cl count rates from the analysed grains were converted to wt% Cl by reference to those from a Durango apatite standard (Melbourne University Standard APT151), analysed at regular intervals. This approach implicitly takes into account atomic number absorption and fluorescence matrix effects, which are normally calculated explicitly when analysing for all elements. A value of 0.43 wt% Cl was used for the Durango standard, based on repeated measurements on the same single fragment using pure rock salt (NaCl) as a standard for chlorine. This approach gives essentially



identical results to Cl contents determined from full compositional measurements, but has the advantage of reducing analytical time by a factor of ten or more.

Chlorine contents in individual grains are listed in the fission track age summary data sheet for each sample in Appendix B. Table B.3 contains fission track age and length data grouped into 0.1 wt% Cl intervals on the basis of chlorine contents of the grains from which the data are derived. A plot of fission track age against Cl content is also shown in the data sheet for each sample, together with a histogram of Cl contents in all individual apatite grains analysed from each sample (i.e. grains analysed for both age and length measurements).

Lower limits of detection for chlorine content have been calculated for typical analytical conditions (beam current, counting time, etc.) and are listed in Table A.2. Errors in wt% composition are given as a percentage and quoted at 1σ for chlorine determinations. A generalised summary of errors for various wt% chlorine values is presented in Table A.3.

Apatite compositions in this study

In most of the samples analysed for this study, apatite grains are dominated by chlorine contents <0.1 wt%, typical of granitic basement rocks from around the world. A small number of samples contain apatites with Cl contents up to 0.4 wt%. In contrast, apatites from one basement sample (GC970-84) contain much higher amounts of chlorine between 1.5 and 2 wt% Cl. This is of note because this sample is close to the region where chlorapatites containing up to 6 wt% Cl are found (e.g. Engvik et al., 2009).

In all samples analysed for this report, the measured distribution of Cl contents has been employed in interpreting the AFTA data, using methods which take explicit, quantitative account of the variation of annealing kinetics with wt% Cl, as outlined in Appendix C.

References

- Engvik, A.K., Golla-Schindler, U., Berndt, J., Austrheim, H., Putnis, A. 2009. Intragranular replacement of chlorapatite by hydroxy-fluor-apatite during metasomatism. *Lithos* 112, 236–246
- Gradstein, F.M., Ogg, J.G., Schmitz, A.G. and Ogg, G.M. 2012. *A geologic time scale 2012*, Elsevier.



Table A.1: Details of fission track samples and apatite yields - outcrop samples from southernmost Norway (Geotrack Report #970A)

Sample number	Source #	Location Digital Lat/Long Elevation (m)	Stratigraphic Subdivision	Stratigraphic age (Ma)	Raw weight (g)	Washed weight (g)	Apatite yield *1
Norwegian coast basement							
GC361-21		Skudenshavn, Karmoy 59.141667 5.250000	Granite (Caledonian)	>?400	1630	979	excellent
GC361-22		Sagvag, Stord 59.777778 5.375000	Sandstone (Silurian)	439-409	2270	1093	excellent
GC361-25		Bergen 60.372222 5.300000	Foliated Granite (Pre Cambrian)	>570	2810	1645	excellent
Lysebotn fjord section							
GC361-74		59.049167 6.657778 75	Precambrian	>570	3010	739	excellent
GC361-75		59.049167 6.657778 440	Precambrian	>570	2140	697	excellent
GC361-76		59.049167 6.657778 990	Precambrian	>570	710	359	excellent
Rjukan vertical section							
GC970-31	norjac07-07	Rjukan, SW Hardangarvidda 59.884559 8.452472 1227	Caledonian Basement	400	790	470	excellent
GC970-32	norjac07-08	Rjukan, SW Hardangarvidda 59.901736 8.497289 1046	Caledonian Basement	400	1780	510	excellent
GC970-33	norjac07-09	Rjukan, SW Hardangarvidda 59.887598 8.586432 866	Caledonian Basement	400	1080	440	fair
GC970-34	norjac07-10	Rjukan, SW Hardangarvidda 59.883471 8.587859 656	Caledonian Basement	400	870	490	excellent
GC970-35	norjac07-11	Rjukan, SW Hardangarvidda 59.881587 8.593956 433	Caledonian Basement	400	730	320	excellent

**Table A.1: Continued**

Sample number	Source #	Location Digital Lat/Long Elevation (m)	Stratigraphic Subdivision	Stratigraphic age (Ma)	Raw weight (g)	Washed weight (g)	Apatite yield *1
Setesdal outcrops							
GC970-71	NOFT13-1	Rogaland, Egersund S, Leknes 58.382700 6.057760 5	Precambrian Anorthite	>540	1000	-	excellent
GC970-72	NOFT13-2	Rogaland, Hauge 58.341580 6.347240 152	Precambrian Anorthite	>540	1250	-	excellent
GC970-73	NOFT13-3	Vest-Agder, Hægeland 58.226090 7.010230 225	Precambrian Biotite gneiss	>540	970	-	excellent
GC970-74	NOFT13-4	Vest-Agder, Vigeland W 58.093050 7.273930 47	Precambrian Basement	>540	960	-	excellent
GC970-75	NOFT13-5	Vest-Agder, Kristianssand, Aukland 58.200710 7.930060 32	Precambrian Biotite gneiss, coarse	>540	1160	-	excellent
GC970-76	NOFT13-6	Vest-Agder, Langevatnet 58.338830 7.810830 229	Precambrian Basement	>540	1230	-	excellent
GC970-77	NOFT13-7	Aust-Agder, Setesdalen, Hornes 58.537220 7.777020 199	Precambrian Biotite gneiss	>540	1390	-	excellent
GC970-78	NOFT13-8	Aust-Agder, Setesdalen, Grendi 58.716500 7.825190 197	Precambrian Biotite gneiss, coarse	>540	930	-	excellent
GC970-79	NOFT13-9	Aust-Agder, Setesdalen, Storestraumer 58.852780 7.739870 220	Precambrian Granitic gneiss	>540	1260	-	excellent
GC970-80	NOFT13-10	Aust-Agder, Setesdalen, Lageid 59.018440 7.553140 229	Precambrian Biotite gneiss	>540	1350	-	excellent
GC970-81	NOFT13-11	Aust-Agder, Setesdalen, Rysslad 59.129370 7.511980 297	Precambrian Biotite gneiss, coarse	>540	1090	-	excellent
GC970-82	NOFT13-12	Aust-Agder, Vegusdal 58.579530 8.155800 197	Precambrian Granitic gneiss	>540	920	-	excellent

**Table A.1: Continued**

Sample number	Source #	Location Digital Lat/Long Elevation (m)	Stratigraphic Subdivision	Stratigraphic age (Ma)	Raw weight (g)	Washed weight (g)	Apatite yield *1
GC970-83	NOFT13-13	Aust-Agder, Arndal 58.506680 8.563830 79	Precambrian Massive granite	>540	1500	-	excellent
GC970-84	NOFT13-14	Telemark, Stabbestad 58.849890 9.397160 26	Precambrian Massive granitic gneiss	>540	1910	-	excellent

*1 Yield based on quantity of mineral suitable for age determination. Excellent: >20 grains; Good: 15-19 grains; Fair: 10-14 grains; Poor: 5-9 grains; Very Poor: <5 grains.



Table A.2: Details of fission track samples and apatite yields - samples from southernmost Norway (Geotrack Report #970A)

Sample number	Depth TVDrKB (m)	Sample type	Stratigraphic Subdivision	Stratigraphic age (Ma)	Present temperature *1 (°C)	Raw weight (g)	Washed weight (g)	Apatite yield *2
19/3-2								
GC361-73	0	surface	Precambrian-Caledonian basement	>400	5	3580	1740	excellent
GC361-71	800	cuttings	Precambrian-Caledonian basement	>400	18	8500	363	excellent
GC361-72	1480	cuttings	Precambrian-Caledonian basement	>400	29	740	316	very poor

*1 See Appendix A for discussion of present temperature data.

*2 Yield based on quantity of mineral suitable for age determination. Excellent: >20 grains; Good: 15-19 grains; Fair: 10-14 grains; Poor: 5-9 grains; Very Poor: <5 grains.



Table A.3: Lower Limits of Detection for Apatite Analyses (Geotrack Report #970A)

Element	LLD (95% c.l.)		LLD (99% c.l.)	
	(wt%)	(ppm)	(wt%)	(ppm)
Cl	0.01	126	0.02	182

Table A.4: Per cent errors in chlorine content (Geotrack Report #970A)

Chlorine content (wt%)	Error (%)
0.01	9.3
0.02	8.7
0.05	7.3
0.10	6.1
0.20	4.7
0.50	3.2
1.00	2.3
1.50	1.9
2.00	1.7
2.50	1.5
3.00	1.4

Errors quoted are at 1σ . See Appendix A for more details.

APPENDIX B

Sample Preparation, Analytical Details and Data Presentation

B.1 Sample Preparation

Core and outcrop samples are crushed in a jaw crusher and then ground to sand grade in a rotary disc mill. Cuttings samples are washed and dried before grinding to sand grade. The ground material is then washed to remove dust, dried and processed by conventional heavy liquid and magnetic separation techniques to recover heavy minerals. Apatite grains are mounted in epoxy resin on glass slides, polished and etched for 20 sec in 5M HNO₃ at 20°C to reveal the fossil fission tracks.

After etching, all mounts are cut down to 1.5 x 1 cm, and cleaned in detergent, alcohol and distilled water. The mounts are then sealed in intimate contact with low-uranium muscovite detectors within heat-shrink plastic film. Each batch of mounts is stacked between two pieces of uranium standard glass, which has been prepared in similar fashion. The stack is then inserted into an aluminium can for irradiation.

After irradiation, the mica detectors are removed from the grain mounts and standard glasses and etched in hydrofluoric acid to reveal the fission tracks produced by induced fission of ²³⁵U in the apatite and standard glass.

B.2 Analytical Details

Fission track ages

Fission track ages are calculated using the standard fission track age equation using the zeta calibration method (equation five of Hurford and Green, 1983), viz:

$$\text{F.T. AGE} = \frac{1}{\lambda_D} \ln \left[1 + \left(\frac{\zeta \lambda_D \rho_s g \rho_D}{\rho_i} \right) \right] \quad \text{B.1}$$

where: λ_D = Total decay constant of ²³⁸U (= 1.55125 x 10⁻¹⁰)
 ζ = Zeta calibration factor
 ρ_s = Spontaneous track density
 ρ_i = Induced track density
 ρ_D = Track density from uranium standard glass
 g = A geometry factor (= 0.5)



Fission track ages are determined by the external detector method or EDM (Gleadow, 1981). The EDM has the advantage of allowing fission track ages to be determined on single grains. In apatite, tracks are counted in 20 grains from each mount wherever possible. In those samples where the desired number is not present, all available grains are counted, the actual number depending on the availability of suitably etched and oriented grains. Only grains oriented with surfaces parallel to the crystallographic *c*-axis are analysed. Such grains can be identified on the basis of the etching characteristics, as well as from morphological evidence in euhedral grains. The grain mount is scanned sequentially, and the first 20 suitably oriented grains identified are analysed.

Tracks are counted within an eyepiece graticule divided into 100 grid squares. In each grain, the number of spontaneous tracks (N_s) within a certain number of grid squares (N_a) is recorded. The number of induced tracks (N_i) in the corresponding location within the mica external detector is then counted. Spontaneous and induced track densities (ρ_s and ρ_i , respectively) are calculated by dividing the track counts by the total area counted, given by the product of N_a and the area of each grid square (determined by calibration against a ruled stage graticule or diffraction grating). Fission track ages may be calculated by substituting track counts (N_s and N_i) for track densities (ρ_s and ρ_i) in equation B.1, since the areas cancel in the ratio.

Translation between apatite grains in the grain mount and external detector locations corresponding to each grain is carried out using AutoscanTM microcomputer-controlled automatic stages (Smith and Leigh Jones, 1985). This system allows repeated movement between grain and detector, and all grain locations are stored for later reference if required.

Neutron irradiations are carried out in a well-thermalised flux (X-7 facility; Cd ratio for Au ~98) in the Australian Atomic Energy Commission's HIFAR research reactor. Total neutron fluence is monitored by counting tracks in mica external detectors attached to two pieces of Corning Glass Works standard glass CN5 (containing ~11 ppm Uranium) included in the irradiation canister at each end of the sample stack. In determining track densities in external detectors irradiated adjacent to uranium standard glasses, 25 fields are normally counted in each detector. The total track count (N_D) is divided by the total area counted to obtain the track density (ρ_D). The positions of the counted fields are arranged in a 5 X 5 grid covering the whole area of the detector. For typical track densities of between $\sim 5 \times 10^5$ and 5×10^6 , this is a convenient arrangement to sample across the detector while gathering sufficient counts to achieve a precision of $\sim \pm 2\%$ in a reasonable time.



A small flux gradient is often present in the irradiation facility over the length of the sample package. If a detectable gradient is present, the track count in the external detector adjacent to each standard glass is converted to a track density (ρ_D) and a value for each mount in the stack is calculated by linear interpolation. When no detectable gradient is present, the track counts in the two external detectors are pooled to give a single value of ρ_D , which is used to calculate fission track ages for each sample.

A Zeta calibration factor (ζ) has been determined empirically for each observer by analysing a set of carefully chosen age standards with independently known K-Ar ages, following the methods outlined by Hurford and Green (1983) and Green (1985).

All track counting is carried out using Zeiss^(R) Axioplan microscopes, with an overall linear magnification of 1068 x using dry objectives.

For further details and background information on practical aspects of fission track age determination, see e.g. Fleischer, Price and Walker (1975), Naeser (1979) and Hurford (1986).

Track length measurements

For track length studies in apatite, the full lengths of "confined" fission tracks are measured. Confined tracks are those which do not intersect the polished surface but have been etched from other tracks or fractures, so that the whole length of the track is etched. Confined track lengths are measured using a digitising tablet connected to a microcomputer, superimposed on the microscope field of view via a projection tube. With this system, calibrated against a stage graticule ruled in 2 μm divisions, individual tracks can be measured to a precision of $\pm 0.2 \mu\text{m}$. Tracks are measured only in prismatic grains, characterised by sharp polishing scratches with well-etched tracks of narrow cone angle in all orientations, because of the anisotropy of annealing of fission tracks in apatite (as discussed by Green et al. 1986). Tracks are also measured following the recommendations of Laslett et al. (1982), the most important of which is that only horizontal tracks should be measured. One hundred tracks are measured whenever possible. In apatite samples with low track density, or in those samples in which only a small number of apatite grains are obtained, fewer confined tracks may be available. In such cases, the whole mount is scanned to measure as many confined tracks as possible.

Integrated fission track age and length measurement

Fission track age determination and length measurement are now made in a single pass of the grain mount, in an integrated approach. The location of each grain in which

tracks are either counted or measured is recorded for future reference. Thus, track length measurements can be tied to age determination in individual grains. As a routine procedure we do not measure the age of every grain in which lengths are determined, as this would be much too time-consuming. Likewise we do not only measure ages in grain in which lengths are measured, as this would bias the age data against low track density grains. Nevertheless, the ability to determine the fission track age of certain grains from which length data originate can be a particularly useful aid to interpretation in some cases. Grain location data are not provided in this report, but are available on request.

B.3 Data Presentation

Fission track age data

Data sheets summarising the apatite fission track age data, including full details of fission track age data for individual apatite grains in each sample, together with the primary counting results and statistical data, are given in the following pages. Individual grain fission track ages are calculated from the ratio of spontaneous to induced fission track counts for each grain using equation B.1, and errors in the single grain ages are calculated using Poissonian statistics, as explained in more detail by Galbraith (1981) and Green (1981). All errors are quoted as $\pm 1\sigma$ throughout this report, unless otherwise stated.

The variability of fission track ages between individual apatite grains within each sample can be assessed using a chi-squared (χ^2) statistic (Galbraith, 1981), the results of which are summarised for each sample in the data sheets. If all the grains counted belong to a single age population, the probability of obtaining the observed χ^2 value, for ν degrees of freedom (where $\nu = \text{number of crystals} - 1$), is listed in the data sheets as $P(\chi^2)$ or $P(\text{chi squared})$.

A $P(\chi^2)$ value greater than 5% can be taken as evidence that all grains are consistent with a single population of fission track age. In this case, the best estimate of the fission track age of the sample is given by the "pooled age", calculated from the ratio of the total spontaneous and induced track counts in all grains analysed. Errors for the pooled age are calculated using the "conventional" technique outlined by Green (1981), based on the total number of tracks counted for each track density measurement (see also Galbraith, 1981).

A $P(\chi^2)$ value of less than 5% denotes a significant spread of single grain ages, suggesting real differences exist between the fission track ages of individual apatite

grains. A significant spread in grain ages can result either from inheritance of detrital grains from mixed source areas (in sedimentary rocks), or from differential annealing in apatite grains of different composition, within a narrow range of temperature.

Calculation of the pooled age inherently assumes that only a single population of ages is present, and is thus not appropriate to samples containing a significant spread of fission track ages. In such cases Galbraith, has recently devised a means of estimating the modal age of a distribution of single grain fission track ages which is referred to as the "central age". Calculation of the central age assumes that all single grain ages belong to a Normal distribution of ages, with a standard deviation (σ) known as the "age dispersion". An iterative algorithm (Galbraith and Laslett, 1993) is used to provide estimates of the central age with its associated error, and the age dispersion, which are all quoted in the data sheets. Note that this treatment replaces use of the "mean age", which has used been in the past for those samples in which $P(\chi^2) < 5\%$. For samples in which $P(\chi^2) > 5\%$, the central age and the pooled age should be equal, and the age dispersion should be less than $\sim 10\%$.

Table B.1 summarises the fission track age data in apatite from each sample analysed.

Construction of radial plots of single grain age data

Single grain age data are best represented in the form of radial plot diagrams (Galbraith, 1988, 1990). As illustrated in Figure B.1, these plots display the variation of individual grain ages in a plot of y against x, where:

$$y = (z_j - z_0) / \sigma_j \quad x = 1/\sigma_j \quad \text{B.2}$$

and;

- z_j = Fission track age of grain j
- z_0 = A reference age
- σ_j = Error in age for grain j

In this plot, all points on a straight line from the origin define a single value of fission track age, and, at any point, the value of x is a measure of the precision of each individual grain age. Therefore, precise individual grain ages fall to the right of the plot (small error, high x), which is useful, for example, in enabling precise, young grains to be identified. The age scale is shown radially around the perimeter of the plot (in Ma). If all grains belong to a single age population, all data should scatter between $y = +2$ and $y = -2$, equivalent to scatter within $\pm 2\sigma$. Scatter outside these boundaries shows a significant spread of individual grain ages, as also reflected in the values of $P(\chi^2)$ and age dispersion.

In detail, rather than using the fission track age for each grain as in equation B.2, we use:

$$z_j = \frac{N_{sj}}{N_{ij}} \quad \sigma_j = \{1/N_{sj} + 1/N_{ij}\} \quad \text{B.3}$$

as we are interested in displaying the scatter within the data from each sample in comparison with that allowed by the Poissonian uncertainty in track counts, without the additional terms which are involved in determination of the fission track age (ρ_D , ζ , etc).

Zero ages cannot be displayed in such a plot. This can be achieved using a modified plot, (Galbraith, 1990) with:

$$z_j = \arcsin \sqrt{\left\{ \frac{N_{sj} + 3/8}{N_{sj} + N_{ij} + 3/4} \right\}} \quad \sigma_j = \frac{1}{2} \sqrt{\left\{ \frac{1}{N_{sj} + N_{ij}} \right\}} \quad \text{B.4}$$

Note that the numerical terms in the equation for z_j are standard terms, introduced for statistical reasons. Using this arc-sin transformation, zero ages plot on a diagonal line which slopes from upper left to lower right. Note that this line does not go through the origin. Figure B.2 illustrates this difference between conventional and arc-sin radial plots, and also provides a simple guide to the structure of radial plots.

Use of arc-sin radial plots is particularly useful in assessing the relative importance of zero ages. For instance, grains with $N_s = 0$, $N_i = 1$ are compatible with ages up to ~900 Ma (at the 95% confidence level), whereas grains with $N_s = 0$, $N_i = 50$ are only compatible with ages up to ~14 Ma. The two data would readily be distinguishable on the radial plot as the 0,50 datum would plot well to the right (high x) compared to the 0,1 datum.

In this report the value of z corresponding to the stratigraphic age of each sample (or the midpoint of the range where appropriate) is adopted as the reference value, z_0 . This allows rapid assessment of the fission track age of individual grains in relation to the stratigraphic age, which is a key component in the interpretation of AFTA data, as explained in more detail in Appendix C.

Note that the x axis of the radial plot is normally not labelled, as this would obscure the age scale around the plot. In general labelling is not considered necessary, as we are concerned only with relative variation within the data, rather than absolute values of precision.

Radial plots of the single grain age data in apatite from each sample analysed in this report are shown on the fission track age data summary sheets at the end of this Appendix. Use of radial plots to provide thermal history information is explained in Appendix C and Figure C.7.

Track length data

Distributions of confined track lengths in apatite from each sample are shown as simple histograms on the fission track age data summary sheets at the end of this Appendix. For every track length measurement, the length is recorded to the nearest 0.1 μm , but the measurements have been grouped into 1 μm intervals for construction of these histograms. Each distribution has been normalised to 100 tracks for each sample to facilitate comparison. A summary of the length distribution in each sample is presented in Table B.2, which also shows the mean track length in each sample and its associated error, the standard deviation of each distribution and the number of tracks (N) measured in each sample. The angle which each confined track makes with the crystallographic c-axis is also routinely recorded, as is the width of each fracture within which tracks are revealed. These data are not provided in this report, but can be supplied on request.

Breakdown of data into compositional groups

In Table B.3, AFTA data are grouped into compositional intervals of 0.1 wt% Cl width. Parameters for each interval represent the data from all grains with Cl contents within each interval. Also shown are the parameters for each compositional interval predicted from the Default Thermal History (see Section 2.1). These data form the basis of interpretation of the AFTA data, which takes full account of the influence of Cl content on annealing kinetics, as described in Appendix C. Distributions of Cl contents in all apatites analysed from each sample (i.e. for both age and length determinations) are shown on the fission track age data summary sheets at the end of this Appendix.

Plots of fission track age against Cl content for individual apatite grains

Fission track ages of single apatite grains within individual samples are plotted against the Cl content of each grain on the fission track age data summary sheets at the end of this Appendix. These plots are useful in assessing the degree of annealing, as expressed by the fission track age data. For example, if grains with a range of Cl contents from zero to some upper limit all give similar fission track ages which are significantly less than the stratigraphic age, then grains with these compositions must have been totally annealed. Alternatively, if fission track age falls rapidly with decreasing Cl content, the sample displays a high degree of partial annealing.



B.4 A note on terminology

Note that throughout this report, the term "fission track age" is understood to denote the parameter calculated from the fission track age equation, using the observed spontaneous and induced track counts (either pooled for all grains or for individual grains). The resulting number (with units of Ma) should not be taken as possessing any significance in terms of events taking place at the time indicated by the measured fission track age, but should rather be regarded as a measure of the integrated thermal history of the sample, and should be interpreted in that light using the principles outlined in Appendix C. Use of the term "apparent age" is not considered to be useful in this regard, as almost every fission track age should be regarded as an apparent age, in the classic sense, and repeated use becomes cumbersome.

References

- Fleischer, R. L., Price, P. B., and Walker, R. M. (1975) Nuclear tracks in solids, University of California Press, Berkeley.
- Galbraith, R. F. (1981) On statistical models for fission-track counts. *Mathematical Geology*, 13, 471-488.
- Galbraith, R. F. (1988) Graphical display of estimates having differing standard errors. *Technometrics*, 30, 271-281.
- Galbraith, R. F. (1990) The radial plot: graphical assessment of spread in ages. *Nuclear Tracks*, 17, 207-214.
- Galbraith R.F. & Laslett G.M. (1993) Statistical methods for mixed fission track ages. *Nuclear Tracks* 21, 459-470.
- Gleadow, A. J. W. (1981) Fission track dating methods; what are the real alternatives? *Nuclear Tracks*, 5, 3-14.
- Green, P. F. (1981) A new look at statistics in fission track dating. *Nuclear Tracks* 5, 77-86.
- Green, P. F. (1985) A comparison of zeta calibration baselines in zircon, sphene and apatite. *Chem. Geol. (Isot. Geol. Sect.)*, 58, 1-22.
- Green, P. F., Duddy, I. R., Gleadow, A. J. W., Tingate, P. R. and Laslett, G. M. (1986) Thermal annealing of fission tracks in apatite 1. A qualitative description. *Chem. Geol. (Isot. Geosci. Sect.)*, 59, 237-253.
- Hurford, A. J. (1986) Application of the fission track dating method to young sediments: Principles, methodology and Examples. *In: Hurford, A. J., Jäger, E. and Ten Cate, J. A. M. (eds), Dating young sediments, CCOP Technical Publication 16, CCOP Technical Secretariat, Bangkok, Thailand.*
- Hurford, A. J. and Green, P. F. (1982) A user's guide to fission track dating calibration. *Earth. Planet. Sci Lett.* 59, 343-354.
- Hurford, A. J. and Green, P. F. (1983) The zeta age calibration of fission track dating. *Isotope Geoscience* 1, 285-317.
- Laslett, G. M., Kendall, W. S., Gleadow, A. J. W. and Duddy, I. R. (1982) Bias in measurement of fission track length distributions. *Nuclear Tracks*, 6, 79-85.
- Naeser, C. W. (1979) Fission track dating and geologic annealing of fission tracks. *In: Jäger, E. and Hunziker, J. C. (eds), Lectures in Isotope Geology, Springer Verlag, Berlin.*
- Smith, M. J. and Leigh-Jones, P. (1985) An automated microscope scanning stage for fission-track dating. *Nuclear Tracks*, 10, 395-400.



Table B.1: Apatite fission track analytical results - samples from southernmost Norway (Geotrack Report #970A)

Sample number	Number of grains	ρ_D (Nd) x10 ⁶ /cm	ρ_S (Ns) x10 ⁶ /cm	ρ_i (Ni) x10 ⁶ /cm	Uranium content (ppm)	P(χ^2) (%)	Age dispersion (%)	Fission track age (Ma)
Norwegian coast basement								
GC361-21	20	1.403 (4414)	0.652 (336)	1.007 (519)	9	5	26	158.3 ± 11.6 <i>155.7 ± 15.3*</i>
GC361-22	20	1.413 (4414)	3.150 (1792)	3.379 (1922)	30	10	8	228.5 ± 8.9
GC361-25	20	1.445 (4414)	1.000 (636)	1.510 (961)	13	24	9	166.7 ± 9.2
19/3-2								
GC361-71	25	1.490 (2351)	0.423 (309)	0.656 (479)	6	2	31	167.7 ± 12.8 <i>162.8 ± 19.1*</i>
GC361-72	4	1.499 (2351)	1.988 (249)	2.683 (336)	22	79	<1	193.4 ± 16.8
GC361-73	20	1.508 (2351)	1.726 (1382)	1.974 (1580)	16	<1	24	229.0 ± 10.0 <i>225.5 ± 16.2*</i>
Lysebotn fjord section								
GC361-74	20	1.517 (2351)	3.412 (979)	4.610 (1323)	38	<1	22	195.5 ± 9.4 <i>204.2 ± 14.5*</i>
GC361-75	20	1.527 (2351)	0.644 (600)	0.849 (791)	7	<1	26	201.5 ± 11.9 <i>197.3 ± 17.1*</i>
GC361-76	20	1.536 (2351)	2.644 (1674)	3.226 (2042)	26	2	10	218.8 ± 8.8 <i>220.3 ± 10.3*</i>
Rjukan vertical section								
GC970-31	20	1.413 (2221)	0.735 (560)	0.781 (595)	6	76	<1	251.4 ± 16.0
GC970-32	20	1.416 (2221)	1.422 (1013)	1.680 (1197)	14	1	19	226.9 ± 11.1 <i>230.0 ± 15.0*</i>
GC970-33	14	1.419 (2221)	0.857 (349)	1.203 (490)	10	70	1	191.9 ± 14.2
GC970-34	20	1.422 (2221)	1.545 (909)	1.992 (1172)	16	23	9	209.1 ± 10.5
GC970-35	20	1.425 (2221)	0.836 (429)	1.396 (716)	11	4	19	162.5 ± 10.7 <i>163.8 ± 13.1*</i>



Table B.1: Continued

Sample number	Number of grains	ρ_D (N_D) x10 ⁶ /cm	ρ_s (N_s) x10 ⁶ /cm	ρ_i (N_i) x10 ⁶ /cm	Uranium content (ppm)	$P(\chi^2)$ (%)	Age dispersion (%)	Fission track age (Ma)
Setesdal outcrops								
GC970-71	20	1.506 (2265)	0.129 (24)	0.177 (33)	1	100	<1	205.1 ± 55.3
GC970-72	20	1.516 (2265)	0.649 (109)	0.863 (145)	6	94	4	213.2 ± 27.6
GC970-73	20	1.299 (2048)	1.807 (407)	1.980 (446)	17	100	<1	221.6 ± 16.3
GC970-74	20	1.299 (2048)	0.874 (116)	1.039 (138)	9	100	<1	204.5 ± 26.3
GC970-75	20	1.300 (2048)	0.433 (147)	0.515 (175)	5	90	<1	204.4 ± 23.5
GC970-76	20	1.300 (2048)	2.046 (354)	2.074 (359)	18	38	1	239.3 ± 19.0
GC970-77	20	1.300 (2048)	3.528 (957)	4.332 (1175)	38	33	1	198.3 ± 10.1
GC970-78	20	1.301 (2048)	0.914 (188)	0.894 (184)	8	97	<1	247.9 ± 26.5
GC970-79	20	1.301 (2048)	0.731 (232)	0.741 (235)	6	76	2	239.7 ± 23.1
GC970-80	20	1.301 (2048)	0.712 (240)	0.934 (315)	8	93	<1	185.8 ± 16.7
GC970-81	20	1.301 (2048)	0.096 (29)	0.146 (44)	1	98	<1	161.1 ± 38.8
GC970-82	20	1.302 (2048)	0.739 (207)	0.843 (236)	7	100	<1	213.6 ± 21.1
GC970-83	20	1.302 (2048)	2.169 (628)	3.043 (881)	27	28	9	174.1 ± 10.2
GC970-84	20	1.302 (2048)	3.766 (647)	4.272 (734)	37	98	<1	214.7 ± 12.9

ρ_s = spontaneous track density; ρ_i = induced track density; ρ_D = track density in glass standard external detector. Brackets show number of tracks counted. ρ_D and ρ_i measured in mica external detectors; ρ_s measured in internal surfaces.

*Central age, used where sample contains a significant spread of single grain ages ($P(\chi^2) < 5\%$). Errors quoted at 1σ

Ages calculated using dosimeter glass CN5, with a zeta of 380.4 ± 5.7 (Analyst: C. O'Brien) for samples; GC970-71 - 84
 CN5, with a zeta of 385.5 ± 4.3 (Analyst: P. F. Green) for samples; GC970-31 - 35
 SRM612, with a zeta of 353 ± 5 (Analyst: D. Coyle) for samples; GC361-21 - 25
 SRM612, with a zeta of 353.5 ± 3.9 (Analyst: P. F. Green) for samples; GC361-71 - 76



Table B.2: Length distribution summary data - samples from southernmost Norway (Geotrack Report #970A)

Sample number	Mean track length (μm)	Standard deviation (μm)	Number of tracks (N)	Number of tracks in Length Intervals (μm)																				
				1	2	3	4	5	6	7	8	9	10	11	12	13	14	15	16	17	18	19	20	
Norwegian coast basement																								
GC361-21	13.07 ± 0.55	2.07	14	-	-	-	-	-	-	-	-	-	-	2	1	-	3	4	2	-	2	-	-	-
GC361-22	13.07 ± 0.17	1.74	106	-	-	1	-	-	-	-	1	1	3	1	9	31	28	24	7	-	-	-	-	-
GC361-25	13.58 ± 0.16	1.41	80	-	-	-	-	-	-	-	-	-	-	2	4	3	14	25	22	9	1	-	-	-
19/3-2																								
GC361-71	11.87 ± 0.34	1.46	18	-	-	-	-	-	-	-	-	-	1	1	2	6	5	1	2	-	-	-	-	-
GC361-72	10.27 ± 0.80	3.47	19	-	-	1	1	-	2	-	1	-	1	2	2	6	2	1	-	-	-	-	-	-
GC361-73	13.35 ± 0.16	1.70	115	-	-	-	-	-	1	-	-	1	2	4	8	28	32	24	6	9	-	-	-	-
Lysebotn fjord section																								
GC361-74	12.87 ± 0.18	1.76	101	-	-	-	-	-	-	1	2	1	-	6	14	28	21	18	8	2	-	-	-	-
GC361-75	13.02 ± 0.13	1.33	106	-	-	-	-	-	-	-	-	-	1	1	5	16	24	37	18	3	-	1	-	-
GC361-76	13.53 ± 0.15	1.63	116	-	-	-	-	1	-	-	1	-	1	4	4	22	37	31	13	2	-	-	-	-
Rjukan vertical section																								
GC970-31	14.41 ± 0.11	1.14	99	-	-	-	-	-	-	-	-	-	-	-	-	4	9	16	40	24	6	-	-	-
GC970-32	13.33 ± 0.11	1.21	111	-	-	-	-	-	-	-	-	-	-	-	4	12	30	29	29	5	2	-	-	-
GC970-33	13.77 ± 0.12	1.21	106	-	-	-	-	-	-	-	-	-	-	-	-	7	24	28	30	15	2	-	-	-
GC970-34	13.30 ± 0.12	1.26	109	-	-	-	-	-	-	-	-	-	-	2	3	12	19	38	28	7	-	-	-	-
GC970-35	13.17 ± 0.12	1.25	105	-	-	-	-	-	-	-	-	-	-	-	4	12	34	29	17	7	2	-	-	-
Setesdal outcrops																								
GC970-71	13.79 ± 0.20	0.28	2	-	-	-	-	-	-	-	-	-	-	-	-	-	-	2	-	-	-	-	-	-
GC970-72	13.47 ± 0.15	1.08	49	-	-	-	-	-	-	-	-	-	-	-	-	6	10	16	15	2	-	-	-	-
GC970-73	13.26 ± 0.13	1.34	101	-	-	-	-	-	-	-	-	-	-	3	-	16	19	30	26	6	1	-	-	-
GC970-74	13.51 ± 0.12	1.21	100	-	-	-	-	-	-	-	-	-	-	2	-	6	21	37	27	5	1	1	-	-
GC970-75	12.56 ± 0.17	1.56	86	-	-	-	-	-	-	1	3	2	5	14	22	25	13	1	-	-	-	-	-	-
GC970-76	12.79 ± 0.13	1.26	100	-	-	-	-	-	-	-	-	-	-	2	7	13	37	24	14	3	-	-	-	-
GC970-77	12.76 ± 0.10	0.99	100	-	-	-	-	-	-	-	-	-	-	1	2	19	40	23	14	1	-	-	-	-
GC970-78	12.68 ± 0.15	1.51	101	-	-	-	-	1	-	-	1	-	9	17	30	23	16	4	-	-	-	-	-	-
GC970-79	12.91 ± 0.14	1.39	100	-	-	-	-	-	-	-	-	1	1	8	12	30	27	17	4	-	-	-	-	-
GC970-80	12.97 ± 0.14	1.40	99	-	-	-	-	-	-	-	-	1	3	4	15	27	24	20	4	1	-	-	-	-
GC970-81	12.40 ± 0.61	2.36	15	-	-	-	-	-	1	-	-	1	2	1	4	1	4	1	-	-	-	-	-	-
GC970-82	13.37 ± 0.25	1.54	38	-	-	-	-	-	-	-	-	-	2	2	1	10	10	9	4	-	-	-	-	-
GC970-83	12.51 ± 0.13	1.34	103	-	-	-	-	-	-	1	-	3	4	29	31	22	9	4	-	-	-	-	-	-
GC970-84	13.99 ± 0.10	1.05	100	-	-	-	-	-	-	-	-	-	-	2	2	14	30	37	13	2	-	-	-	-

Track length measurements by: C. O'Brien for samples; GC970-71 - 84
D. Coyle for samples; GC361-21 - 25
P. F. Green for samples; GC361-71 - 76
GC970-31 - 35



Table B.3: Continued - (Geotrack Report #970A)

Cl	Default fission track age* (Ma)	Measured fission track age (Ma)	Error in age (Ma)	P (χ^2)	Number of grains	Default fission track length* (μm)	Mean Track length (μm)	Error in length (μm)	Std deviation (μm)	Number of lengths	Number of grains	Number of tracks in length interval (μm)																			
												1	2	3	4	5	6	7	8	9	10	11	12	13	14	15	16	17	18	19	20
Lysebotn fjord section																															
361-74†	570	204.2	14.5	0.0	20	14.8	12.9	0.2	1.8	100	29	0	0	0	0	1	2	1	0	6	14	28	21	18	8	2	0	0	0		
0.0 - 0.1	569	190.4	11.6	5.0	12	14.7	12.9	0.2	1.9	58	15	0	0	0	0	1	2	0	0	3	6	15	14	11	5	1	0	0	0		
0.1 - 0.2	571	225.9	28.0	0.0	8	14.8	12.8	0.2	1.6	41	13	0	0	0	0	0	1	0	3	8	13	6	7	2	1	0	0	0			
0.2 - 0.3	572	0.0	0.0	0.0	0	14.8	15.8	0.0	0.0	1	1	0	0	0	0	0	0	0	0	0	0	0	0	0	1	0	0	0			
361-75†	569	197.3	17.1	0.5	20	14.7	13.0	0.1	1.3	106	49	0	0	0	0	0	1	1	5	16	24	37	18	3	0	1	0	0			
0.0 - 0.1	569	192.7	11.7	5.3	19	14.7	13.0	0.1	1.3	105	48	0	0	0	0	0	1	1	5	16	24	37	17	3	0	1	0	0			
0.1 - 0.2	571	388.9	85.5	100.0	1	14.8	14.5	0.0	0.0	1	1	0	0	0	0	0	0	0	0	0	0	0	0	1	0	0	0	0			
361-76†	569	220.3	10.3	2.5	20	14.7	13.5	0.2	1.6	114	19	0	0	0	1	0	1	0	1	4	22	37	31	13	2	0	0	0			
0.0 - 0.1	569	220.3	10.3	2.5	20	14.7	13.5	0.2	1.6	114	19	0	0	0	1	0	1	0	1	4	22	36	30	13	2	0	0	0			
Rjukan vertical section																															
970-31†	401	251.4	16.0	75.8	20	14.8	14.4	0.1	1.1	99	47	0	0	0	0	0	0	0	0	4	9	16	40	24	6	0	0	0			
0.0 - 0.1	401	251.4	16.0	75.8	20	14.8	14.4	0.1	1.1	99	47	0	0	0	0	0	0	0	0	4	9	16	40	24	6	0	0	0			
970-32†	401	230.0	15.0	0.5	20	14.8	13.3	0.1	1.2	111	50	0	0	0	0	0	0	0	4	12	30	29	29	5	2	0	0	0			
0.0 - 0.1	401	230.0	15.0	0.5	20	14.8	13.3	0.1	1.2	111	50	0	0	0	0	0	0	0	4	12	30	29	29	5	2	0	0	0			
970-33†	401	191.9	14.2	70.1	14	14.8	13.8	0.1	1.2	106	54	0	0	0	0	0	0	0	0	7	24	28	30	15	2	0	0	0			
0.0 - 0.1	401	191.9	14.2	70.1	14	14.8	13.8	0.1	1.2	106	54	0	0	0	0	0	0	0	0	7	24	28	30	15	2	0	0	0			
970-34†	401	209.1	10.5	22.9	20	14.8	13.3	0.1	1.3	109	39	0	0	0	0	0	0	0	2	3	12	19	38	28	7	0	0	0	0		
0.0 - 0.1	401	209.1	10.5	22.9	20	14.8	13.3	0.1	1.3	108	38	0	0	0	0	0	0	0	2	3	12	19	38	28	6	0	0	0	0		
0.1 - 0.2	-	-	-	-	-	-	-	-	-	-	-	-	-	-	-	-	-	-	-	-	-	-	-	-	-	-	-	-			
0.2 - 0.3	-	-	-	-	-	-	-	-	-	-	-	-	-	-	-	-	-	-	-	-	-	-	-	-	-	-	-	-			
0.3 - 0.4	404	0.0	0.0	0.0	0	14.9	15.4	0.0	0.0	1	1	0	0	0	0	0	0	0	0	0	0	0	0	0	1	0	0	0			
970-35†	401	163.8	13.1	4.5	20	14.8	13.2	0.1	1.2	104	48	0	0	0	0	0	0	0	4	12	34	29	17	7	2	0	0	0			
0.0 - 0.1	401	163.8	13.1	4.5	20	14.8	13.2	0.1	1.2	104	48	0	0	0	0	0	0	0	4	12	33	29	17	7	2	0	0	0			

*Fission Track Age and Mean Track Length predicted from the Default Thermal History (i.e. if the sample has not been hotter in the past)

†Combined data for all compositional groups



Table B.3: Continued - (Geotrack Report #970A)

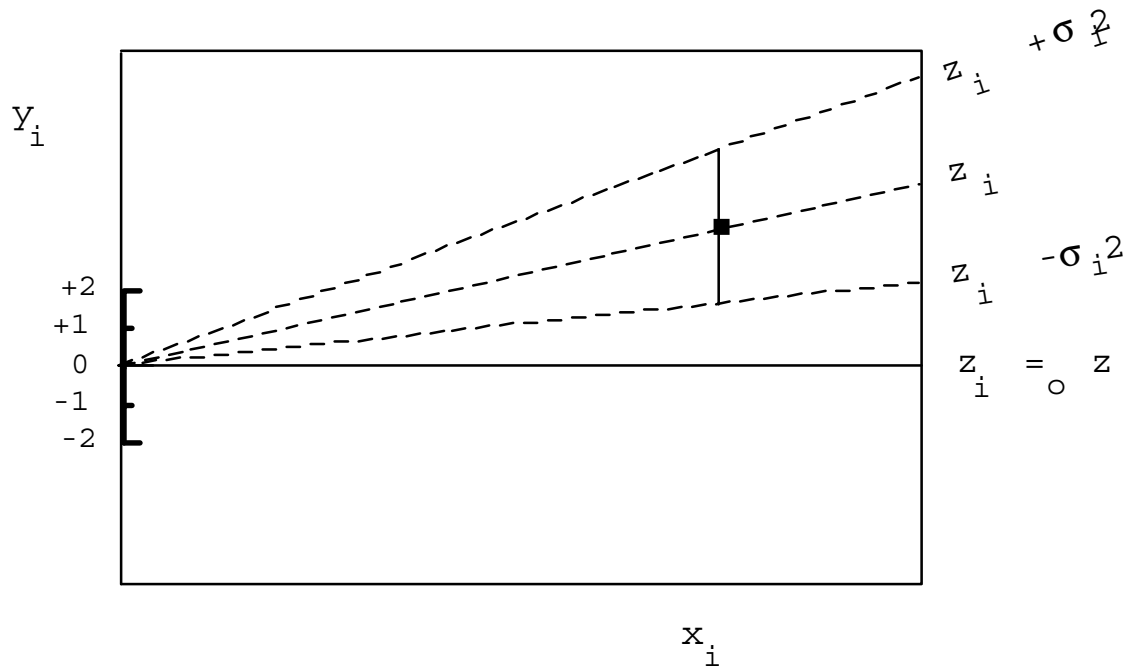
Cl	Wt %	Default fission track age* (Ma)	Measured fission track age (Ma)	Error in age (Ma)	P (χ^2)	Number of grains	Default fission track length* (μm)	Mean Track length (μm)	Error in length (μm)	Std deviation (μm)	Number of lengths	Number of grains	Number of tracks in length interval (μm)																			
													1	2	3	4	5	6	7	8	9	10	11	12	13	14	15	16	17	18	19	20
970-78 [†]	0.0 - 0.1	540	247.9	26.5	96.9	20	14.7	12.7	0.2	1.5	101	47	0	0	0	0	1	0	0	1	0	9	17	30	23	16	4	0	0	0	0	
		540	247.9	26.5	96.9	20	14.7	12.7	0.2	1.5	101	47	0	0	0	0	1	0	0	1	0	9	17	30	23	16	4	0	0	0	0	
970-79 [†]	0.0 - 0.1	540	239.7	23.1	76.2	20	14.7	12.9	0.1	1.4	99	50	0	0	0	0	0	1	1	8	12	30	27	17	4	0	0	0	0	0		
		540	237.3	23.7	71.5	19	14.7	12.9	0.1	1.4	96	48	0	0	0	0	0	1	1	8	11	28	26	17	4	0	0	0	0	0	0	
		541	272.5	93.9	100.0	1	14.8	12.4	0.5	0.8	3	2	0	0	0	0	0	0	0	0	0	1	1	1	0	0	0	0	0	0	0	
970-80 [†]	0.0 - 0.1	540	185.8	16.7	92.8	20	14.7	13.0	0.1	1.4	98	48	0	0	0	0	0	0	1	3	4	15	27	24	20	4	1	0	0	0	0	
		540	185.8	16.7	92.8	20	14.7	13.0	0.1	1.4	98	48	0	0	0	0	0	0	1	3	4	15	27	23	20	4	1	0	0	0	0	
970-81 [†]	0.0 - 0.1	540	161.1	38.8	98.2	20	14.7	12.4	0.6	2.4	15	10	0	0	0	0	1	0	0	1	2	1	4	1	4	1	0	0	0	0	0	
		540	161.1	38.8	98.2	20	14.7	12.4	0.6	2.4	15	10	0	0	0	0	1	0	0	1	2	1	4	1	4	1	0	0	0	0	0	0
970-82 [†]	0.0 - 0.1	540	213.6	21.1	99.9	20	14.7	13.4	0.2	1.5	38	23	0	0	0	0	0	0	0	0	2	2	1	10	10	9	4	0	0	0	0	0
		540	213.6	21.1	99.9	20	14.7	13.4	0.2	1.5	38	23	0	0	0	0	0	0	0	0	2	2	1	10	10	9	4	0	0	0	0	0
970-83 [†]	0.0 - 0.1	540	174.1	10.2	27.5	20	14.7	12.5	0.1	1.3	102	17	0	0	0	0	0	1	0	3	4	29	31	22	9	4	0	0	0	0	0	0
		540	174.1	10.2	27.5	20	14.7	12.5	0.1	1.3	102	17	0	0	0	0	0	1	0	3	4	28	31	22	9	4	0	0	0	0	0	0

*Fission Track Age and Mean Track Length predicted from the Default Thermal History (i.e. if the sample has not been hotter in the past)

[†]Combined data for all compositional groups

Estimates	z_i
Standard errors	σ_i
Reference value	z_0
Standardised estimates	$y_i = (z_i - z_0) / \sigma_i$
Precision	$x_i = 1 / \sigma_i$

PLOT y_i against x_i



Slope of line from origin through data point

$$= y_i / x_i$$

$$= \{(z_i - z_0) / \sigma_i\} / \{1 / \sigma_i\}$$

$$= z_i - z_0$$

Key Points:

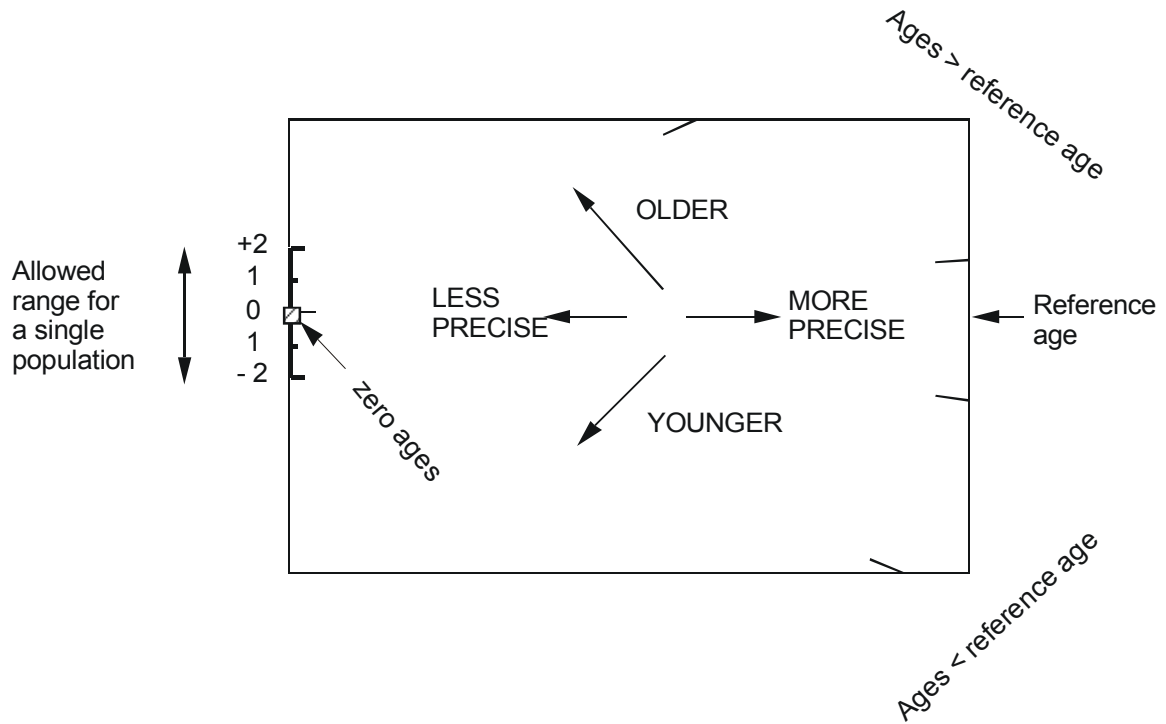
Radial lines emanating from the origin correspond to fixed values of z

Data points with higher values of x_i have greater precision.

Error bars on all points are the same size in this plot.

Figure B.1 Basic construction of a radial plot. In AFTA, the estimates z_i correspond to the fission track age values for individual apatite grains. Any convenient value of age can be chosen as the reference value corresponding to the horizontal in the radial plot. Radial lines emanating from the origin with positive slopes correspond to fission track ages greater than the reference value. Lines with negative slopes correspond to fission track ages less than the reference value.

Normal radial plot (equations B.2 and B.3)



Arc-sin radial plot (equations B.2 and B.4)

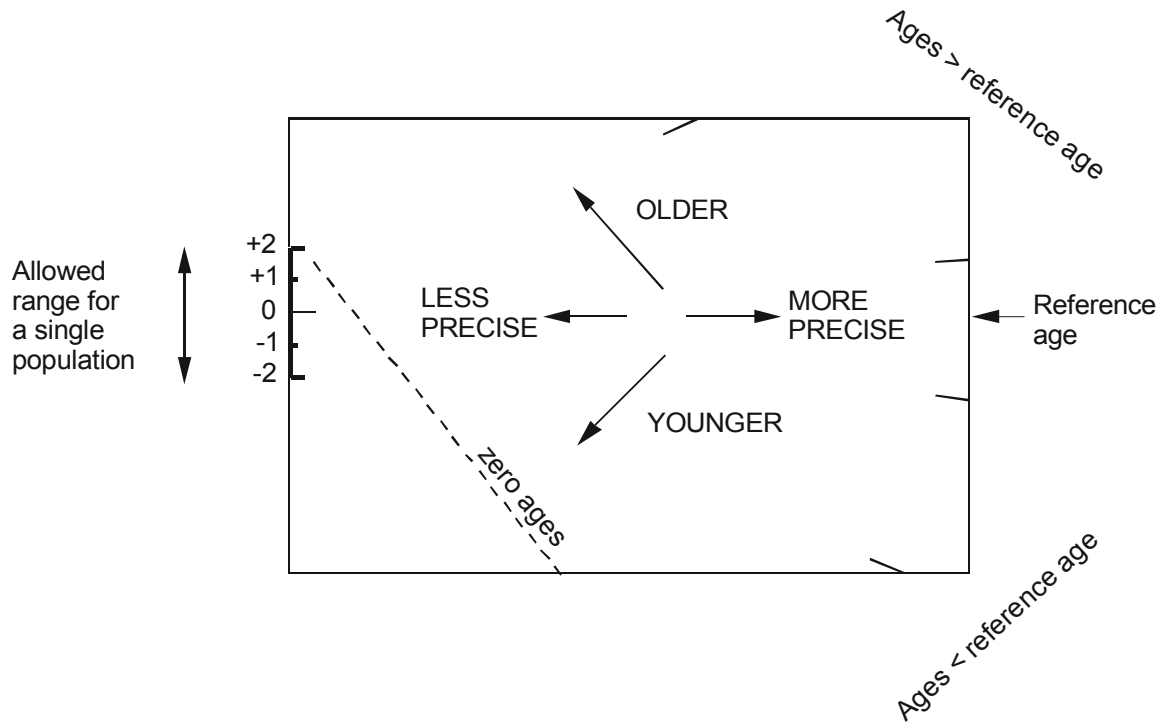


Figure B.2 Simplified structure of Normal and Arc-sin radial plots.

Fission Track Age Data Sheets - Glossary

N_s	=	Number of spontaneous tracks in N_a grid squares
N_i	=	Number of induced tracks in N_a grid squares
N_a	=	Number of grid squares counted in each grain
RATIO	=	N_s/N_i
U (ppm)	=	Uranium content of each grain (= U content of standard glass * ρ_i/ρ_D)
Cl (wt%)	=	Weight percent chlorine content of each grain
ρ_s	=	Spontaneous track density (ρ_s) = $N_s/(N_a \cdot \text{area of basic unit})$
ρ_i	=	Induced track density (ρ_i) = $N_i/(N_a \cdot \text{area of basic unit})$
F.T. AGE	=	Fission track age, calculated using equation B.1
Area of basic unit	=	Area of one grid square
Chi squared	=	χ^2 parameter, used to assess variation of single grain ages within the sample
P(chi squared)	=	Probability of obtaining observed χ^2 value for the relevant number of degrees of freedom, if all grains belong to a single population
Age Dispersion	=	% variation in single grain ages - see discussion in text re "Central age"
N_s/N_i	=	Pooled ratio, total spontaneous tracks divided by total induced tracks for all grains
Mean ratio	=	Mean of (N_s/N_i) for individual grains
Zeta	=	Calibration constant, determined empirically for each observer
ρ_D	=	Track density (ρ_D) from uranium standard glass (interpolated from values at each end of stack)
ND	=	Total number of tracks counted for determining ρ_D
POOLED AGE	=	Fission track age calculated from pooled ratio N_s/N_i . Valid only when $P(\chi^2) > 5\%$
CENTRAL AGE	=	Alternative to pooled age when $P(\chi^2) < 5\%$

Key to Figures:

A: Radial plot of single grain ages <i>(See Figures B.1 and B.2 for details of radial plot construction)</i>	B: Distribution of Cl contents in apatite grains
C: Single grain age vs weight % Cl for individual apatite grains.	D: Distribution of confined track lengths



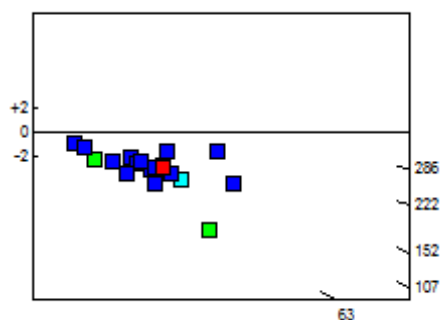
GC361-21 Apatite
Counted by: DAC

Slide ref	Current grain no	N _s	N _i	N _a	ρ _s	ρ _i	RATIO	U (ppm)	Cl (wt%)	F.T. AGE (Ma)
G229-8	1	12	16	70	2.724E+05	3.632E+05	0.750	3.2	0.02	183.1 ± 70.0
G229-8	3	2	3	90	3.531E+04	5.297E+04	0.667	0.5	0.00	163.0 ± 148.8
G229-8	5	2	3	25	1.271E+05	1.907E+05	0.667	1.7	0.05	163.0 ± 148.8
G229-8	6	12	19	36	5.297E+05	8.387E+05	0.632	7.5	0.01	154.5 ± 57.1
G229-8	7	3	8	80	5.959E+04	1.589E+05	0.375	1.4	0.16	92.2 ± 62.4
G229-8	8	23	39	20	1.827E+06	3.099E+06	0.590	27.6	0.27	144.4 ± 38.1
G229-8	9	49	66	48	1.622E+06	2.185E+06	0.742	19.5	0.05	181.3 ± 34.4
G229-8	11	27	25	49	8.756E+05	8.107E+05	1.080	7.2	0.00	262.0 ± 72.9
G229-8	13	3	5	25	1.907E+05	3.178E+05	0.600	2.8	0.03	146.9 ± 107.3
G229-8	14	13	30	42	4.919E+05	1.135E+06	0.433	10.1	0.08	106.4 ± 35.4
G229-8	16	20	28	36	8.828E+05	1.236E+06	0.714	11.0	0.01	174.5 ± 51.2
G229-8	18	21	33	16	2.086E+06	3.277E+06	0.636	29.2	0.00	155.7 ± 43.6
G229-8	19	15	25	28	8.513E+05	1.419E+06	0.600	12.6	0.00	146.9 ± 48.1
G229-8	20	52	44	36	2.295E+06	1.942E+06	1.182	17.3	0.02	286.2 ± 58.9
G229-8	22	17	26	24	1.126E+06	1.721E+06	0.654	15.3	0.00	159.9 ± 50.0
G229-8	23	20	29	25	1.271E+06	1.843E+06	0.690	16.4	0.38	168.5 ± 49.1
G229-8	24	6	12	49	1.946E+05	3.892E+05	0.500	3.5	0.00	122.6 ± 61.4
G229-8	25	7	18	30	3.708E+05	9.534E+05	0.389	8.5	0.00	95.6 ± 42.6
G229-8	30	18	70	20	1.430E+06	5.562E+06	0.257	49.6	0.11	63.4 ± 16.8
G229-8	31	14	20	70	3.178E+05	4.540E+05	0.700	4.0	0.00	171.0 ± 59.7
		336	519		6.519E+05	1.007E+06		9.0		

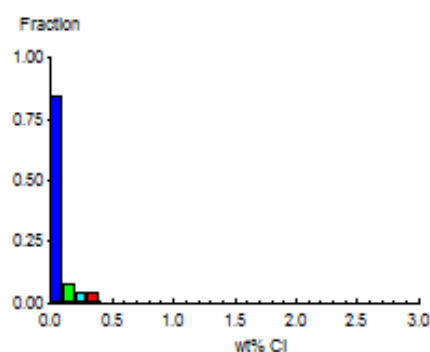
Area of basic unit = 6.293E-07 cm²
 $\chi^2 = 30.315$ with 19 degrees of freedom
 $P(\chi^2) = 4.8\%$
 Age Dispersion = 26.010%
 $N_s / N_i = 0.647 \pm 0.045$
 Mean Ratio = 0.643 ± 0.048

Ages calculated using a zeta of 353 ± 5 for SRM612 glass
 $\rho = 1.403E+06 \text{ cm}^{-2}$ ND=4414
 ρ_D interpolated between top of can; $\rho = 1.328E+06 \text{ cm}^{-2}$ ND=2090
 bottom of can; $\rho = 1.477E+06 \text{ cm}^{-2}$ ND=2324
 POOLED AGE = 158.3 ± 11.6 Ma
CENTRAL AGE = 155.7 ± 15.3 Ma

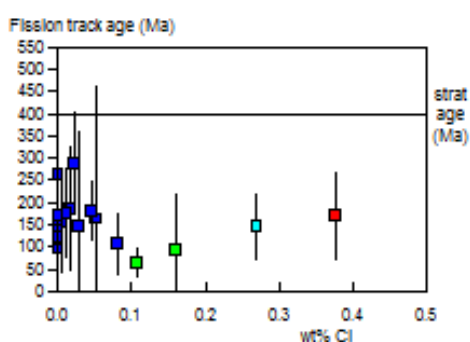
A:



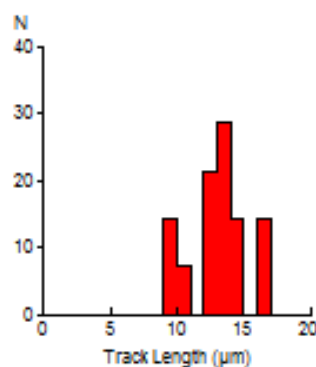
B:



C:



D:



Mean track length 13.07 ± 0.55 μm Std. Dev. 2.07 μm 14 tracks



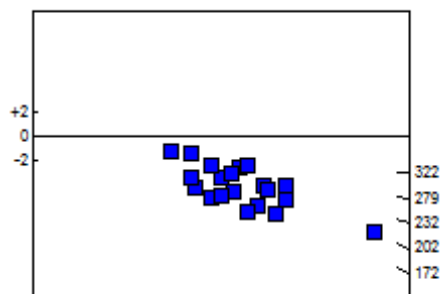
GC361-22 Apatite
Counted by: DAC

Slide ref	Current grain no	N _s	N _i	N _a	ρ _s	ρ _i	RATIO	U (ppm)	Cl (wt%)	F.T. AGE (Ma)
G229-9	1	77	89	42	2.913E+06	3.367E+06	0.865	29.8	0.06	212.3 ± 33.3
G229-9	2	109	109	36	4.811E+06	4.811E+06	1.000	42.5	0.03	244.8 ± 33.5
G229-9	3	45	34	25	2.860E+06	2.161E+06	1.324	19.1	0.04	322.0 ± 73.5
G229-9	4	58	44	56	1.646E+06	1.249E+06	1.318	11.0	0.06	320.7 ± 64.5
G229-9	5	219	255	100	3.480E+06	4.052E+06	0.859	35.8	0.05	210.8 ± 19.9
G229-9	6	92	115	63	2.321E+06	2.901E+06	0.800	25.7	0.05	196.6 ± 27.8
G229-9	7	104	136	70	2.361E+06	3.087E+06	0.765	27.3	0.03	188.0 ± 24.8
G229-9	8	48	61	42	1.816E+06	2.308E+06	0.787	20.4	0.05	193.4 ± 37.5
G229-9	9	55	76	35	2.497E+06	3.451E+06	0.724	30.5	0.07	178.1 ± 31.7
G229-9	10	48	54	24	3.178E+06	3.575E+06	0.889	31.6	0.05	218.0 ± 43.5
G229-9	11	77	110	45	2.719E+06	3.884E+06	0.700	34.4	0.04	172.3 ± 25.8
G229-9	12	73	73	20	5.800E+06	5.800E+06	1.000	51.3	0.04	244.8 ± 40.8
G229-9	13	111	115	48	3.675E+06	3.807E+06	0.965	33.7	0.04	236.4 ± 31.8
G229-9	14	95	81	40	3.774E+06	3.218E+06	1.173	28.5	0.06	286.1 ± 43.7
G229-9	15	134	128	48	4.436E+06	4.238E+06	1.047	37.5	0.07	256.0 ± 32.1
G229-9	16	84	78	30	4.449E+06	4.132E+06	1.077	36.5	0.04	263.2 ± 41.7
G229-9	17	125	136	70	2.838E+06	3.087E+06	0.919	27.3	0.06	225.3 ± 28.3
G229-9	18	69	61	25	4.386E+06	3.877E+06	1.131	34.3	0.09	276.2 ± 48.9
G229-9	19	105	85	50	3.337E+06	2.701E+06	1.235	23.9	0.00	301.0 ± 44.4
G229-9	20	64	82	35	2.906E+06	3.723E+06	0.780	32.9	0.05	191.8 ± 32.2
		1792	1922		3.150E+06	3.379E+06		29.9		

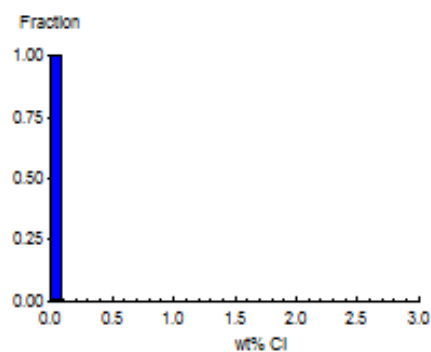
Area of basic unit = 6.293E-07 cm²
 $\chi^2 = 27.278$ with 19 degrees of freedom
 $P(\chi^2) = 9.8\%$
 Age Dispersion = 8.078% (did not converge)
 $N_s / N_i = 0.932 \pm 0.031$
 Mean Ratio = 0.968 ± 0.043

Ages calculated using a zeta of 353 ± 5 for SRM612 glass
 $\rho = 1.413E+06 \text{ cm}^{-2}$ ND=4414
 ρ_D interpolated between top of can; $\rho = 1.328E+06 \text{ cm}^{-2}$ ND=2090
 bottom of can; $\rho = 1.477E+06 \text{ cm}^{-2}$ ND=2324
POOLED AGE = 228.5 ± 8.9 Ma
CENTRAL AGE = 229.5 ± 9.9 Ma

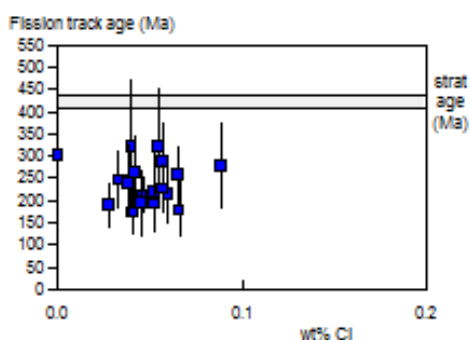
A:



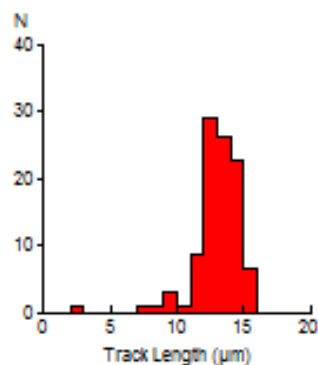
B:



C:



D:



Mean track length 13.07 ± 0.17 µm Std. Dev. 1.74 µm 106 tracks



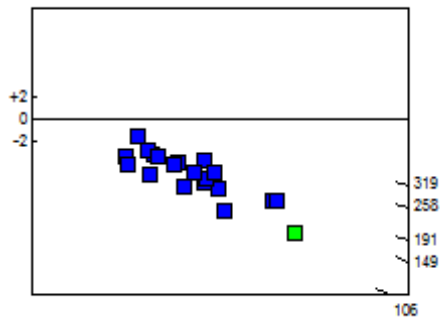
GC361-25 Apatite
Counted by: DAC

Slide ref	Current grain no	N _s	N _i	N _a	ρ _s	ρ _i	RATIO	U (ppm)	Cl (wt%)	F.T. AGE (Ma)
G229-12	3	9	16	12	1.192E+06	2.119E+06	0.563	18.3	0.00	141.9 ± 59.2
G229-12	4	32	74	49	1.038E+06	2.400E+06	0.432	20.8	0.01	109.4 ± 23.3
G229-12	7	27	34	20	2.145E+06	2.701E+06	0.794	23.4	0.00	199.5 ± 51.6
G229-12	12	68	97	50	2.161E+06	3.083E+06	0.701	26.7	0.00	176.4 ± 28.1
G229-12	13	37	61	100	5.880E+05	9.693E+05	0.607	8.4	0.00	152.9 ± 32.0
G229-12	18	33	52	36	1.457E+06	2.295E+06	0.635	19.9	0.01	159.9 ± 35.7
G229-12	19	25	33	16	2.483E+06	3.277E+06	0.758	28.3	0.01	190.4 ± 50.6
G229-12	20	12	28	100	1.907E+05	4.449E+05	0.429	3.8	0.00	108.4 ± 37.5
G229-12	21	19	23	12	2.516E+06	3.046E+06	0.826	26.3	0.03	207.4 ± 64.4
G229-12	23	36	51	30	1.907E+06	2.701E+06	0.706	23.4	0.00	177.6 ± 38.8
G229-12	28	18	21	70	4.086E+05	4.767E+05	0.857	4.1	0.00	215.0 ± 69.2
G229-12	29	18	14	24	1.192E+06	9.270E+05	1.286	8.0	0.00	319.9 ± 114.2
G229-12	30	21	45	30	1.112E+06	2.384E+06	0.467	20.6	0.00	118.0 ± 31.3
G229-12	32	42	43	40	1.669E+06	1.708E+06	0.977	14.8	0.01	244.5 ± 53.3
G229-12	35	20	25	32	9.932E+05	1.241E+06	0.800	10.7	0.00	200.9 ± 60.4
G229-12	36	71	99	100	1.128E+06	1.573E+06	0.717	13.6	0.00	180.4 ± 28.3
G229-12	37	42	52	81	8.240E+05	1.020E+06	0.808	8.8	0.00	202.8 ± 42.3
G229-12	40	66	130	70	1.498E+06	2.951E+06	0.508	25.5	0.15	128.2 ± 19.6
G229-12	41	32	44	49	1.038E+06	1.427E+06	0.727	12.3	0.01	182.9 ± 42.7
G229-12	51	8	19	90	1.413E+05	3.355E+05	0.421	2.9	0.00	106.5 ± 45.0
		636	961		9.997E+05	1.510E+06		13.1		

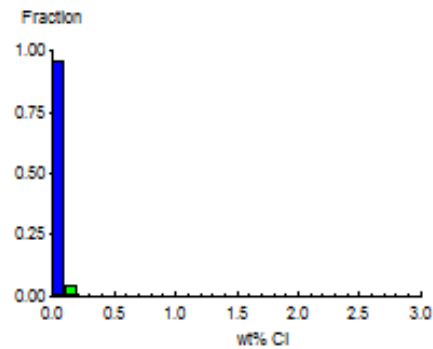
Area of basic unit = 6.293E-07 cm²
 $\chi^2 = 22.880$ with 19 degrees of freedom
 $P(\chi^2) = 24.3\%$
 Age Dispersion = 9.184% (did not converge)
 N_s / N_i = 0.662 ± 0.034
 Mean Ratio = 0.701 ± 0.047

Ages calculated using a zeta of 353 ± 5 for SRM612 glass
 $\rho = 1.445E+06 \text{ cm}^{-2}$ ND=4414
 ρ_D interpolated between top of can; $\rho = 1.328E+06 \text{ cm}^{-2}$ ND=2090
 bottom of can; $\rho = 1.477E+06 \text{ cm}^{-2}$ ND=2324
POOLED AGE = 166.7 ± 9.2 Ma
CENTRAL AGE = 167.5 ± 10.0 Ma

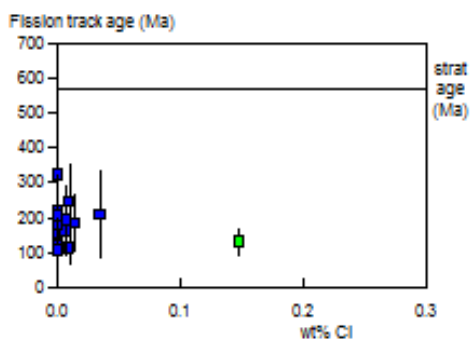
A:



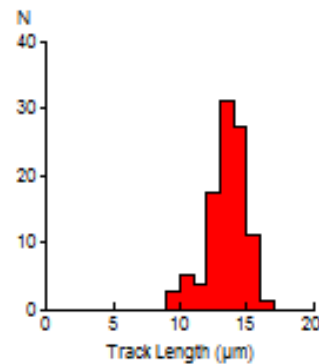
B:



C:



D:



Mean track length 13.58 ± 0.16 μm Std. Dev. 1.41 μm 80 tracks



GC361-71 Apatite
Counted by: PFG

19/3-2 800-m -

Slide ref	Current grain no	N _s	N _i	N _a	ρ _s	ρ _i	RATIO	U (ppm)	Cl (wt%)	F.T. AGE (Ma)
G235-9	1	1	2	49	3.243E+04	6.486E+04	0.500	0.5	0.00	130.3 ± 159.7
G235-9	2	35	100	50	1.112E+06	3.178E+06	0.350	26.7	0.00	91.5 ± 18.1
G235-9	4	2	3	49	6.486E+04	9.729E+04	0.667	0.8	0.00	173.2 ± 158.2
G235-9	5	10	7	9	1.766E+06	1.236E+06	1.429	10.4	0.00	365.6 ± 180.4
G235-9	6	1	1	32	4.966E+04	4.966E+04	1.000	0.4	0.00	258.1 ± 365.0
G235-9	8	1	3	50	3.178E+04	9.534E+04	0.333	0.8	0.00	87.2 ± 100.7
G235-9	9	2	8	80	3.973E+04	1.589E+05	0.250	1.3	0.00	65.5 ± 51.8
G235-9	10	2	7	60	5.297E+04	1.854E+05	0.286	1.6	0.00	74.8 ± 60.0
G235-9	11	2	3	100	3.178E+04	4.767E+04	0.667	0.4	0.00	173.2 ± 158.2
G235-9	12	0	2	50	0.000E+00	6.356E+04	0.000	0.5	0.00	0.0 ± 427.5
G235-9	16	25	27	60	6.621E+05	7.151E+05	0.926	6.0	0.28	239.3 ± 66.7
G235-9	17	2	4	70	4.540E+04	9.080E+04	0.500	0.8	0.00	130.3 ± 112.9
G235-9	18	5	3	50	1.589E+05	9.534E+04	1.667	0.8	0.00	424.6 ± 310.2
G235-9	21	1	6	50	3.178E+04	1.907E+05	0.167	1.6	0.00	43.7 ± 47.3
G235-9	22	3	4	50	9.534E+04	1.271E+05	0.750	1.1	0.00	194.5 ± 148.6
G235-9	23	17	21	15	1.801E+06	2.225E+06	0.810	18.7	0.00	209.7 ± 68.6
G235-9	27	2	1	50	6.356E+04	3.178E+04	2.000	0.3	0.00	506.2 ± 620.1
G235-9	28	24	31	40	9.534E+05	1.232E+06	0.774	10.3	0.00	200.7 ± 54.8
G235-9	29	106	113	70	2.406E+06	2.565E+06	0.938	21.5	0.07	242.4 ± 33.3
G235-9	30	15	47	20	1.192E+06	3.734E+06	0.319	31.3	0.00	83.5 ± 24.8
G235-9	32	10	16	20	7.945E+05	1.271E+06	0.625	10.7	0.00	162.5 ± 65.6
G235-9	35	19	22	21	1.438E+06	1.665E+06	0.864	14.0	0.00	223.5 ± 70.2
G235-9	37	7	9	40	2.781E+05	3.575E+05	0.778	3.0	0.24	201.6 ± 101.7
G235-9	39	3	7	50	9.534E+04	2.225E+05	0.429	1.9	0.00	111.9 ± 77.2
G235-9	40	14	32	25	8.899E+05	2.034E+06	0.438	17.1	0.00	114.2 ± 36.7
		309	479		4.233E+05	6.562E+05		5.5		

Area of basic unit = 6.293E-07 cm⁻²

χ² = 41.011 with 24 degrees of freedom

P(χ²) = 1.7%

Age Dispersion = 31.322%

N_s / N_i = 0.645 ± 0.047

Mean Ratio = 0.699 ± 0.093

Ages calculated using a zeta of 353.5 ± 3.9 for SRM612 glass

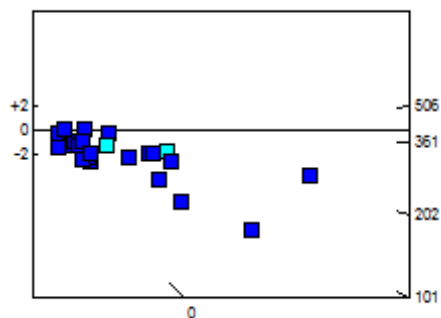
ρ = 1.490E+06cm⁻² ND=2351

ρ_D interpolated between top of can; ρ = 1.416E+06cm⁻² ND=1114
bottom of can; ρ = 1.573E+06cm⁻² ND=1237

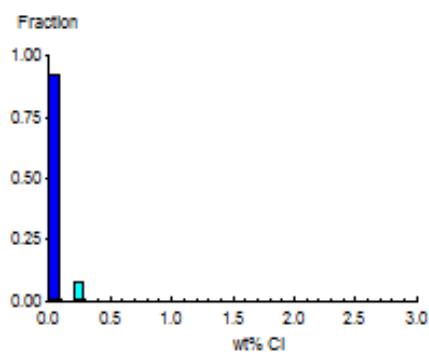
POOLED AGE = 167.7 ± 12.8 Ma

CENTRAL AGE = 162.8 ± 19.1 Ma

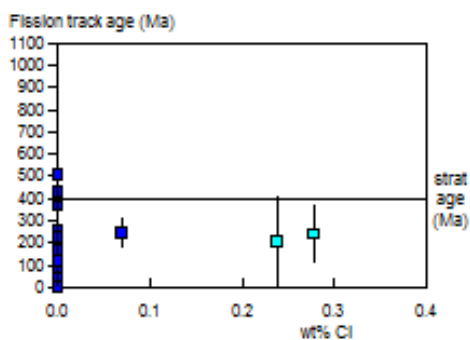
A:



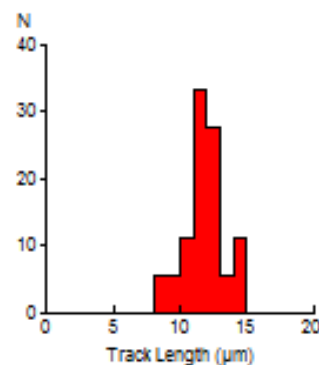
B:



C:



D:



Mean track length 11.87 ± 0.34 μm Std. Dev. 1.46 μm 18 tracks



GC361-72 Apatite
Counted by: PFG

19/3-2 1480-m -

Slide ref	Current grain no	N _s	N _i	N _a	ρ _s	ρ _i	RATIO	U (ppm)	Cl (wt%)	F.T. AGE (Ma)
G235-10	2	5	10	49	1.621E+05	3.243E+05	0.500	2.7	0.01	131.1 ± 71.9
G235-10	3	44	66	30	2.331E+06	3.496E+06	0.667	29.2	0.00	174.3 ± 34.2
G235-10	4	180	232	50	5.721E+06	7.373E+06	0.776	61.5	0.00	202.3 ± 20.6
G235-10	5	20	28	70	4.540E+05	6.356E+05	0.714	5.3	0.00	186.5 ± 54.8
		249	336		1.988E+06	2.683E+06		22.4		

Area of basic unit = 6.293E-07 cm²

χ² = 1.048 with 3 degrees of freedom

P(χ²) = 79.0%

Age Dispersion = 0.000% (did not converge)

N_s / N_i = 0.741 ± 0.062

Mean Ratio = 0.664 ± 0.059

Ages calculated using a zeta of 353.5 ± 3.9 for SRM612 glass

ρ = 1.499E+06cm⁻² ND = 2351

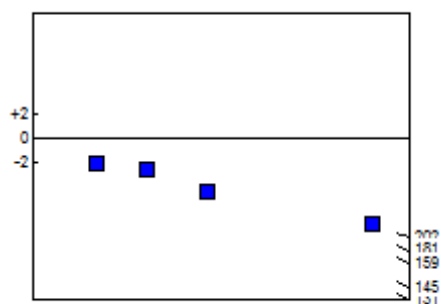
ρ_D interpolated between top of can; ρ = 1.416E+06cm⁻² ND = 1114

bottom of can; ρ = 1.573E+06cm⁻² ND = 1237

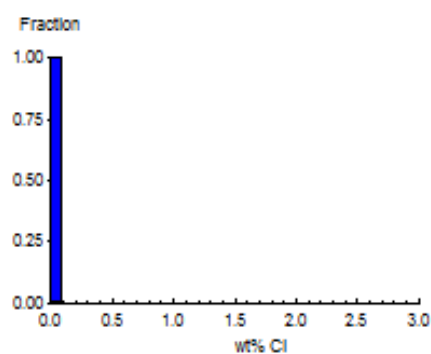
POOLED AGE = 193.4 ± 16.8 Ma

CENTRAL AGE = 193.4 ± 16.8 Ma

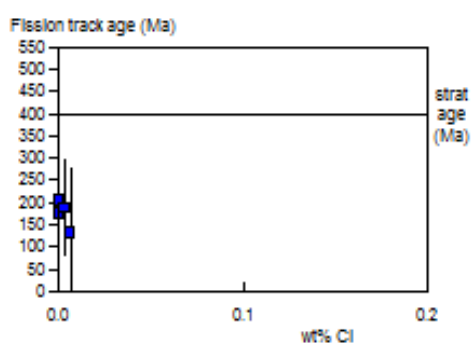
A:



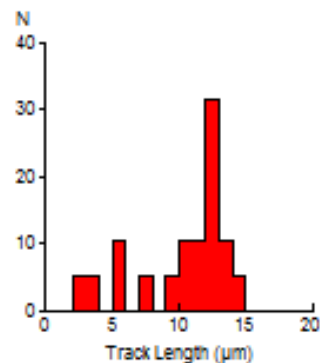
B:



C:



D:



Mean track length 10.27 ± 0.80 μm Std. Dev. 3.47 μm 19 tracks



GC361-73 Apatite
Counted by: PFG

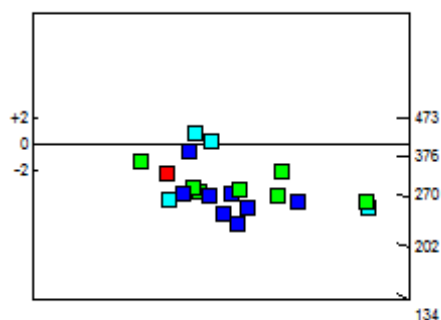
19/3-2

Slide ref	Current grain no	N _s	N _i	N _a	ρ _s	ρ _i	RATIO	U (ppm)	Cl (wt%)	F.T. AGE (Ma)
G235-11	1	40	56	80	7.945E+05	1.112E+06	0.714	9.2	0.12	187.6 ± 39.1
G235-11	2	38	51	36	1.677E+06	2.251E+06	0.745	18.7	0.13	195.6 ± 42.2
G235-11	3	60	76	100	9.534E+05	1.208E+06	0.789	10.0	0.07	207.1 ± 36.1
G235-11	4	65	94	70	1.476E+06	2.134E+06	0.691	17.7	0.08	181.7 ± 29.6
G235-11	5	48	36	50	1.526E+06	1.144E+06	1.333	9.5	0.06	346.0 ± 76.7
G235-11	6	96	109	50	3.051E+06	3.464E+06	0.881	28.7	0.14	230.6 ± 32.7
G235-11	7	67	42	90	1.183E+06	7.416E+05	1.595	6.1	0.26	411.8 ± 81.6
G235-11	8	51	94	50	1.621E+06	2.987E+06	0.543	24.8	0.07	143.0 ± 25.1
G235-11	9	67	79	80	1.331E+06	1.569E+06	0.848	13.0	0.11	222.2 ± 37.3
G235-11	10	186	199	100	2.956E+06	3.162E+06	0.935	26.2	0.24	244.5 ± 25.6
G235-11	11	114	100	36	5.032E+06	4.414E+06	1.140	36.6	0.12	296.9 ± 41.3
G235-11	12	22	43	50	6.992E+05	1.367E+06	0.512	11.3	0.22	135.0 ± 35.5
G235-11	13	188	195	90	3.319E+06	3.443E+06	0.964	28.5	0.17	252.0 ± 26.4
G235-11	14	29	34	60	7.680E+05	9.005E+05	0.853	7.5	0.34	223.4 ± 56.7
G235-11	15	59	32	60	1.563E+06	8.475E+05	1.844	7.0	0.21	473.6 ± 104.6
G235-11	16	30	48	60	7.945E+05	1.271E+06	0.625	10.5	0.10	164.5 ± 38.5
G235-11	17	46	79	60	1.218E+06	2.092E+06	0.582	17.3	0.08	153.4 ± 28.7
G235-11	18	44	63	50	1.398E+06	2.002E+06	0.698	16.6	0.10	183.5 ± 36.3
G235-11	19	20	20	40	7.945E+05	7.945E+05	1.000	6.6	0.18	261.2 ± 82.8
G235-11	20	112	130	60	2.966E+06	3.443E+06	0.862	28.5	0.07	225.7 ± 29.6
		1382	1580		1.726E+06	1.974E+06		16.4		

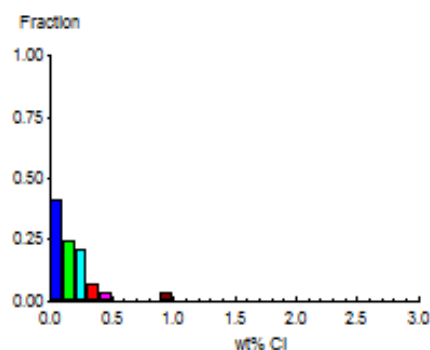
Area of basic unit = 6.293E-07 cm²
 $\chi^2 = 55.012$ with 19 degrees of freedom
 $P(\chi^2) = 0.0\%$
 Age Dispersion = 24.297%
 N_s / N_i = 0.875 ± 0.032
 Mean Ratio = 0.908 ± 0.077

Ages calculated using a zeta of 353.5 ± 3.9 for SRM612 glass
 $\rho = 1.508E+06\text{cm}^{-2}$ ND=2351
 ρ_D interpolated between top of can; $\rho = 1.416E+06\text{cm}^{-2}$ ND=1114
 bottom of can; $\rho = 1.573E+06\text{cm}^{-2}$ ND=1237
 POOLED AGE = 229.0 ± 10.0 Ma
CENTRAL AGE = 225.5 ± 16.2 Ma

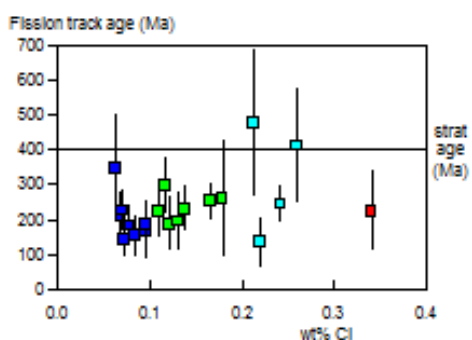
A:



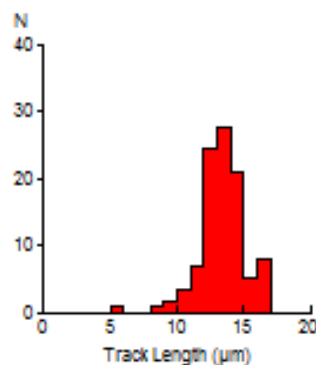
B:



C:



D:



Mean track length 13.35 ± 0.16 μm Std. Dev. 1.70 μm 115 tracks



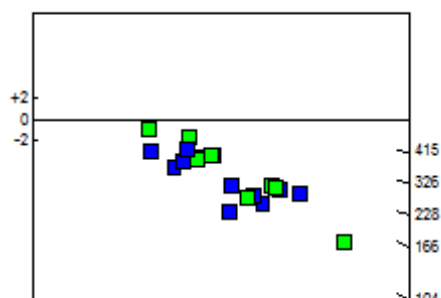
GC361-74 Apatite
Counted by: PFG

Slide ref	Current grain no	N _s	N _i	N _a	ρ _s	ρ _i	RATIO	U (ppm)	Cl (wt%)	F.T. AGE (Ma)
G235-12	1	95	181	40	3.774E+06	7.191E+06	0.525	59.2	0.13	139.2 ± 17.9
G235-12	2	18	22	16	1.788E+06	2.185E+06	0.818	18.0	0.07	215.8 ± 68.8
G235-12	3	22	35	16	2.185E+06	3.476E+06	0.629	28.6	0.07	166.4 ± 45.4
G235-12	4	28	36	20	2.225E+06	2.860E+06	0.778	23.6	0.07	205.3 ± 52.0
G235-12	5	47	45	16	4.668E+06	4.469E+06	1.044	36.8	0.06	274.2 ± 57.5
G235-12	6	77	97	24	5.098E+06	6.422E+06	0.794	52.9	0.09	209.5 ± 32.3
G235-12	8	55	95	32	2.731E+06	4.718E+06	0.579	38.9	0.09	153.4 ± 26.2
G235-12	11	24	15	15	2.543E+06	1.589E+06	1.600	13.1	0.10	415.4 ± 137.1
G235-12	12	38	40	20	3.019E+06	3.178E+06	0.950	26.2	0.06	249.9 ± 56.9
G235-12	13	47	44	10	7.469E+06	6.992E+06	1.068	57.6	0.13	280.3 ± 59.2
G235-12	14	37	40	12	4.900E+06	5.297E+06	0.925	43.6	0.15	243.4 ± 55.8
G235-12	17	73	90	16	7.250E+06	8.939E+06	0.811	73.6	0.13	213.9 ± 34.1
G235-12	18	74	94	48	2.450E+06	3.112E+06	0.787	25.6	0.13	207.7 ± 32.6
G235-12	19	54	85	40	2.145E+06	3.377E+06	0.635	27.8	0.05	168.2 ± 29.5
G235-12	20	41	28	18	3.620E+06	2.472E+06	1.464	20.4	0.14	381.2 ± 93.9
G235-12	21	35	33	12	4.635E+06	4.370E+06	1.061	36.0	0.10	278.3 ± 67.9
G235-12	22	49	83	25	3.115E+06	5.276E+06	0.590	43.5	0.13	156.4 ± 28.4
G235-12	24	44	68	30	2.331E+06	3.602E+06	0.647	29.7	0.10	171.2 ± 33.4
G235-12	25	31	79	16	3.079E+06	7.846E+06	0.392	64.6	0.06	104.4 ± 22.3
G235-12	26	90	113	30	4.767E+06	5.985E+06	0.796	49.3	0.08	210.1 ± 30.1
		979	1323		3.412E+06	4.610E+06		38.0		

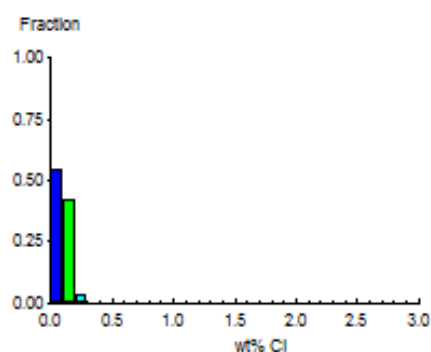
Area of basic unit = 6.293E-07 cm²
 $\chi^2 = 47.191$ with 19 degrees of freedom
 $P(\chi^2) = 0.0\%$
 Age Dispersion = 22.316%
 N_s / N_i = 0.740 ± 0.031
 Mean Ratio = 0.845 ± 0.067

Ages calculated using a zeta of 353.5 ± 3.9 for SRM612 glass
 $\rho = 1.517E+06\text{cm}^{-2}$ ND=2351
 ρ_D interpolated between top of can; $\rho = 1.416E+06\text{cm}^{-2}$ ND=1114
 bottom of can; $\rho = 1.573E+06\text{cm}^{-2}$ ND=1237
 POOLED AGE = 195.5 ± 9.4 Ma
CENTRAL AGE = 204.2 ± 14.5 Ma

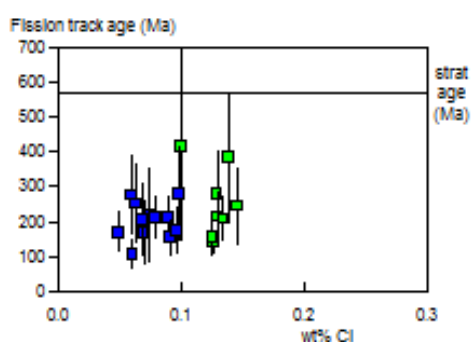
A:



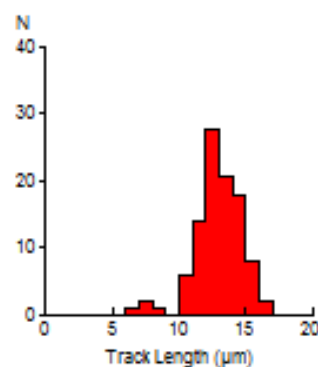
B:



C:



D:



Mean track length 12.87 ± 0.18 μm Std. Dev. 1.76 μm 101 tracks



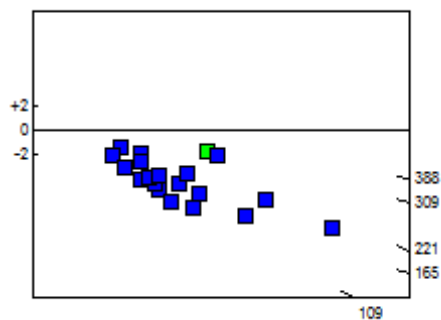
GC361-75 Apatite
Counted by: PFG

Slide ref	Current grain no	N _s	N _i	N _a	ρ _s	ρ _i	RATIO	U (ppm)	Cl (wt%)	F.T. AGE (Ma)
G235-13	1	110	143	50	3.496E+06	4.545E+06	0.769	37.2	0.08	204.3 ± 26.3
G235-13	2	17	16	100	2.701E+05	2.543E+05	1.063	2.1	0.04	280.5 ± 97.9
G235-13	3	31	48	70	7.037E+05	1.090E+06	0.646	8.9	0.02	171.9 ± 39.8
G235-13	4	16	18	80	3.178E+05	3.575E+05	0.889	2.9	0.02	235.5 ± 81.1
G235-13	5	25	36	60	6.621E+05	9.534E+05	0.694	7.8	0.02	184.7 ± 48.3
G235-13	6	15	31	80	2.980E+05	6.158E+05	0.484	5.0	0.02	129.3 ± 40.8
G235-13	7	15	28	100	2.384E+05	4.449E+05	0.536	3.6	0.01	142.9 ± 45.9
G235-13	8	11	22	70	2.497E+05	4.994E+05	0.500	4.1	0.02	133.5 ± 49.4
G235-13	9	70	83	90	1.236E+06	1.465E+06	0.843	12.0	0.04	223.6 ± 36.7
G235-13	10	16	39	100	2.543E+05	6.197E+05	0.410	5.1	0.01	109.8 ± 32.7
G235-13	11	14	24	60	3.708E+05	6.356E+05	0.583	5.2	0.05	155.5 ± 52.4
G235-13	12	19	27	60	5.032E+05	7.151E+05	0.704	5.9	0.01	187.1 ± 56.2
G235-13	13	12	10	60	3.178E+05	2.648E+05	1.200	2.2	0.02	315.9 ± 135.5
G235-13	14	32	36	100	5.085E+05	5.721E+05	0.889	4.7	0.04	235.5 ± 57.5
G235-13	15	8	10	50	2.543E+05	3.178E+05	0.800	2.6	0.01	212.3 ± 100.8
G235-13	16	52	35	20	4.132E+06	2.781E+06	1.486	22.8	0.11	388.9 ± 85.5
G235-13	17	57	40	100	9.058E+05	6.356E+05	1.425	5.2	0.01	373.5 ± 77.5
G235-13	18	48	80	100	7.628E+05	1.271E+06	0.600	10.4	0.04	159.9 ± 29.4
G235-13	19	9	15	50	2.860E+05	4.767E+05	0.600	3.9	0.04	159.9 ± 67.5
G235-13	20	23	50	80	4.569E+05	9.932E+05	0.460	8.1	0.03	122.9 ± 31.1
		600	791		6.442E+05	8.493E+05		7.0		

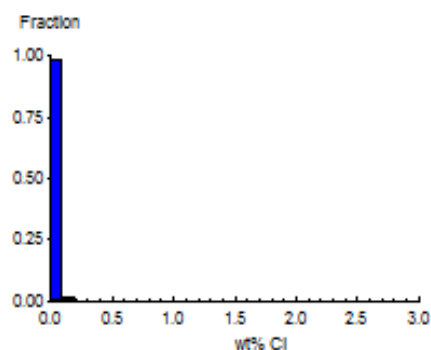
Area of basic unit = 6.293E-07 cm²
 $\chi^2 = 38.936$ with 19 degrees of freedom
 $P(\chi^2) = 0.5\%$
 Age Dispersion = 25.647%
 N_s / N_i = 0.759 ± 0.041
 Mean Ratio = 0.779 ± 0.069

Ages calculated using a zeta of 353.5 ± 3.9 for SRM612 glass
 $\rho = 1.527E+06 \text{ cm}^{-2}$ ND=2351
 ρ_D interpolated between top of can; $\rho = 1.416E+06 \text{ cm}^{-2}$ ND=1114
 bottom of can; $\rho = 1.573E+06 \text{ cm}^{-2}$ ND=1237
 POOLED AGE = 201.5 ± 11.9 Ma
CENTRAL AGE = 197.3 ± 17.1 Ma

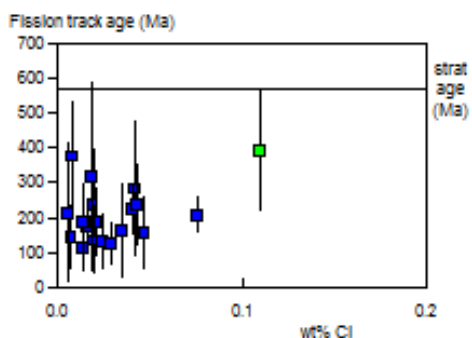
A:



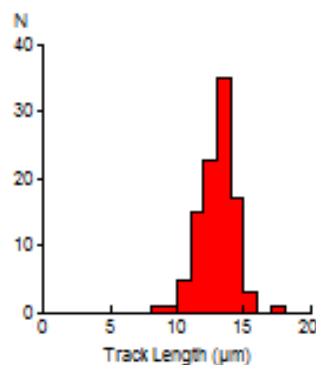
B:



C:



D:



Mean track length 13.02 ± 0.13 μm Std. Dev. 1.33 μm 106 tracks



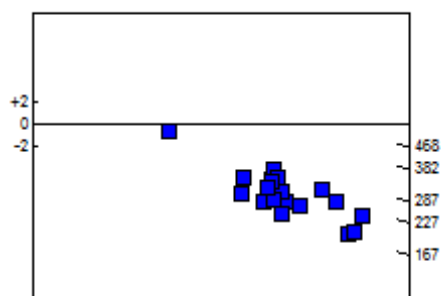
GC361-76 Apatite
Counted by: PFG

Slide ref	Current grain no	N _s	N _i	N _a	ρ _s	ρ _i	RATIO	U (ppm)	Cl (wt%)	F.T. AGE (Ma)
G235-14	1	139	168	70	3.155E+06	3.814E+06	0.827	31.0	0.02	220.8 ± 25.8
G235-14	2	34	19	36	1.501E+06	8.387E+05	1.789	6.8	0.02	468.3 ± 134.6
G235-14	3	83	83	50	2.638E+06	2.638E+06	1.000	21.5	0.01	265.9 ± 41.7
G235-14	4	79	83	50	2.511E+06	2.638E+06	0.952	21.5	0.01	253.3 ± 40.3
G235-14	5	122	139	60	3.231E+06	3.681E+06	0.878	30.0	0.05	233.9 ± 29.5
G235-14	6	49	74	30	2.595E+06	3.920E+06	0.662	31.9	0.01	177.3 ± 32.9
G235-14	7	61	91	28	3.462E+06	5.164E+06	0.670	42.0	0.00	179.4 ± 30.0
G235-14	8	111	171	80	2.205E+06	3.397E+06	0.649	27.6	0.03	173.8 ± 21.6
G235-14	9	118	174	70	2.679E+06	3.950E+06	0.678	32.2	0.03	181.5 ± 22.1
G235-14	10	77	105	50	2.447E+06	3.337E+06	0.733	27.2	0.10	196.0 ± 29.8
G235-14	11	86	78	36	3.796E+06	3.443E+06	1.103	28.0	0.03	292.5 ± 46.3
G235-14	12	60	67	36	2.648E+06	2.957E+06	0.896	24.1	0.01	238.6 ± 42.8
G235-14	13	80	96	50	2.543E+06	3.051E+06	0.833	24.8	0.03	222.3 ± 34.1
G235-14	14	68	109	40	2.701E+06	4.330E+06	0.624	35.2	0.02	167.2 ± 26.1
G235-14	15	70	96	50	2.225E+06	3.051E+06	0.729	24.8	0.01	194.9 ± 31.0
G235-14	16	85	116	50	2.701E+06	3.687E+06	0.733	30.0	0.01	195.9 ± 28.3
G235-14	17	85	84	60	2.251E+06	2.225E+06	1.012	18.1	0.04	269.0 ± 41.9
G235-14	18	118	120	50	3.750E+06	3.814E+06	0.983	31.0	0.02	261.5 ± 34.5
G235-14	19	77	84	50	2.447E+06	2.670E+06	0.917	21.7	0.01	244.1 ± 38.9
G235-14	20	72	85	60	1.907E+06	2.251E+06	0.847	18.3	0.00	225.9 ± 36.6
		1674	2042		2.644E+06	3.226E+06		26.3		

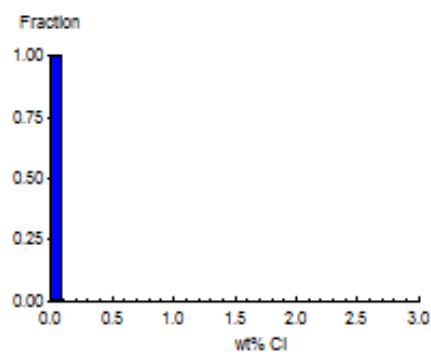
Area of basic unit = 6.293E-07 cm²
 $\chi^2 = 32.870$ with 19 degrees of freedom
 $P(\chi^2) = 2.5\%$
 Age Dispersion = 10.340%
 N_s / N_i = 0.820 ± 0.027
 Mean Ratio = 0.876 ± 0.057

Ages calculated using a zeta of 353.5 ± 3.9 for SRM612 glass
 $\rho = 1.536E+06\text{cm}^{-2}$ ND=2351
 ρ_D interpolated between top of can; $\rho = 1.416E+06\text{cm}^{-2}$ ND=1114
 bottom of can; $\rho = 1.573E+06\text{cm}^{-2}$ ND=1237
 POOLED AGE = 218.8 ± 8.8 Ma
CENTRAL AGE = 220.3 ± 10.3 Ma

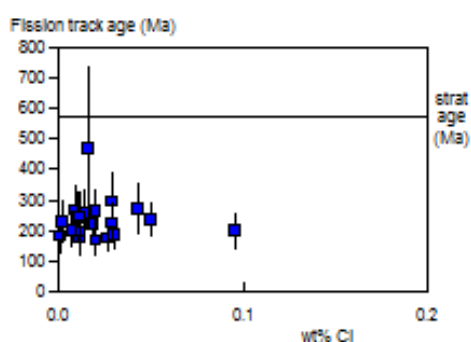
A:



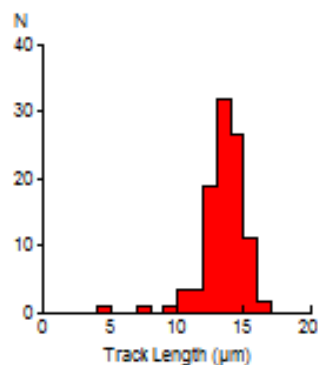
B:



C:



D:



Mean track length 13.53 ± 0.15 μm Std. Dev. 1.63 μm 116 tracks



GC970-31 Apatite
Counted by: PFG

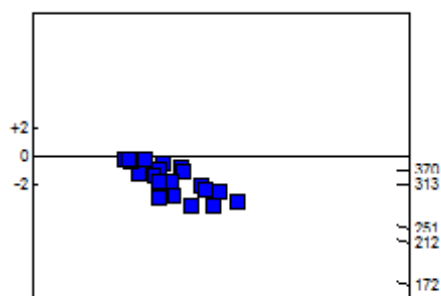
norjac07-07

Slide ref	Current grain no	N _s	N _i	N _a	ρ _s	ρ _i	RATIO	U (ppm)	Cl (wt%)	F.T. AGE (Ma)
G1075-7	3	28	43	40	1.112E+06	1.708E+06	0.651	13.8	0.01	175.0 ± 42.7
G1075-7	5	14	10	21	1.059E+06	7.567E+05	1.400	6.1	0.02	370.5 ± 153.7
G1075-7	11	35	28	64	8.690E+05	6.952E+05	1.250	5.6	0.00	331.8 ± 84.5
G1075-7	14	16	16	40	6.356E+05	6.356E+05	1.000	5.1	0.03	266.8 ± 94.5
G1075-7	21	21	15	36	9.270E+05	6.621E+05	1.400	5.3	0.00	370.5 ± 125.6
G1075-7	25	27	21	60	7.151E+05	5.562E+05	1.286	4.5	0.01	341.0 ± 99.6
G1075-7	26	39	41	100	6.197E+05	6.515E+05	0.951	5.3	0.00	254.0 ± 57.1
G1075-7	28	16	12	50	5.085E+05	3.814E+05	1.333	3.1	0.00	353.3 ± 135.2
G1075-7	31	35	30	36	1.545E+06	1.324E+06	1.167	10.7	0.01	310.2 ± 77.5
G1075-7	33	24	21	58	6.575E+05	5.754E+05	1.143	4.6	0.01	304.0 ± 91.1
G1075-7	34	21	21	50	6.674E+05	6.674E+05	1.000	5.4	0.01	266.8 ± 82.6
G1075-7	37	47	52	56	1.334E+06	1.476E+06	0.904	11.9	0.00	241.6 ± 49.0
G1075-7	38	26	28	70	5.902E+05	6.356E+05	0.929	5.1	0.00	248.1 ± 67.8
G1075-7	41	39	53	90	6.886E+05	9.358E+05	0.736	7.5	0.00	197.4 ± 41.9
G1075-7	45	15	11	50	4.767E+05	3.496E+05	1.364	2.8	0.00	361.1 ± 143.6
G1075-7	50	21	24	40	8.343E+05	9.534E+05	0.875	7.7	0.00	234.0 ± 70.2
G1075-7	53	54	64	90	9.534E+05	1.130E+06	0.844	9.1	0.01	225.8 ± 42.1
G1075-7	58	24	33	100	3.814E+05	5.244E+05	0.727	4.2	0.00	195.1 ± 52.6
G1075-7	60	40	44	60	1.059E+06	1.165E+06	0.909	9.4	0.00	243.0 ± 53.4
G1075-7	64	18	28	100	2.860E+05	4.449E+05	0.643	3.6	0.00	172.8 ± 52.4
		560	595		7.348E+05	7.808E+05		6.3		

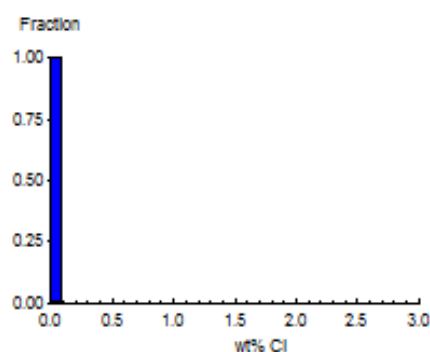
Area of basic unit = 6.293E-07 cm²
 $\chi^2 = 14.427$ with 19 degrees of freedom
 $P(\chi^2) = 75.8\%$
 Age Dispersion = 0.371% (did not converge)
 N_s / N_i = 0.941 ± 0.055
 Mean Ratio = 1.026 ± 0.056

Ages calculated using a zeta of 385.5 ± 4.3 for CN5 glass
 $\rho = 1.413E+06\text{cm}^{-2}$ ND=2221
 ρ_D interpolated between top of can; $\rho = 1.396E+06\text{cm}^{-2}$ ND=1098
 bottom of can; $\rho = 1.428E+06\text{cm}^{-2}$ ND=1123
POOLED AGE = 251.4 ± 16.0 Ma
CENTRAL AGE = 251.4 ± 16.0 Ma

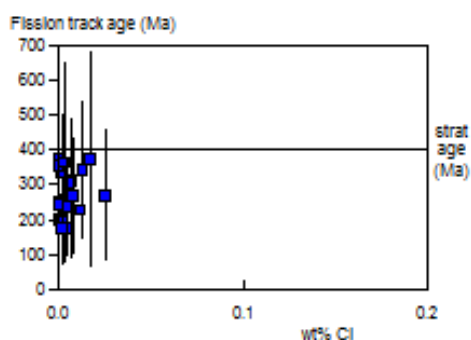
A:



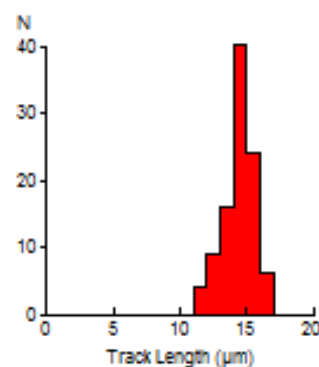
B:



C:



D:



Mean track length 14.41 ± 0.11 μm Std. Dev. 1.14 μm 99 tracks



GC970-32 Apatite
Counted by: PFG

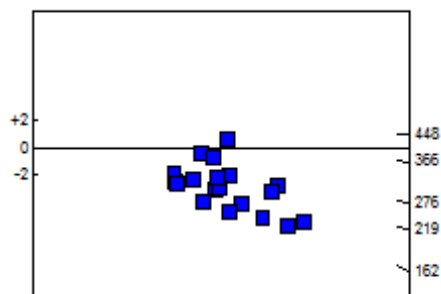
norjac07-08

Slide ref	Current grain no	N _s	N _i	N _a	ρ _s	ρ _i	RATIO	U (ppm)	Cl (wt%)	F.T. AGE (Ma)
G1075-8	6	25	33	100	3.973E+05	5.244E+05	0.758	4.2	0.00	203.5 ± 54.2
G1075-8	7	42	53	50	1.335E+06	1.684E+06	0.792	13.6	0.01	212.7 ± 44.2
G1075-8	8	31	51	48	1.026E+06	1.688E+06	0.608	13.6	0.01	163.8 ± 37.5
G1075-8	11	27	30	35	1.226E+06	1.362E+06	0.900	11.0	0.00	241.1 ± 64.2
G1075-8	13	34	39	60	9.005E+05	1.033E+06	0.872	8.3	0.00	233.7 ± 55.1
G1075-8	15	25	34	50	7.945E+05	1.081E+06	0.735	8.7	0.00	197.6 ± 52.3
G1075-8	18	46	34	21	3.481E+06	2.573E+06	1.353	20.7	0.01	359.1 ± 81.7
G1075-8	19	68	40	50	2.161E+06	1.271E+06	1.700	10.2	0.00	448.1 ± 89.9
G1075-8	20	47	49	40	1.867E+06	1.947E+06	0.959	15.7	0.02	256.6 ± 52.8
G1075-8	21	86	122	60	2.278E+06	3.231E+06	0.705	26.0	0.01	189.6 ± 27.1
G1075-8	22	55	54	50	1.748E+06	1.716E+06	1.019	13.8	0.00	272.2 ± 52.5
G1075-8	24	45	54	28	2.554E+06	3.065E+06	0.833	24.7	0.01	223.5 ± 45.4
G1075-8	28	84	86	60	2.225E+06	2.278E+06	0.977	18.3	0.00	261.2 ± 40.6
G1075-8	29	59	91	70	1.339E+06	2.066E+06	0.648	16.6	0.01	174.6 ± 29.5
G1075-8	32	76	85	80	1.510E+06	1.688E+06	0.894	13.6	0.00	239.5 ± 38.2
G1075-8	37	72	113	100	1.144E+06	1.796E+06	0.637	14.5	0.00	171.6 ± 26.2
G1075-8	38	52	40	60	1.377E+06	1.059E+06	1.300	8.5	0.01	345.4 ± 73.1
G1075-8	43	51	72	70	1.158E+06	1.634E+06	0.708	13.2	0.01	190.5 ± 35.2
G1075-8	55	41	68	50	1.303E+06	2.161E+06	0.603	17.4	0.00	162.5 ± 32.4
G1075-8	60	47	49	50	1.494E+06	1.557E+06	0.959	12.5	0.00	256.6 ± 52.8
		1013	1197		1.422E+06	1.680E+06		13.5		

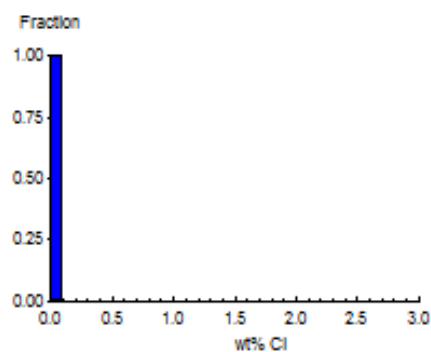
Area of basic unit = 6.293E-07 cm²
 $\chi^2 = 38.555$ with 19 degrees of freedom
 $P(\chi^2) = 0.5\%$
 Age Dispersion = 18.765%
 $N_s / N_i = 0.846 \pm 0.036$
 Mean Ratio = 0.898 ± 0.062

Ages calculated using a zeta of 385.5 ± 4.3 for CN5 glass
 $\rho = 1.416E+06 \text{ cm}^{-2}$ ND=2221
 ρ_D interpolated between top of can; $\rho = 1.396E+06 \text{ cm}^{-2}$ ND=1098
 bottom of can; $\rho = 1.428E+06 \text{ cm}^{-2}$ ND=1123
 POOLED AGE = 226.9 ± 11.1 Ma
CENTRAL AGE = 230.0 ± 15.0 Ma

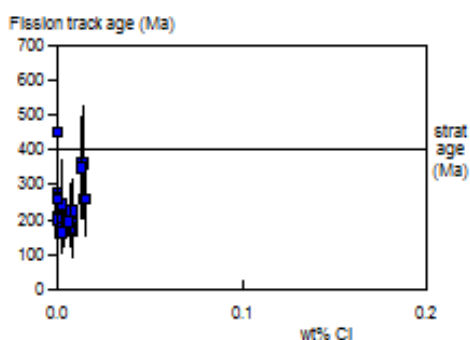
A:



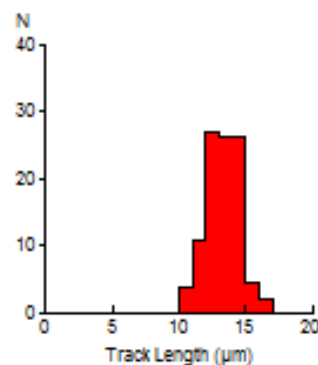
B:



C:



D:



Mean track length 13.33 ± 0.11 μm Std. Dev. 1.21 μm 111 tracks



GC970-33 Apatite
Counted by: PFG

norjac07-09

Slide ref	Current grain no	N _s	N _i	N _a	ρ _s	ρ _i	RATIO	U (ppm)	Cl (wt%)	F.T. AGE (Ma)
G1075-9	13	14	24	60	3.708E+05	6.356E+05	0.583	5.1	0.00	157.6 ± 53.1
G1075-9	14	29	41	40	1.152E+06	1.629E+06	0.707	13.1	0.00	190.6 ± 46.5
G1075-9	20	48	55	40	1.907E+06	2.185E+06	0.873	17.6	0.00	234.4 ± 46.6
G1075-9	24	14	30	40	5.562E+05	1.192E+06	0.467	9.6	0.00	126.4 ± 41.0
G1075-9	28	26	31	30	1.377E+06	1.642E+06	0.839	13.2	0.00	225.4 ± 60.2
G1075-9	29	7	17	60	1.854E+05	4.502E+05	0.412	3.6	0.00	111.6 ± 50.2
G1075-9	37	56	70	30	2.966E+06	3.708E+06	0.800	29.8	0.01	215.2 ± 38.9
G1075-9	39	8	13	60	2.119E+05	3.443E+05	0.615	2.8	0.01	166.1 ± 74.8
G1075-9	41	12	27	60	3.178E+05	7.151E+05	0.444	5.7	0.01	120.4 ± 41.9
G1075-9	42	12	24	30	6.356E+05	1.271E+06	0.500	10.2	0.00	135.3 ± 48.0
G1075-9	50	26	38	25	1.653E+06	2.415E+06	0.684	19.4	0.01	184.5 ± 47.2
G1075-9	51	15	21	42	5.675E+05	7.945E+05	0.714	6.4	0.00	192.5 ± 65.2
G1075-9	55	59	67	70	1.339E+06	1.521E+06	0.881	12.2	0.00	236.5 ± 42.6
G1075-9	59	23	32	60	6.091E+05	8.475E+05	0.719	6.8	0.00	193.6 ± 53.1
		349	490		8.572E+05	1.203E+06		9.7		

Area of basic unit = 6.293E-07 cm²

χ² = 9.918 with 13 degrees of freedom

P(χ²) = 70.1%

Age Dispersion = 0.529% (did not converge)

N_s / N_i = 0.712 ± 0.050

Mean Ratio = 0.660 ± 0.043

Ages calculated using a zeta of 385.5 ± 4.3 for CN5 glass

ρ = 1.419E+06cm⁻² ND=2221

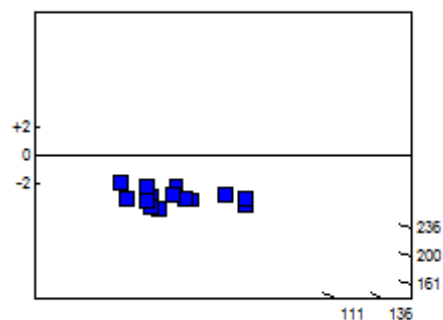
ρ_D interpolated between top of can; ρ = 1.396E+06cm⁻² ND=1098

bottom of can; ρ = 1.428E+06cm⁻² ND=1123

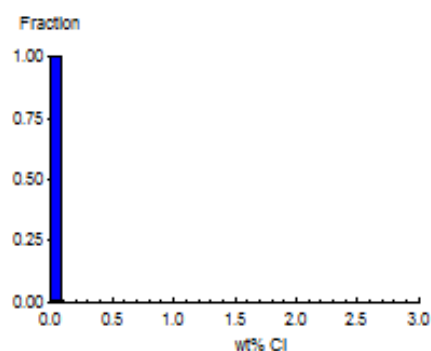
POOLED AGE = 191.9 ± 14.2 Ma

CENTRAL AGE = 191.9 ± 14.2 Ma

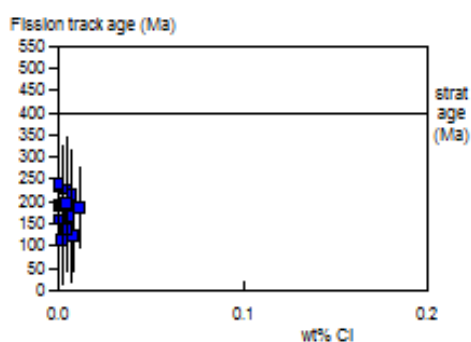
A:



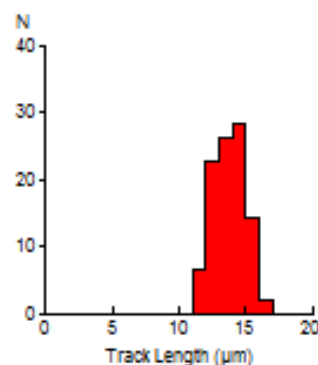
B:



C:



D:



Mean track length 13.77 ± 0.12 μm Std. Dev. 1.21 μm 106 tracks



GC970-34 Apatite
Counted by: PFG

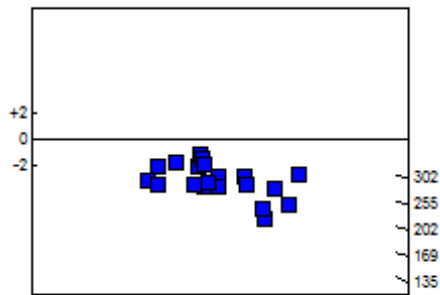
norjac07-10

Slide ref	Current grain no	N _s	N _i	N _a	ρ _s	ρ _i	RATIO	U (ppm)	Cl (wt%)	F.T. AGE (Ma)
G1075-10	3	33	51	40	1.311E+06	2.026E+06	0.647	16.2	0.00	174.9 ± 39.3
G1075-10	4	61	68	50	1.939E+06	2.161E+06	0.897	17.3	0.00	241.3 ± 42.9
G1075-10	10	101	101	50	3.210E+06	3.210E+06	1.000	25.7	0.00	268.4 ± 38.3
G1075-10	12	38	41	80	7.548E+05	8.144E+05	0.927	6.5	0.01	249.1 ± 56.4
G1075-10	13	58	72	28	3.292E+06	4.086E+06	0.806	32.8	0.01	217.1 ± 38.7
G1075-10	14	43	38	25	2.733E+06	2.415E+06	1.132	19.4	0.00	302.9 ± 67.8
G1075-10	17	13	26	40	5.164E+05	1.033E+06	0.500	8.3	0.00	135.6 ± 46.2
G1075-10	18	15	30	80	2.980E+05	5.959E+05	0.500	4.8	0.00	135.6 ± 43.0
G1075-10	20	42	40	50	1.335E+06	1.271E+06	1.050	10.2	0.00	281.5 ± 62.6
G1075-10	22	20	26	36	8.828E+05	1.148E+06	0.769	9.2	0.01	207.4 ± 61.9
G1075-10	26	44	54	50	1.398E+06	1.716E+06	0.815	13.8	0.01	219.5 ± 44.9
G1075-10	30	75	92	50	2.384E+06	2.924E+06	0.815	23.4	0.02	219.6 ± 34.6
G1075-10	39	30	46	40	1.192E+06	1.827E+06	0.652	14.7	0.00	176.3 ± 41.6
G1075-10	40	77	110	49	2.497E+06	3.567E+06	0.700	28.6	0.01	189.0 ± 28.5
G1075-10	41	55	100	36	2.428E+06	4.414E+06	0.550	35.4	0.01	149.0 ± 25.3
G1075-10	42	57	94	35	2.588E+06	4.268E+06	0.606	34.2	0.00	164.1 ± 27.8
G1075-10	44	41	43	30	2.172E+06	2.278E+06	0.953	18.3	0.00	256.2 ± 56.2
G1075-10	47	40	58	36	1.766E+06	2.560E+06	0.690	20.5	0.00	186.3 ± 38.5
G1075-10	51	29	31	30	1.536E+06	1.642E+06	0.935	13.2	0.01	251.4 ± 65.2
G1075-10	52	37	51	100	5.880E+05	8.104E+05	0.725	6.5	0.01	195.8 ± 42.5
		909	1172		1.545E+06	1.992E+06		16.0		

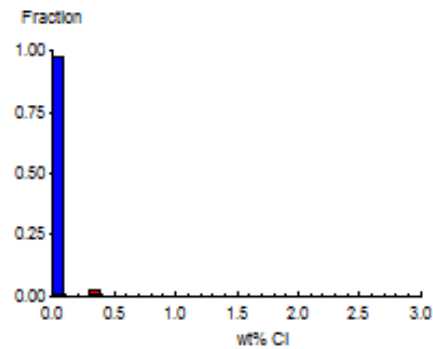
Area of basic unit = 6.293E-07 cm²
 $\chi^2 = 23.185$ with 19 degrees of freedom
 $P(\chi^2) = 22.9\%$
 Age Dispersion = 9.024% (did not converge)
 $N_s / N_i = 0.776 \pm 0.034$
 Mean Ratio = 0.784 ± 0.041

Ages calculated using a zeta of 385.5 ± 4.3 for CN5 glass
 $\rho = 1.422E+06 \text{ cm}^{-2}$ ND=2221
 ρ_D interpolated between top of can; $\rho = 1.396E+06 \text{ cm}^{-2}$ ND=1098
 bottom of can; $\rho = 1.428E+06 \text{ cm}^{-2}$ ND=1123
POOLED AGE = 209.1 ± 10.5 Ma
CENTRAL AGE = 209.0 ± 11.4 Ma

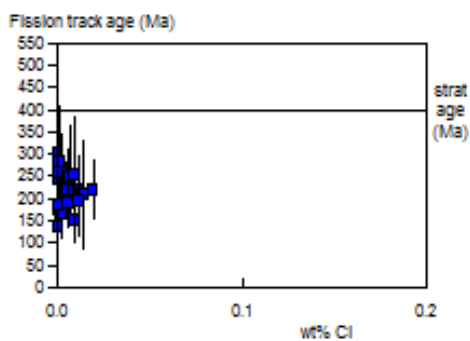
A:



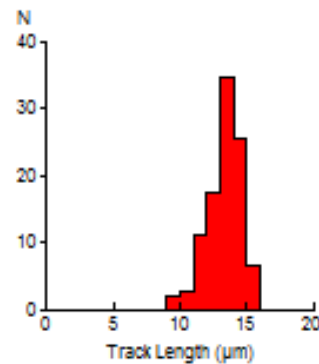
B:



C:



D:



Mean track length 13.30 ± 0.12 μm Std. Dev. 1.26 μm 109 tracks



GC970-35 Apatite
Counted by: PFG

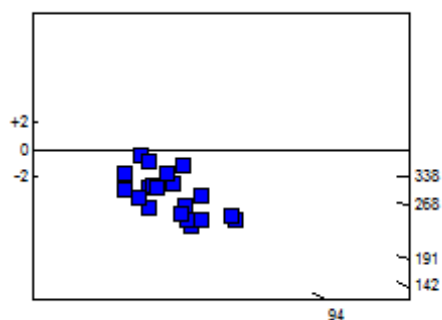
norjac07-11

Slide ref	Current grain no	N _s	N _i	N _a	ρ _s	ρ _i	RATIO	U (ppm)	Cl (wt%)	F.T. AGE (Ma)
G1075-11	5	14	24	36	6.180E+05	1.059E+06	0.583	8.5	0.00	158.2 ± 53.3
G1075-11	6	34	31	18	3.002E+06	2.737E+06	1.097	21.9	0.07	294.4 ± 73.4
G1075-11	13	16	25	50	5.085E+05	7.945E+05	0.640	6.4	0.01	173.4 ± 55.7
G1075-11	23	10	29	50	3.178E+05	9.217E+05	0.345	7.4	0.00	94.0 ± 34.5
G1075-11	24	19	15	25	1.208E+06	9.534E+05	1.267	7.6	0.01	338.8 ± 117.3
G1075-11	27	20	52	50	6.356E+05	1.653E+06	0.385	13.2	0.01	104.8 ± 27.7
G1075-11	28	25	55	40	9.932E+05	2.185E+06	0.455	17.5	0.00	123.6 ± 30.0
G1075-11	29	42	74	60	1.112E+06	1.960E+06	0.568	15.7	0.01	154.0 ± 30.0
G1075-11	30	20	48	36	8.828E+05	2.119E+06	0.417	17.0	0.00	113.4 ± 30.3
G1075-11	38	9	23	50	2.860E+05	7.310E+05	0.391	5.8	0.01	106.6 ± 42.0
G1075-11	45	7	17	60	1.854E+05	4.502E+05	0.412	3.6	0.00	112.1 ± 50.4
G1075-11	46	23	44	24	1.523E+06	2.913E+06	0.523	23.3	0.01	142.0 ± 36.7
G1075-11	48	17	27	25	1.081E+06	1.716E+06	0.630	13.7	0.02	170.6 ± 53.0
G1075-11	49	20	18	30	1.059E+06	9.534E+05	1.111	7.6	0.01	298.1 ± 97.1
G1075-11	52	19	43	45	6.709E+05	1.518E+06	0.442	12.1	0.01	120.2 ± 33.2
G1075-11	56	33	47	40	1.311E+06	1.867E+06	0.702	14.9	0.00	190.0 ± 43.4
G1075-11	61	24	32	60	6.356E+05	8.475E+05	0.750	6.8	0.00	202.7 ± 55.0
G1075-11	62	25	27	30	1.324E+06	1.430E+06	0.926	11.4	0.01	249.4 ± 69.5
G1075-11	64	10	14	36	4.414E+05	6.180E+05	0.714	4.9	0.00	193.2 ± 80.1
G1075-11	66	42	71	50	1.335E+06	2.256E+06	0.592	18.1	0.01	160.4 ± 31.5
		429	716		8.365E+05	1.396E+06		11.2		

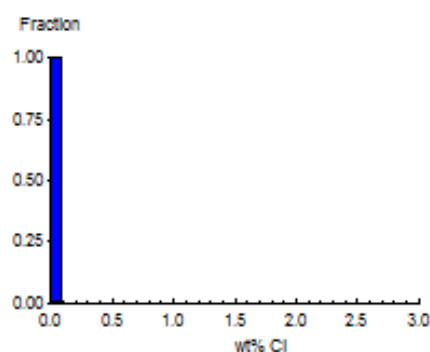
Area of basic unit = 6.293E-07 cm²
 $\chi^2 = 30.608$ with 19 degrees of freedom
 $P(\chi^2) = 4.5\%$
 Age Dispersion = 19.457%
 N_s / N_i = 0.599 ± 0.037
 Mean Ratio = 0.647 ± 0.059

Ages calculated using a zeta of 385.5 ± 4.3 for CN5 glass
 $\rho = 1.425E+06\text{cm}^{-2}$ ND=2221
 ρ_D interpolated between top of can; $\rho = 1.396E+06\text{cm}^{-2}$ ND=1098
 bottom of can; $\rho = 1.428E+06\text{cm}^{-2}$ ND=1123
 POOLED AGE = 162.5 ± 10.7 Ma
CENTRAL AGE = 163.8 ± 13.1 Ma

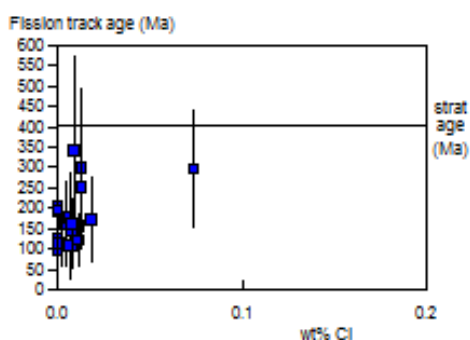
A:



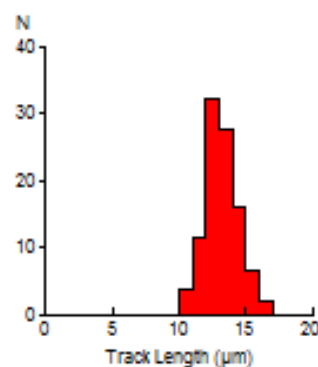
B:



C:



D:



Mean track length 13.17 ± 0.12 μm Std. Dev. 1.25 μm 105 tracks



GC970-71 Apatite
Counted by: COB

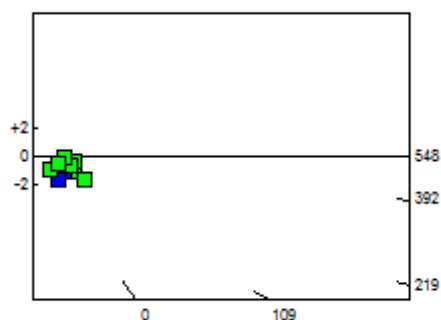
NOFT13-1

Slide ref	Current grain no	N _s	N _i	N _a	ρ _s	ρ _i	RATIO	U (ppm)	Cl (wt%)	F.T. AGE (Ma)
G1243-17	3	0	1	15	0.000E+00	1.059E+05	0.000	0.8	0.08	0.0 ± 1973.3
G1243-17	4	2	2	16	1.986E+05	1.986E+05	1.000	1.5	0.12	280.3 ± 280.4
G1243-17	5	1	1	4	3.973E+05	3.973E+05	1.000	3.0	0.13	280.3 ± 396.5
G1243-17	6	1	1	9	1.766E+05	1.766E+05	1.000	1.3	0.12	280.3 ± 396.5
G1243-17	7	1	2	25	6.356E+04	1.271E+05	0.500	1.0	0.09	141.7 ± 173.6
G1243-17	8	2	3	21	1.513E+05	2.270E+05	0.667	1.7	0.14	188.2 ± 171.9
G1243-17	9	1	1	18	8.828E+04	8.828E+04	1.000	0.7	0.13	280.3 ± 396.5
G1243-17	10	1	1	18	8.828E+04	8.828E+04	1.000	0.7	0.05	280.3 ± 396.5
G1243-17	11	0	1	15	0.000E+00	1.059E+05	0.000	0.8	0.09	0.0 ± 1973.3
G1243-17	12	3	2	8	5.959E+05	3.973E+05	1.500	3.0	0.12	416.1 ± 380.0
G1243-17	13	1	2	10	1.589E+05	3.178E+05	0.500	2.4	0.09	141.7 ± 173.6
G1243-17	14	3	5	42	1.135E+05	1.892E+05	0.600	1.4	0.11	169.7 ± 124.0
G1243-17	15	2	2	9	3.531E+05	3.531E+05	1.000	2.7	0.09	280.3 ± 280.4
G1243-17	16	0	2	15	0.000E+00	2.119E+05	0.000	1.6	0.06	0.0 ± 462.6
G1243-17	17	0	1	9	0.000E+00	1.766E+05	0.000	1.3	0.13	0.0 ± 1973.3
G1243-17	18	2	2	9	3.531E+05	3.531E+05	1.000	2.7	0.12	280.3 ± 280.4
G1243-17	19	0	1	18	0.000E+00	8.828E+04	0.000	0.7	0.12	0.0 ± 1973.3
G1243-17	20	1	1	14	1.135E+05	1.135E+05	1.000	0.9	0.09	280.3 ± 396.5
G1243-17	21	2	1	12	2.648E+05	1.324E+05	2.000	1.0	0.12	549.0 ± 672.5
G1243-17	22	1	1	9	1.766E+05	1.766E+05	1.000	1.3	0.15	280.3 ± 396.5
		24	33		1.288E+05	1.772E+05		1.3		

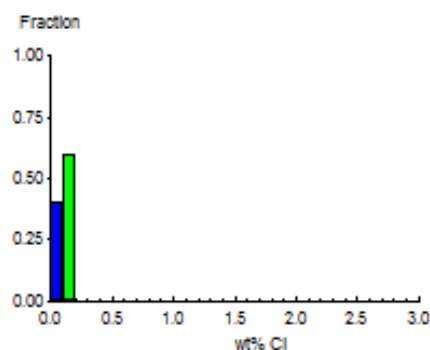
Area of basic unit = 6.293E-07 cm²
 $\chi^2 = 6.645$ with 19 degrees of freedom
 $P(\chi^2) = 99.6\%$
 Age Dispersion = 0.000% (did not converge)
 N_s / N_i = 0.727 ± 0.195
 Mean Ratio = 0.738 ± 0.122

Ages calculated using a zeta of 380.4 ± 5.7 for CN5 glass
 $\rho = 1.506E+06\text{cm}^{-2}$ ND=2265
 ρ_D interpolated between top of can; $\rho = 1.354E+06\text{cm}^{-2}$ ND=1065
 bottom of can; $\rho = 1.526E+06\text{cm}^{-2}$ ND=1200
POOLED AGE = 205.1 ± 55.3 Ma
CENTRAL AGE = 205.1 ± 55.3 Ma

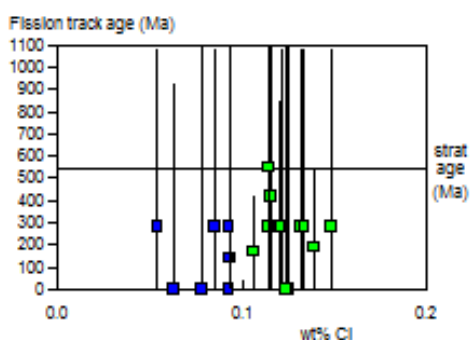
A:



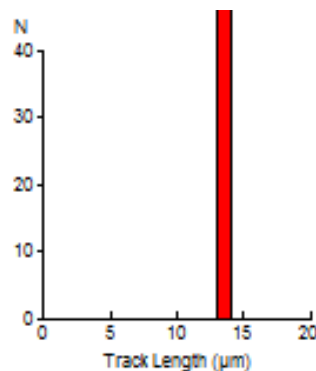
B:



C:



D:



Mean track length 13.79 ± 0.20 μm Std. Dev. 0.28 μm 2 tracks



GC970-72 Apatite
Counted by: COB

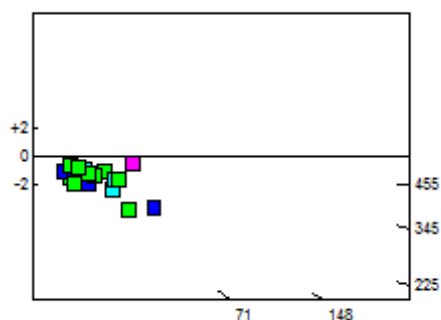
NOFT13-2

Slide ref	Current grain no	N _s	N _i	N _a	ρ _s	ρ _i	RATIO	U (ppm)	Cl (wt%)	F.T. AGE (Ma)
G1243-18	4	2	4	6	5.297E+05	1.059E+06	0.500	8.0	0.26	142.6 ± 123.5
G1243-18	7	3	5	8	5.959E+05	9.932E+05	0.600	7.5	0.15	170.7 ± 124.8
G1243-18	8	3	6	4	1.192E+06	2.384E+06	0.500	17.9	0.10	142.6 ± 100.9
G1243-18	10	1	3	8	1.986E+05	5.959E+05	0.333	4.5	0.16	95.4 ± 110.2
G1243-18	11	2	3	5	6.356E+05	9.534E+05	0.667	7.2	0.11	189.4 ± 173.0
G1243-18	12	8	7	10	1.271E+06	1.112E+06	1.143	8.4	0.12	321.4 ± 166.5
G1243-18	14	7	11	8	1.390E+06	2.185E+06	0.636	16.4	0.24	180.9 ± 87.6
G1243-18	15	1	2	12	1.324E+05	2.648E+05	0.500	2.0	0.09	142.6 ± 174.7
G1243-18	16	5	6	9	8.828E+05	1.059E+06	0.833	8.0	0.18	235.9 ± 143.0
G1243-18	17	2	3	20	1.589E+05	2.384E+05	0.667	1.8	0.08	189.4 ± 173.0
G1243-18	18	8	19	35	3.632E+05	8.626E+05	0.421	6.5	0.12	120.3 ± 50.8
G1243-18	19	4	4	28	2.270E+05	2.270E+05	1.000	1.7	0.20	282.1 ± 199.6
G1243-18	20	4	5	12	5.297E+05	6.621E+05	0.800	5.0	0.11	226.6 ± 152.1
G1243-18	21	9	10	8	1.788E+06	1.986E+06	0.900	14.9	0.21	254.4 ± 117.1
G1243-18	22	2	2	4	7.945E+05	7.945E+05	1.000	6.0	0.16	282.1 ± 282.2
G1243-18	23	1	4	8	1.986E+05	7.945E+05	0.250	6.0	0.14	71.7 ± 80.2
G1243-18	24	10	11	12	1.324E+06	1.457E+06	0.909	11.0	0.11	256.9 ± 112.5
G1243-18	25	3	3	10	4.767E+05	4.767E+05	1.000	3.6	0.18	282.1 ± 230.4
G1243-18	26	16	26	42	6.054E+05	9.837E+05	0.615	7.4	0.10	175.0 ± 55.8
G1243-18	27	18	11	18	1.589E+06	9.711E+05	1.636	7.3	0.45	455.4 ± 174.7
		109	145		6.487E+05	8.630E+05		6.5		

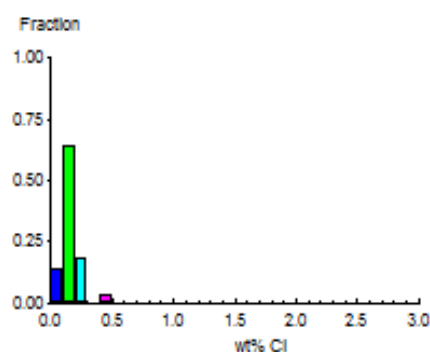
Area of basic unit = 6.293E-07 cm²
 $\chi^2 = 10.621$ with 19 degrees of freedom
 $P(\chi^2) = 93.6\%$
 Age Dispersion = 4.488% (did not converge)
 N_s / N_i = 0.752 ± 0.095
 Mean Ratio = 0.746 ± 0.072

Ages calculated using a zeta of 380.4 ± 5.7 for CN5 glass
 $\rho = 1.516E+06 \text{ cm}^{-2}$ ND=2265
 ρ_D interpolated between top of can; $\rho = 1.354E+06 \text{ cm}^{-2}$ ND=1065
 bottom of can; $\rho = 1.526E+06 \text{ cm}^{-2}$ ND=1200
POOLED AGE = 213.2 ± 27.6 Ma
CENTRAL AGE = 213.2 ± 27.7 Ma

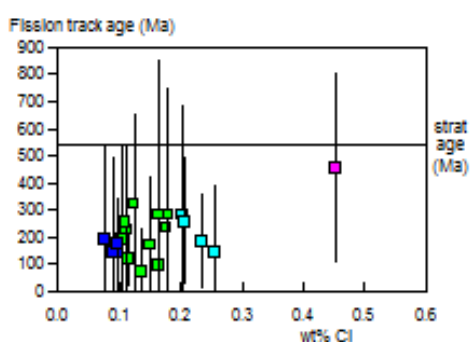
A:



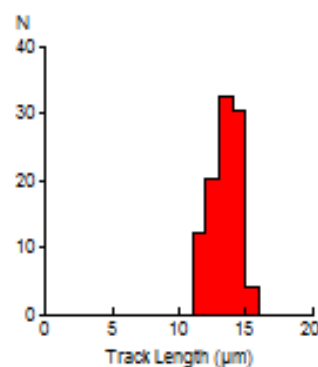
B:



C:



D:



Mean track length 13.47 ± 0.15 μm Std. Dev. 1.08 μm 49 tracks



GC970-73 Apatite
Counted by: COB

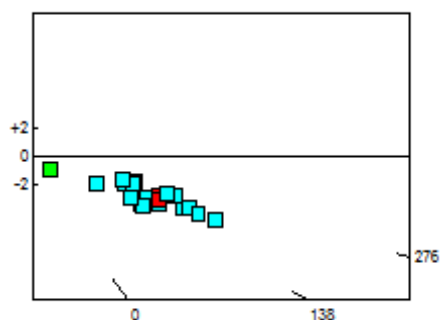
NOFT13-3

Slide ref	Current grain no	N _s	N _i	N _a	ρ _s	ρ _i	RATIO	U (ppm)	Cl (wt%)	F.T. AGE (Ma)
G1244-1	3	0	1	9	0.000E+00	1.766E+05	0.000	1.5	0.18	0.0 ± 1763.6
G1244-1	5	12	12	9	2.119E+06	2.119E+06	1.000	18.6	0.30	242.5 ± 99.2
G1244-1	6	21	24	9	3.708E+06	4.238E+06	0.875	37.2	0.22	212.7 ± 63.8
G1244-1	7	21	25	15	2.225E+06	2.648E+06	0.840	23.2	0.24	204.3 ± 60.7
G1244-1	9	14	20	15	1.483E+06	2.119E+06	0.700	18.6	0.26	170.7 ± 59.7
G1244-1	10	5	7	15	5.297E+05	7.416E+05	0.714	6.5	0.28	174.1 ± 102.1
G1244-1	12	31	34	20	2.463E+06	2.701E+06	0.912	23.7	0.23	221.5 ± 55.3
G1244-1	14	17	20	40	6.754E+05	7.945E+05	0.850	7.0	0.27	206.7 ± 68.4
G1244-1	15	45	50	25	2.860E+06	3.178E+06	0.900	27.9	0.21	218.7 ± 45.3
G1244-1	16	33	36	24	2.185E+06	2.384E+06	0.917	20.9	0.25	222.6 ± 54.0
G1244-1	18	23	23	16	2.284E+06	2.284E+06	1.000	20.0	0.31	242.5 ± 71.8
G1244-1	19	14	21	15	1.483E+06	2.225E+06	0.667	19.5	0.28	162.7 ± 56.3
G1244-1	20	22	24	12	2.913E+06	3.178E+06	0.917	27.9	0.30	222.6 ± 66.0
G1244-1	21	12	16	10	1.907E+06	2.543E+06	0.750	22.3	0.25	182.7 ± 69.9
G1244-1	22	16	14	24	1.059E+06	9.270E+05	1.143	8.1	0.22	276.4 ± 101.4
G1244-1	23	30	28	16	2.980E+06	2.781E+06	1.071	24.4	0.26	259.5 ± 68.5
G1244-1	26	27	25	15	2.860E+06	2.648E+06	1.080	23.2	0.25	261.5 ± 72.9
G1244-1	27	15	14	15	1.589E+06	1.483E+06	1.071	13.0	0.26	259.5 ± 96.7
G1244-1	30	37	41	30	1.960E+06	2.172E+06	0.902	19.1	0.29	219.2 ± 50.1
G1244-1	31	12	11	24	7.945E+05	7.283E+05	1.091	6.4	0.30	264.1 ± 110.5
		407	446		1.807E+06	1.980E+06		17.4		

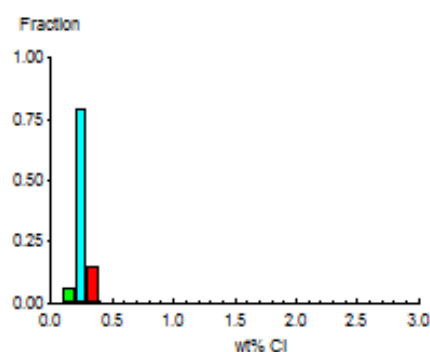
Area of basic unit = 6.293E-07 cm²
 $\chi^2 = 4.562$ with 19 degrees of freedom
 $P(\chi^2) = 100.0\%$
 Age Dispersion = 0.000% (did not converge)
 N_s / N_i = 0.913 ± 0.063
 Mean Ratio = 0.870 ± 0.055

Ages calculated using a zeta of 380.4 ± 5.7 for CN5 glass
 $\rho = 1.299E+06\text{cm}^{-2}$ ND=2048
 ρ_D interpolated between top of can; $\rho = 1.299E+06\text{cm}^{-2}$ ND=1022
 bottom of can; $\rho = 1.304E+06\text{cm}^{-2}$ ND=1026
POOLED AGE = 221.6 ± 16.3 Ma
CENTRAL AGE = 221.6 ± 16.3 Ma

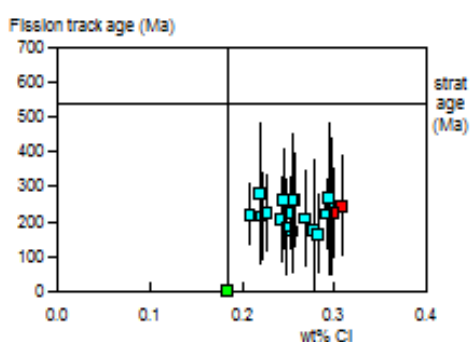
A:



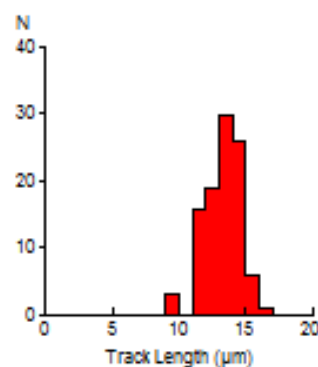
B:



C:



D:



Mean track length 13.26 ± 0.13 µm Std. Dev. 1.34 µm 101 tracks



GC970-74 Apatite
Counted by: COB

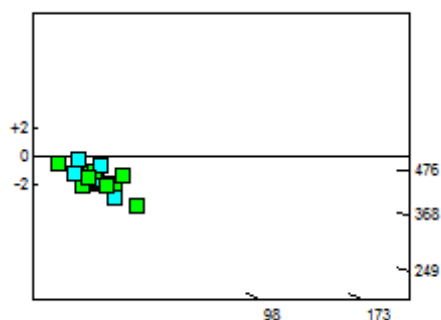
NOFT13-4

Slide ref	Current grain no	N _s	N _i	N _a	ρ _s	ρ _i	RATIO	U (ppm)	Cl (wt%)	F.T. AGE (Ma)
G1244-2	3	1	1	9	1.766E+05	1.766E+05	1.000	1.5	0.15	242.5 ± 343.1
G1244-2	4	6	8	12	7.945E+05	1.059E+06	0.750	9.3	0.21	182.8 ± 98.8
G1244-2	5	5	5	6	1.324E+06	1.324E+06	1.000	11.6	0.16	242.5 ± 153.5
G1244-2	6	5	7	8	9.932E+05	1.390E+06	0.714	12.2	0.15	174.2 ± 102.1
G1244-2	7	6	6	6	1.589E+06	1.589E+06	1.000	13.9	0.16	242.5 ± 140.2
G1244-2	8	4	2	4	1.589E+06	7.945E+05	2.000	7.0	0.28	476.3 ± 412.7
G1244-2	10	8	11	10	1.271E+06	1.748E+06	0.727	15.3	0.17	177.3 ± 82.5
G1244-2	11	4	6	6	1.059E+06	1.589E+06	0.667	13.9	0.10	162.7 ± 105.1
G1244-2	13	12	19	15	1.271E+06	2.013E+06	0.632	17.7	0.16	154.2 ± 57.0
G1244-2	14	9	10	15	9.534E+05	1.059E+06	0.900	9.3	0.14	218.7 ± 100.7
G1244-2	16	7	12	45	2.472E+05	4.238E+05	0.583	3.7	0.20	142.6 ± 67.9
G1244-2	17	2	3	12	2.648E+05	3.973E+05	0.667	3.5	0.15	162.7 ± 148.6
G1244-2	20	5	6	4	1.986E+06	2.384E+06	0.833	20.9	0.22	202.7 ± 122.9
G1244-2	21	2	5	9	3.531E+05	8.828E+05	0.400	7.7	0.19	98.1 ± 82.1
G1244-2	23	2	3	6	5.297E+05	7.945E+05	0.667	7.0	0.22	162.7 ± 148.6
G1244-2	26	13	10	9	2.295E+06	1.766E+06	1.300	15.5	0.18	313.6 ± 132.2
G1244-2	28	6	5	9	1.059E+06	8.828E+05	1.200	7.7	0.19	290.0 ± 175.8
G1244-2	29	7	9	12	9.270E+05	1.192E+06	0.778	10.5	0.20	189.4 ± 95.6
G1244-2	31	8	5	8	1.589E+06	9.932E+05	1.600	8.7	0.21	383.8 ± 219.0
G1244-2	34	4	5	6	1.059E+06	1.324E+06	0.800	11.6	0.19	194.8 ± 130.8
		116	138		8.736E+05	1.039E+06		9.1		

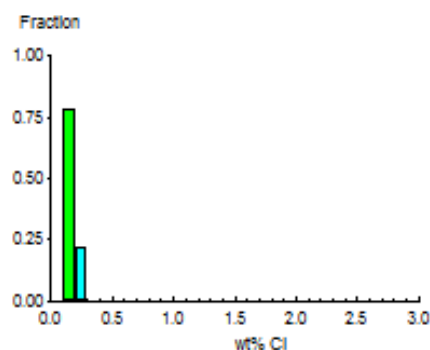
Area of basic unit = 6.293E-07 cm²
 $\chi^2 = 6.564$ with 19 degrees of freedom
 $P(\chi^2) = 99.6\%$
 Age Dispersion = 0.002% (did not converge)
 N_s / N_i = 0.841 ± 0.106
 Mean Ratio = 0.911 ± 0.084

Ages calculated using a zeta of 380.4 ± 5.7 for CN5 glass
 $\rho = 1.299E+06 \text{ cm}^{-2}$ ND=2048
 ρ_D interpolated between top of can; $\rho = 1.299E+06 \text{ cm}^{-2}$ ND=1022
 bottom of can; $\rho = 1.304E+06 \text{ cm}^{-2}$ ND=1026
POOLED AGE = 204.5 ± 26.3 Ma
CENTRAL AGE = 204.5 ± 26.3 Ma

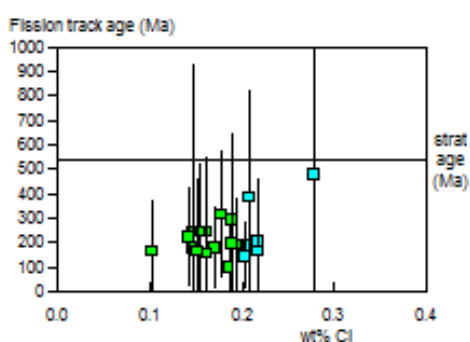
A:



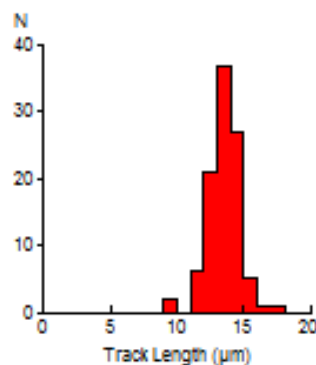
B:



C:



D:



Mean track length 13.51 ± 0.12 μm Std. Dev. 1.21 μm 100 tracks



GC970-75 Apatite
Counted by: COB

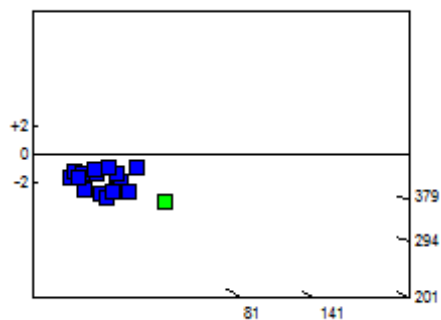
NOFT13-5

Slide ref	Current grain no	N _s	N _i	N _a	ρ _s	ρ _i	RATIO	U (ppm)	Cl (wt%)	F.T. AGE (Ma)
G1244-3	3	9	11	30	4.767E+05	5.827E+05	0.818	5.1	0.04	199.2 ± 89.7
G1244-3	4	1	3	21	7.567E+04	2.270E+05	0.333	2.0	0.07	81.9 ± 94.6
G1244-3	5	3	5	21	2.270E+05	3.783E+05	0.600	3.3	0.06	146.6 ± 107.2
G1244-3	6	9	12	10	1.430E+06	1.907E+06	0.750	16.7	0.13	182.8 ± 80.8
G1244-3	7	2	6	24	1.324E+05	3.973E+05	0.333	3.5	0.08	81.9 ± 66.9
G1244-3	8	4	9	30	2.119E+05	4.767E+05	0.444	4.2	0.07	108.9 ± 65.5
G1244-3	9	5	11	21	3.783E+05	8.324E+05	0.455	7.3	0.06	111.4 ± 60.2
G1244-3	10	11	11	32	5.462E+05	5.462E+05	1.000	4.8	0.09	242.6 ± 103.6
G1244-3	11	19	12	36	8.387E+05	5.297E+05	1.583	4.6	0.07	380.0 ± 140.5
G1244-3	12	7	11	40	2.781E+05	4.370E+05	0.636	3.8	0.06	155.4 ± 75.3
G1244-3	13	23	27	24	1.523E+06	1.788E+06	0.852	15.7	0.12	207.2 ± 59.1
G1244-3	15	6	6	32	2.980E+05	2.980E+05	1.000	2.6	0.07	242.6 ± 140.2
G1244-3	16	11	9	18	9.711E+05	7.945E+05	1.222	7.0	0.06	295.3 ± 133.0
G1244-3	17	2	3	24	1.324E+05	1.986E+05	0.667	1.7	0.09	162.7 ± 148.6
G1244-3	18	12	15	60	3.178E+05	3.973E+05	0.800	3.5	0.07	194.8 ± 75.6
G1244-3	19	3	4	20	2.384E+05	3.178E+05	0.750	2.8	0.07	182.8 ± 139.7
G1244-3	20	10	7	45	3.531E+05	2.472E+05	1.429	2.2	0.05	343.8 ± 169.7
G1244-3	21	6	5	24	3.973E+05	3.311E+05	1.200	2.9	0.07	290.0 ± 175.8
G1244-3	22	2	4	16	1.986E+05	3.973E+05	0.500	3.5	0.10	122.4 ± 106.1
G1244-3	23	2	4	12	2.648E+05	5.297E+05	0.500	4.6	0.07	122.4 ± 106.1
		147	175		4.326E+05	5.150E+05		4.5		

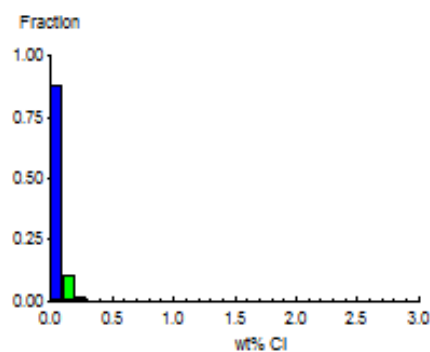
Area of basic unit = 6.293E-07 cm²
 $\chi^2 = 11.574$ with 19 degrees of freedom
 $P(\chi^2) = 90.3\%$
 Age Dispersion = 0.296% (did not converge)
 N_s / N_i = 0.840 ± 0.094
 Mean Ratio = 0.794 ± 0.079

Ages calculated using a zeta of 380.4 ± 5.7 for CN5 glass
 $\rho = 1.300E+06 \text{ cm}^{-2}$ ND=2048
 ρ_D interpolated between top of can; $\rho = 1.299E+06 \text{ cm}^{-2}$ ND=1022
 bottom of can; $\rho = 1.304E+06 \text{ cm}^{-2}$ ND=1026
POOLED AGE = 204.4 ± 23.5 Ma
CENTRAL AGE = 204.4 ± 23.5 Ma

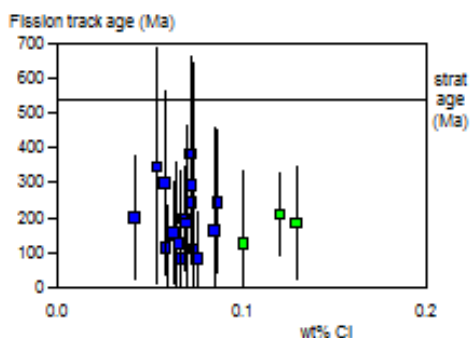
A:



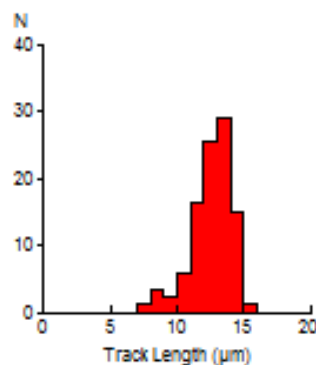
B:



C:



D:



Mean track length 12.56 ± 0.17 μm Std. Dev. 1.56 μm 86 tracks



GC970-76 Apatite
Counted by: COB

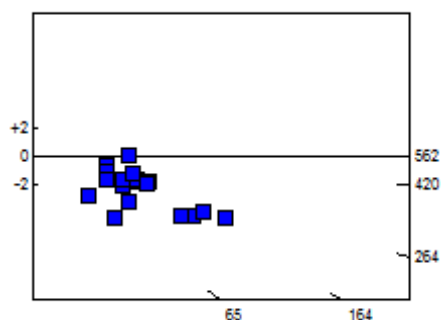
NOFT13-6

Slide ref	Current grain no	N _s	N _i	N _a	ρ _s	ρ _i	RATIO	U (ppm)	Cl (wt%)	F.T. AGE (Ma)
G1244-4	3	4	15	4	1.589E+06	5.959E+06	0.267	52.3	0.01	65.6 ± 37.0
G1244-4	4	15	13	12	1.986E+06	1.721E+06	1.154	15.1	0.01	279.2 ± 106.0
G1244-4	5	10	6	8	1.986E+06	1.192E+06	1.667	10.5	0.00	399.5 ± 206.6
G1244-4	6	34	40	35	1.544E+06	1.816E+06	0.850	15.9	0.00	206.8 ± 48.6
G1244-4	7	15	13	8	2.980E+06	2.582E+06	1.154	22.6	0.01	279.2 ± 106.0
G1244-4	8	10	16	15	1.059E+06	1.695E+06	0.625	14.9	0.00	152.7 ± 61.7
G1244-4	9	9	7	6	2.384E+06	1.854E+06	1.286	16.3	0.00	310.3 ± 156.6
G1244-4	10	40	43	50	1.271E+06	1.367E+06	0.930	12.0	0.01	226.0 ± 50.0
G1244-4	11	19	8	12	2.516E+06	1.059E+06	2.375	9.3	0.00	562.0 ± 237.3
G1244-4	12	11	12	10	1.748E+06	1.907E+06	0.917	16.7	0.00	222.8 ± 93.2
G1244-4	13	8	8	10	1.271E+06	1.271E+06	1.000	11.1	0.00	242.6 ± 121.5
G1244-4	14	51	54	16	5.065E+06	5.363E+06	0.944	47.0	0.00	229.4 ± 45.2
G1244-4	16	12	11	10	1.907E+06	1.748E+06	1.091	15.3	0.01	264.3 ± 110.5
G1244-4	17	27	35	12	3.575E+06	4.635E+06	0.771	40.6	0.00	188.0 ± 48.4
G1244-4	18	17	14	15	1.801E+06	1.483E+06	1.214	13.0	0.00	293.5 ± 106.2
G1244-4	19	2	7	10	3.178E+05	1.112E+06	0.286	9.8	0.01	70.3 ± 56.4
G1244-4	20	12	11	12	1.589E+06	1.457E+06	1.091	12.8	0.00	264.3 ± 110.5
G1244-4	21	17	12	12	2.251E+06	1.589E+06	1.417	13.9	0.00	341.1 ± 128.9
G1244-4	22	21	17	8	4.171E+06	3.377E+06	1.235	29.6	0.00	298.4 ± 97.7
G1244-4	23	20	17	10	3.178E+06	2.701E+06	1.176	23.7	0.00	284.5 ± 94.2
		354	359		2.046E+06	2.074E+06		18.2		

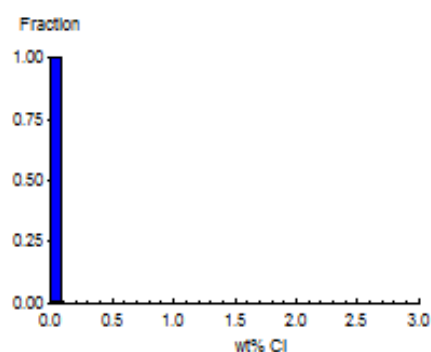
Area of basic unit = 6.293E-07 cm²
 $\chi^2 = 20.174$ with 19 degrees of freedom
 $P(\chi^2) = 38.4\%$
 Age Dispersion = 0.892% (did not converge)
 N_s / N_i = 0.986 ± 0.074
 Mean Ratio = 1.072 ± 0.102

Ages calculated using a zeta of 380.4 ± 5.7 for CN5 glass
 $\rho = 1.300E+06\text{cm}^{-2}$ ND=2048
 ρ_D interpolated between top of can; $\rho = 1.299E+06\text{cm}^{-2}$ ND=1022
 bottom of can; $\rho = 1.304E+06\text{cm}^{-2}$ ND=1026
POOLED AGE = 239.3 ± 19.0 Ma
CENTRAL AGE = 239.3 ± 19.0 Ma

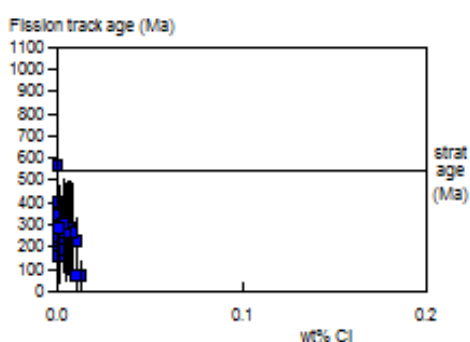
A:



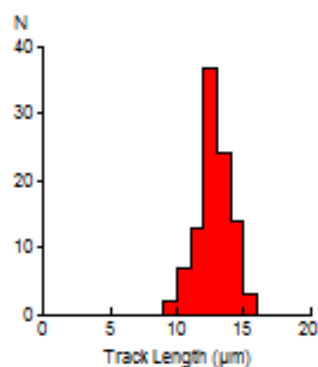
B:



C:



D:



Mean track length 12.79 ± 0.13 μm Std. Dev. 1.26 μm 100 tracks



GC970-77 Apatite
Counted by: COB

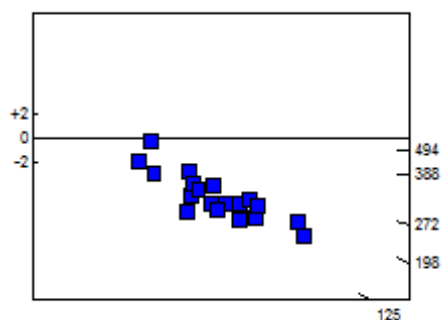
NOFT13-7

Slide ref	Current grain no	N _s	N _i	N _a	ρ _s	ρ _i	RATIO	U (ppm)	Cl (wt%)	F.T. AGE (Ma)
G1244-5	3	20	22	8	3.973E+06	4.370E+06	0.909	38.3	0.02	221.0 ± 68.5
G1244-5	4	46	59	9	8.122E+06	1.042E+07	0.780	91.3	0.01	190.0 ± 37.7
G1244-5	5	91	107	40	3.615E+06	4.251E+06	0.850	37.3	0.00	207.0 ± 30.0
G1244-5	6	27	13	9	4.767E+06	2.295E+06	2.077	20.1	0.03	494.2 ± 167.4
G1244-5	7	89	120	36	3.929E+06	5.297E+06	0.742	46.4	0.02	180.9 ± 25.8
G1244-5	8	37	32	12	4.900E+06	4.238E+06	1.156	37.2	0.02	279.8 ± 68.0
G1244-5	9	48	73	24	3.178E+06	4.833E+06	0.658	42.4	0.02	160.6 ± 30.2
G1244-5	10	55	66	24	3.642E+06	4.370E+06	0.833	38.3	0.01	202.9 ± 37.4
G1244-5	11	30	41	18	2.648E+06	3.620E+06	0.732	31.7	0.01	178.5 ± 43.1
G1244-5	12	38	53	18	3.355E+06	4.679E+06	0.717	41.0	0.00	174.9 ± 37.5
G1244-5	13	39	58	20	3.099E+06	4.608E+06	0.672	40.4	0.03	164.2 ± 34.3
G1244-5	14	35	38	15	3.708E+06	4.026E+06	0.921	35.3	0.01	223.9 ± 52.8
G1244-5	15	46	46	25	2.924E+06	2.924E+06	1.000	25.6	0.00	242.7 ± 51.0
G1244-5	16	88	120	50	2.797E+06	3.814E+06	0.733	33.4	0.01	178.9 ± 25.6
G1244-5	17	17	15	10	2.701E+06	2.384E+06	1.133	20.9	0.01	274.4 ± 97.5
G1244-5	18	36	42	21	2.724E+06	3.178E+06	0.857	27.9	0.01	208.6 ± 47.7
G1244-5	19	60	80	20	4.767E+06	6.356E+06	0.750	55.7	0.02	182.9 ± 31.6
G1244-5	20	65	69	28	3.689E+06	3.916E+06	0.942	34.3	0.02	228.9 ± 40.0
G1244-5	21	67	76	32	3.327E+06	3.774E+06	0.882	33.1	0.04	214.4 ± 36.4
G1244-5	22	23	45	12	3.046E+06	5.959E+06	0.511	52.2	0.02	125.2 ± 32.3
		957	1175		3.528E+06	4.332E+06		38.0		

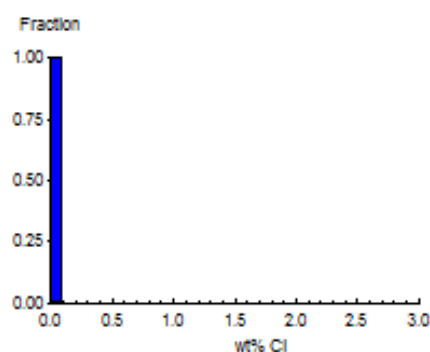
Area of basic unit = 6.293E-07 cm²
 $\chi^2 = 21.146$ with 19 degrees of freedom
 $P(\chi^2) = 32.9\%$
 Age Dispersion = 0.600% (did not converge)
 N_s / N_i = 0.814 ± 0.035
 Mean Ratio = 0.893 ± 0.071

Ages calculated using a zeta of 380.4 ± 5.7 for CN5 glass
 $\rho = 1.300E+06\text{cm}^{-2}$ ND=2048
 ρ_D interpolated between top of can; $\rho = 1.299E+06\text{cm}^{-2}$ ND=1022
 bottom of can; $\rho = 1.304E+06\text{cm}^{-2}$ ND=1026
POOLED AGE = 198.3 ± 10.1 Ma
CENTRAL AGE = 198.4 ± 10.1 Ma

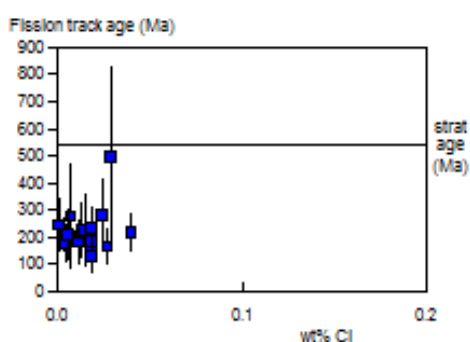
A:



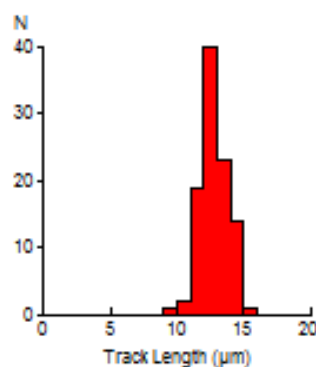
B:



C:



D:



Mean track length 12.76 ± 0.10 μm Std. Dev. 0.99 μm 100 tracks



GC970-78 Apatite
Counted by: COB

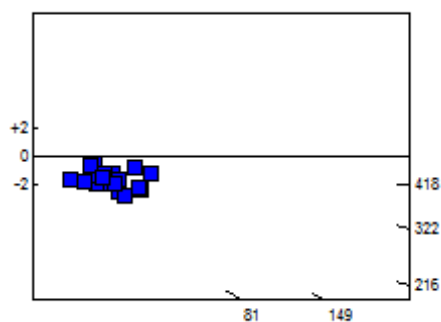
NOFT13-8

Slide ref	Current grain no	N _s	N _i	N _a	ρ _s	ρ _i	RATIO	U (ppm)	Cl (wt%)	F.T. AGE (Ma)
G1244-6	3	17	17	24	1.126E+06	1.126E+06	1.000	9.9	0.01	242.7 ± 83.5
G1244-6	5	10	8	32	4.966E+05	3.973E+05	1.250	3.5	0.01	302.0 ± 143.5
G1244-6	6	7	4	24	4.635E+05	2.648E+05	1.750	2.3	0.02	419.0 ± 262.8
G1244-6	7	5	7	6	1.324E+06	1.854E+06	0.714	16.3	0.01	174.3 ± 102.2
G1244-6	8	16	16	30	8.475E+05	8.475E+05	1.000	7.4	0.00	242.7 ± 86.1
G1244-6	10	9	12	8	1.788E+06	2.384E+06	0.750	20.9	0.01	182.9 ± 80.8
G1244-6	11	6	8	10	9.534E+05	1.271E+06	0.750	11.1	0.02	182.9 ± 98.9
G1244-6	12	5	7	15	5.297E+05	7.416E+05	0.714	6.5	0.01	174.3 ± 102.2
G1244-6	15	9	12	9	1.589E+06	2.119E+06	0.750	18.6	0.01	182.9 ± 80.8
G1244-6	16	6	6	18	5.297E+05	5.297E+05	1.000	4.6	0.00	242.7 ± 140.3
G1244-6	19	1	3	25	6.356E+04	1.907E+05	0.333	1.7	0.02	81.9 ± 94.6
G1244-6	20	3	5	8	5.959E+05	9.932E+05	0.600	8.7	0.01	146.7 ± 107.2
G1244-6	21	8	7	8	1.589E+06	1.390E+06	1.143	12.2	0.01	276.7 ± 143.4
G1244-6	22	11	10	24	7.283E+05	6.621E+05	1.100	5.8	0.01	266.5 ± 116.7
G1244-6	24	6	4	15	6.356E+05	4.238E+05	1.500	3.7	0.01	360.8 ± 233.1
G1244-6	25	19	11	10	3.019E+06	1.748E+06	1.727	15.3	0.01	413.7 ± 157.1
G1244-6	26	24	16	14	2.724E+06	1.816E+06	1.500	15.9	0.01	360.8 ± 116.8
G1244-6	28	10	14	18	8.828E+05	1.236E+06	0.714	10.8	0.03	174.3 ± 72.3
G1244-6	29	9	10	15	9.534E+05	1.059E+06	0.900	9.3	0.03	218.9 ± 100.7
G1244-6	31	7	7	14	7.945E+05	7.945E+05	1.000	7.0	0.00	242.7 ± 129.9
		188	184		9.136E+05	8.942E+05		7.8		

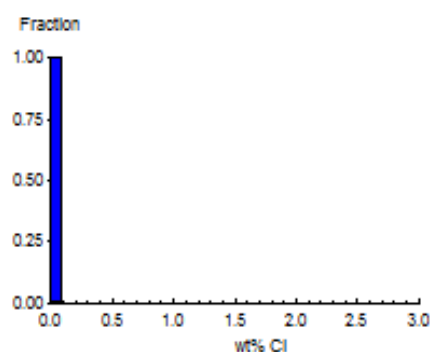
Area of basic unit = 6.293E-07 cm²
 $\chi^2 = 9.275$ with 19 degrees of freedom
 $P(\chi^2) = 96.9\%$
 Age Dispersion = 0.047% (did not converge)
 N_s / N_i = 1.022 ± 0.106
 Mean Ratio = 1.010 ± 0.085

Ages calculated using a zeta of 380.4 ± 5.7 for CN5 glass
 $\rho = 1.301E+06 \text{ cm}^{-2}$ ND=2048
 ρ_D interpolated between top of can; $\rho = 1.299E+06 \text{ cm}^{-2}$ ND=1022
 bottom of can; $\rho = 1.304E+06 \text{ cm}^{-2}$ ND=1026
POOLED AGE = 247.9 ± 26.5 Ma
CENTRAL AGE = 247.9 ± 26.5 Ma

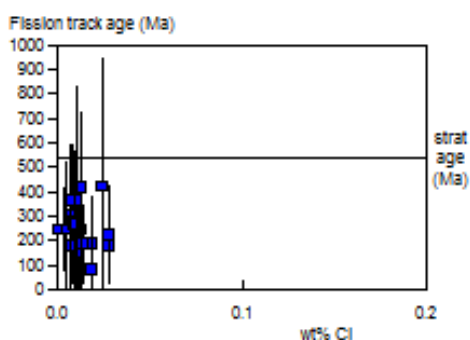
A:



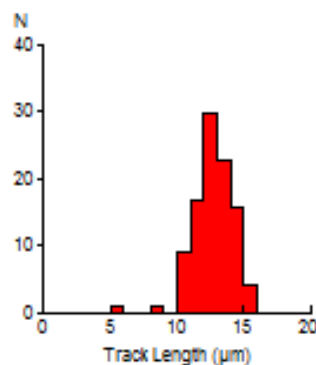
B:



C:



D:



Mean track length 12.68 ± 0.15 μm Std. Dev. 1.51 μm 101 tracks



GC970-79 Apatite
Counted by: COB

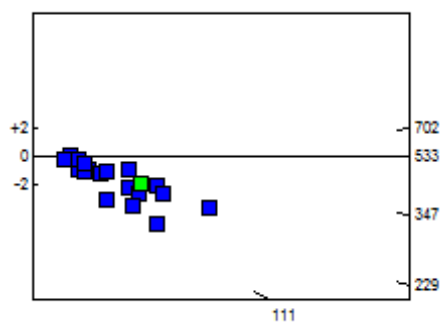
NOFT13-9

Slide ref	Current grain no	N _s	N _i	N _a	ρ _s	ρ _i	RATIO	U (ppm)	Cl (wt%)	F.T. AGE (Ma)
G1244-7	3	13	14	40	5.164E+05	5.562E+05	0.929	4.9	0.06	225.7 ± 87.2
G1244-7	4	5	4	15	5.297E+05	4.238E+05	1.250	3.7	0.05	302.1 ± 202.8
G1244-7	5	3	3	18	2.648E+05	2.648E+05	1.000	2.3	0.06	242.8 ± 198.3
G1244-7	6	7	6	64	1.738E+05	1.490E+05	1.167	1.3	0.05	282.4 ± 157.3
G1244-7	7	3	1	18	2.648E+05	8.828E+04	3.000	0.8	0.03	702.5 ± 811.4
G1244-7	8	9	7	32	4.469E+05	3.476E+05	1.286	3.0	0.03	310.5 ± 156.7
G1244-7	16	5	11	18	4.414E+05	9.711E+05	0.455	8.5	0.06	111.5 ± 60.2
G1244-7	18	3	1	40	1.192E+05	3.973E+04	3.000	0.3	0.02	702.5 ± 811.4
G1244-7	20	16	10	16	1.589E+06	9.932E+05	1.600	8.7	0.04	384.2 ± 155.2
G1244-7	21	15	29	15	1.589E+06	3.072E+06	0.517	26.9	0.07	126.7 ± 40.4
G1244-7	22	15	17	40	5.959E+05	6.754E+05	0.882	5.9	0.06	214.7 ± 76.3
G1244-7	23	4	2	15	4.238E+05	2.119E+05	2.000	1.9	0.04	476.8 ± 413.1
G1244-7	24	11	18	20	8.740E+05	1.430E+06	0.611	12.5	0.06	149.5 ± 57.3
G1244-7	25	4	4	9	7.063E+05	7.063E+05	1.000	6.2	0.02	242.8 ± 171.8
G1244-7	27	5	3	15	5.297E+05	3.178E+05	1.667	2.8	0.05	399.7 ± 292.1
G1244-7	29	18	16	20	1.430E+06	1.271E+06	1.125	11.1	0.15	272.5 ± 93.9
G1244-7	30	24	20	25	1.526E+06	1.271E+06	1.200	11.1	0.03	290.3 ± 88.2
G1244-7	31	25	24	40	9.932E+05	9.534E+05	1.042	8.4	0.03	252.7 ± 72.5
G1244-7	32	45	44	32	2.235E+06	2.185E+06	1.023	19.1	0.02	248.2 ± 53.0
G1244-7	33	2	1	12	2.648E+05	1.324E+05	2.000	1.2	0.06	476.8 ± 584.1
		232	235		7.315E+05	7.409E+05		6.5		

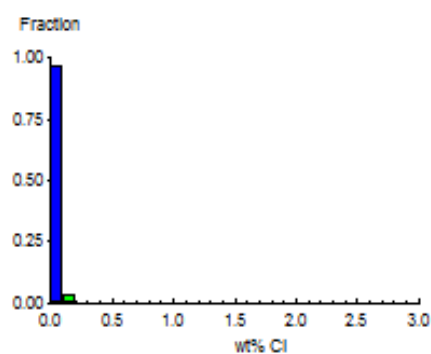
Area of basic unit = 6.293E-07 cm²
 $\chi^2 = 14.373$ with 19 degrees of freedom
 $P(\chi^2) = 76.2\%$
 Age Dispersion = 1.595% (did not converge)
 N_s / N_i = 0.987 ± 0.091
 Mean Ratio = 1.338 ± 0.158

Ages calculated using a zeta of 380.4 ± 5.7 for CN5 glass
 $\rho = 1.301E+06\text{cm}^{-2}$ ND=2048
 ρ_D interpolated between top of can; $\rho = 1.299E+06\text{cm}^{-2}$ ND=1022
 bottom of can; $\rho = 1.304E+06\text{cm}^{-2}$ ND=1026
POOLED AGE = 239.7 ± 23.1 Ma
CENTRAL AGE = 239.8 ± 23.1 Ma

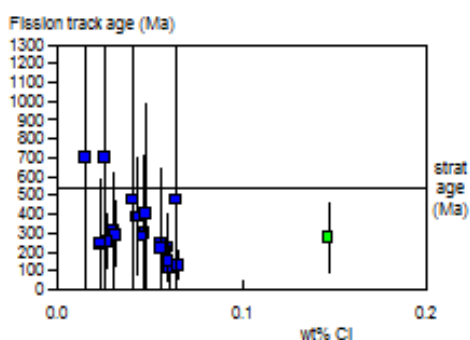
A:



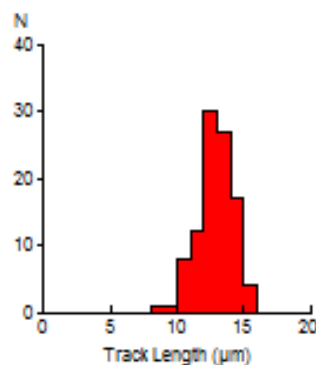
B:



C:



D:



Mean track length 12.91 ± 0.14 µm Std. Dev. 1.39 µm 100 tracks



GC970-80 Apatite
Counted by: COB

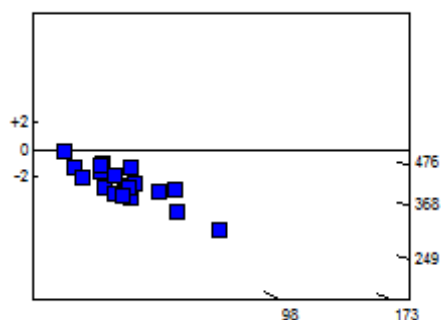
NOFT13-10

Slide ref	Current grain no	N _s	N _i	N _a	ρ _s	ρ _i	RATIO	U (ppm)	Cl (wt%)	F.T. AGE (Ma)
G1244-8	3	6	7	8	1.192E+06	1.390E+06	0.857	12.2	0.02	208.7 ± 116.2
G1244-8	4	12	15	36	5.297E+05	6.621E+05	0.800	5.8	0.01	195.0 ± 75.7
G1244-8	5	2	1	8	3.973E+05	1.986E+05	2.000	1.7	0.03	476.9 ± 584.2
G1244-8	6	5	10	63	1.261E+05	2.522E+05	0.500	2.2	0.02	122.6 ± 67.2
G1244-8	7	2	3	12	2.648E+05	3.973E+05	0.667	3.5	0.02	162.9 ± 148.8
G1244-8	8	14	16	25	8.899E+05	1.017E+06	0.875	8.9	0.02	213.0 ± 78.1
G1244-8	9	9	15	6	2.384E+06	3.973E+06	0.600	34.8	0.04	146.8 ± 62.0
G1244-8	10	39	59	30	2.066E+06	3.125E+06	0.661	27.4	0.02	161.5 ± 33.6
G1244-8	11	8	6	25	5.085E+05	3.814E+05	1.333	3.3	0.01	321.8 ± 174.0
G1244-8	12	21	24	24	1.390E+06	1.589E+06	0.875	13.9	0.06	213.0 ± 63.9
G1244-8	13	6	13	28	3.405E+05	7.378E+05	0.462	6.5	0.01	113.2 ± 56.0
G1244-8	14	2	5	18	1.766E+05	4.414E+05	0.400	3.9	0.01	98.2 ± 82.2
G1244-8	15	10	18	24	6.621E+05	1.192E+06	0.556	10.4	0.02	136.0 ± 53.8
G1244-8	16	16	12	16	1.589E+06	1.192E+06	1.333	10.4	0.01	321.8 ± 123.2
G1244-8	17	7	6	30	3.708E+05	3.178E+05	1.167	2.8	0.02	282.4 ± 157.3
G1244-8	18	24	36	70	5.448E+05	8.172E+05	0.667	7.2	0.04	162.9 ± 43.1
G1244-8	19	11	15	36	4.855E+05	6.621E+05	0.733	5.8	0.02	179.0 ± 71.2
G1244-8	20	8	15	50	2.543E+05	4.767E+05	0.533	4.2	0.04	130.7 ± 57.3
G1244-8	21	29	29	18	2.560E+06	2.560E+06	1.000	22.4	0.02	242.8 ± 64.1
G1244-8	22	9	10	9	1.589E+06	1.766E+06	0.900	15.5	0.02	219.0 ± 100.8
		240	315		7.115E+05	9.339E+05		8.2		

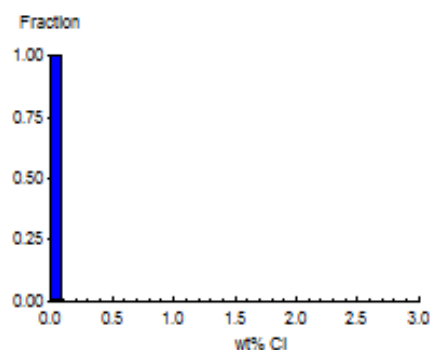
Area of basic unit = 6.293E-07 cm²
 $\chi^2 = 10.872$ with 19 degrees of freedom
 $P(\chi^2) = 92.8\%$
 Age Dispersion = 0.068% (did not converge)
 N_s / N_i = 0.762 ± 0.065
 Mean Ratio = 0.846 ± 0.085

Ages calculated using a zeta of 380.4 ± 5.7 for CN5 glass
 $\rho = 1.301E+06\text{cm}^{-2}$ ND=2048
 ρ_D interpolated between top of can; $\rho = 1.299E+06\text{cm}^{-2}$ ND=1022
 bottom of can; $\rho = 1.304E+06\text{cm}^{-2}$ ND=1026
POOLED AGE = 185.8 ± 16.7 Ma
CENTRAL AGE = 185.8 ± 16.7 Ma

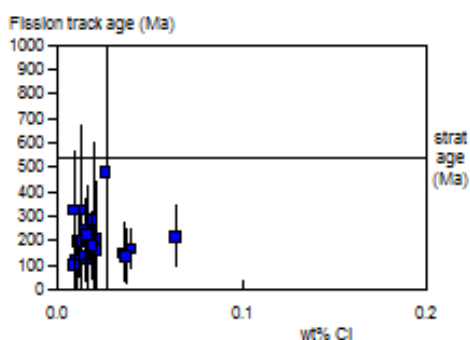
A:



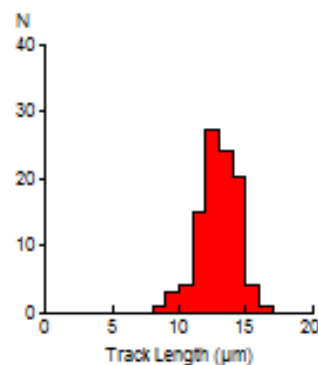
B:



C:



D:



Mean track length 12.97 ± 0.14 μm Std. Dev. 1.40 μm 99 tracks



GC970-81 Apatite
Counted by: COB

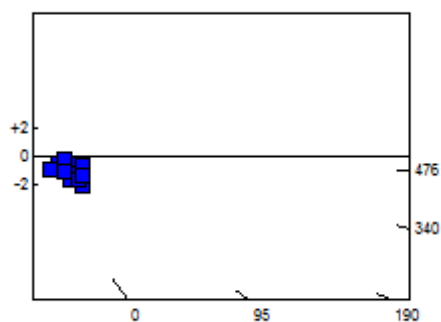
NOFT13-11

Slide ref	Current grain no	N _s	N _i	N _a	ρ _s	ρ _i	RATIO	U (ppm)	Cl (wt%)	F.T. AGE (Ma)
G1244-9	5	1	2	12	1.324E+05	2.648E+05	0.500	2.3	0.00	122.6 ± 150.2
G1244-9	7	0	1	9	0.000E+00	1.766E+05	0.000	1.5	0.01	0.0 ± 1765.8
G1244-9	8	1	1	10	1.589E+05	1.589E+05	1.000	1.4	0.02	242.9 ± 343.6
G1244-9	9	2	3	25	1.271E+05	1.907E+05	0.667	1.7	0.00	162.9 ± 148.8
G1244-9	10	1	3	30	5.297E+04	1.589E+05	0.333	1.4	0.00	82.0 ± 94.7
G1244-9	11	0	1	9	0.000E+00	1.766E+05	0.000	1.5	0.01	0.0 ± 1765.8
G1244-9	13	0	1	25	0.000E+00	6.356E+04	0.000	0.6	0.01	0.0 ± 1765.8
G1244-9	14	2	2	18	1.766E+05	1.766E+05	1.000	1.5	0.00	242.9 ± 243.0
G1244-9	15	3	2	40	1.192E+05	7.945E+04	1.500	0.7	0.02	361.0 ± 329.7
G1244-9	16	2	1	40	7.945E+04	3.973E+04	2.000	0.3	0.00	477.0 ± 584.3
G1244-9	17	2	3	30	1.059E+05	1.589E+05	0.667	1.4	0.02	162.9 ± 148.8
G1244-9	18	1	3	30	5.297E+04	1.589E+05	0.333	1.4	0.00	82.0 ± 94.7
G1244-9	20	0	1	30	0.000E+00	5.297E+04	0.000	0.5	0.02	0.0 ± 1765.8
G1244-9	21	2	1	40	7.945E+04	3.973E+04	2.000	0.3	0.01	477.0 ± 584.3
G1244-9	22	2	5	30	1.059E+05	2.648E+05	0.400	2.3	0.01	98.3 ± 82.2
G1244-9	23	4	3	10	6.356E+05	4.767E+05	1.333	4.2	0.02	321.9 ± 246.0
G1244-9	24	1	2	20	7.945E+04	1.589E+05	0.500	1.4	0.00	122.6 ± 150.2
G1244-9	25	2	4	20	1.589E+05	3.178E+05	0.500	2.8	0.00	122.6 ± 106.2
G1244-9	27	0	1	30	0.000E+00	5.297E+04	0.000	0.5	0.00	0.0 ± 1765.8
G1244-9	28	3	4	21	2.270E+05	3.027E+05	0.750	2.7	0.02	183.0 ± 139.9
		29	44		9.621E+04	1.460E+05		1.3		

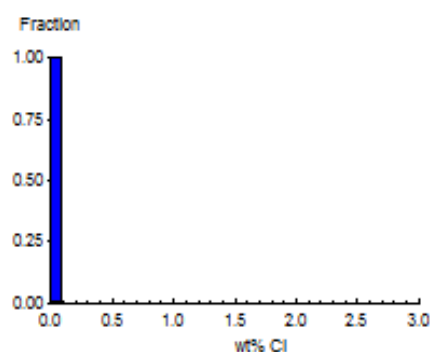
Area of basic unit = 6.293E-07 cm²
 $\chi^2 = 8.446$ with 19 degrees of freedom
 $P(\chi^2) = 98.2\%$
 Age Dispersion = 0.004% (did not converge)
 N_s / N_i = 0.659 ± 0.158
 Mean Ratio = 0.674 ± 0.141

Ages calculated using a zeta of 380.4 ± 5.7 for CN5 glass
 $\rho = 1.301E+06 \text{ cm}^{-2}$ ND=2048
 ρ_D interpolated between top of can; $\rho = 1.299E+06 \text{ cm}^{-2}$ ND=1022
 bottom of can; $\rho = 1.304E+06 \text{ cm}^{-2}$ ND=1026
POOLED AGE = 161.1 ± 38.8 Ma
CENTRAL AGE = 161.1 ± 38.8 Ma

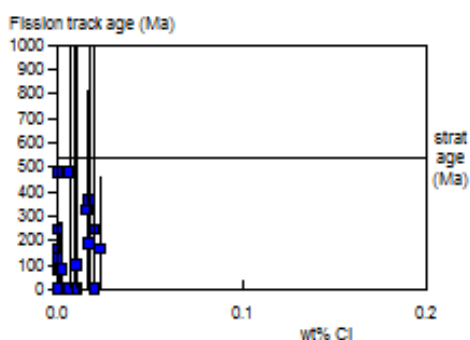
A:



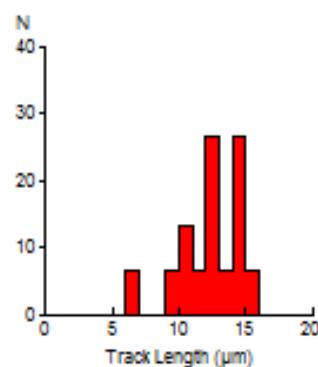
B:



C:



D:



Mean track length 12.40 ± 0.61 μm Std. Dev. 2.36 μm 15 tracks



GC970-82 Apatite
Counted by: COB

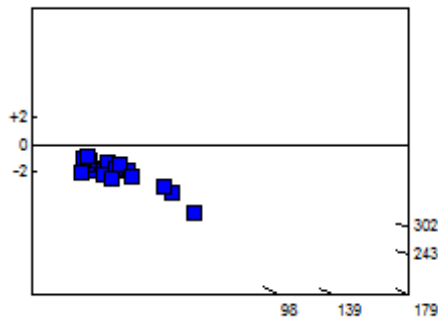
NOFT13-12

Slide ref	Current grain no	N _s	N _i	N _a	ρ _s	ρ _i	RATIO	U (ppm)	Cl (wt%)	F.T. AGE (Ma)
G1244-10	3	26	30	40	1.033E+06	1.192E+06	0.867	10.4	0.02	211.1 ± 56.8
G1244-10	5	31	45	30	1.642E+06	2.384E+06	0.689	20.9	0.02	168.3 ± 39.5
G1244-10	7	7	8	12	9.270E+05	1.059E+06	0.875	9.3	0.01	213.1 ± 110.4
G1244-10	8	5	7	30	2.648E+05	3.708E+05	0.714	3.2	0.03	174.5 ± 102.3
G1244-10	9	8	9	49	2.594E+05	2.919E+05	0.889	2.6	0.02	216.4 ± 105.3
G1244-10	11	9	8	21	6.810E+05	6.054E+05	1.125	5.3	0.01	272.7 ± 132.7
G1244-10	12	5	4	9	8.828E+05	7.063E+05	1.250	6.2	0.01	302.3 ± 202.9
G1244-10	13	4	5	8	7.945E+05	9.932E+05	0.800	8.7	0.03	195.1 ± 131.0
G1244-10	14	14	13	28	7.945E+05	7.378E+05	1.077	6.5	0.02	261.2 ± 100.9
G1244-10	15	5	5	21	3.783E+05	3.783E+05	1.000	3.3	0.02	242.9 ± 153.8
G1244-10	17	4	4	30	2.119E+05	2.119E+05	1.000	1.9	0.01	242.9 ± 171.9
G1244-10	18	9	8	15	9.534E+05	8.475E+05	1.125	7.4	0.02	272.7 ± 132.7
G1244-10	19	2	5	16	1.986E+05	4.966E+05	0.400	4.3	0.02	98.3 ± 82.3
G1244-10	20	5	4	16	4.966E+05	3.973E+05	1.250	3.5	0.01	302.3 ± 202.9
G1244-10	21	6	9	25	3.814E+05	5.721E+05	0.667	5.0	0.01	163.0 ± 86.0
G1244-10	23	10	10	18	8.828E+05	8.828E+05	1.000	7.7	0.02	242.9 ± 108.8
G1244-10	24	7	11	16	6.952E+05	1.092E+06	0.636	9.6	0.02	155.7 ± 75.4
G1244-10	28	24	26	16	2.384E+06	2.582E+06	0.923	22.6	0.01	224.6 ± 63.9
G1244-10	29	12	10	21	9.080E+05	7.567E+05	1.200	6.6	0.02	290.4 ± 124.6
G1244-10	30	14	15	24	9.270E+05	9.932E+05	0.933	8.7	0.03	227.0 ± 84.6
		207	236		7.392E+05	8.427E+05		7.4		

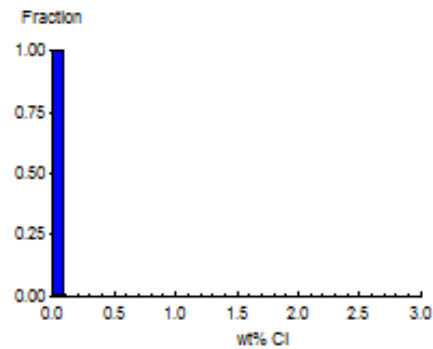
Area of basic unit = 6.293E-07 cm²
 $\chi^2 = 5.005$ with 19 degrees of freedom
 $P(\chi^2) = 99.9\%$
 Age Dispersion = 0.000% (did not converge)
 N_s / N_i = 0.877 ± 0.084
 Mean Ratio = 0.921 ± 0.050

Ages calculated using a zeta of 380.4 ± 5.7 for CN5 glass
 $\rho = 1.302E+06\text{cm}^{-2}$ ND=2048
 ρ_D interpolated between top of can; $\rho = 1.299E+06\text{cm}^{-2}$ ND=1022
 bottom of can; $\rho = 1.304E+06\text{cm}^{-2}$ ND=1026
POOLED AGE = 213.6 ± 21.1 Ma
CENTRAL AGE = 213.6 ± 21.1 Ma

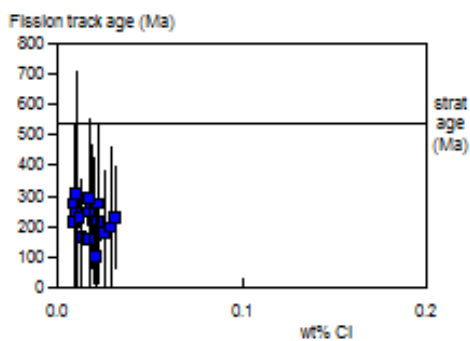
A:



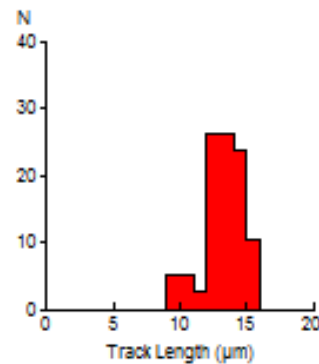
B:



C:



D:



Mean track length 13.37 ± 0.25 μm Std. Dev. 1.54 μm 38 tracks



GC970-83 Apatite
Counted by: COB

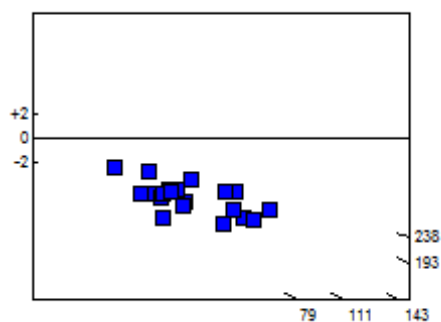
NOFT13-13

Slide ref	Current grain no	N _s	N _i	N _a	ρ _s	ρ _i	RATIO	U (ppm)	Cl (wt%)	F.T. AGE (Ma)
G1244-11	3	25	41	24	1.655E+06	2.715E+06	0.610	23.8	0.03	149.2 ± 38.1
G1244-11	5	52	75	40	2.066E+06	2.980E+06	0.693	26.1	0.02	169.4 ± 30.9
G1244-11	6	37	67	20	2.940E+06	5.323E+06	0.552	46.6	0.03	135.3 ± 28.0
G1244-11	7	12	37	12	1.589E+06	4.900E+06	0.324	42.9	0.06	79.8 ± 26.6
G1244-11	8	18	20	9	3.178E+06	3.531E+06	0.900	30.9	0.04	219.1 ± 71.4
G1244-11	9	8	11	8	1.589E+06	2.185E+06	0.727	19.1	0.04	177.6 ± 82.7
G1244-11	10	25	34	15	2.648E+06	3.602E+06	0.735	31.5	0.02	179.6 ± 47.5
G1244-11	11	14	27	12	1.854E+06	3.575E+06	0.519	31.3	0.02	127.1 ± 42.0
G1244-11	12	10	23	10	1.589E+06	3.655E+06	0.435	32.0	0.01	106.8 ± 40.5
G1244-11	13	49	66	35	2.225E+06	2.997E+06	0.742	26.2	0.03	181.3 ± 34.5
G1244-11	14	22	31	36	9.711E+05	1.368E+06	0.710	12.0	0.01	173.4 ± 48.6
G1244-11	15	58	80	60	1.536E+06	2.119E+06	0.725	18.6	0.02	177.1 ± 30.9
G1244-11	16	16	31	8	3.178E+06	6.158E+06	0.516	53.9	0.05	126.6 ± 39.1
G1244-11	17	18	30	15	1.907E+06	3.178E+06	0.600	27.8	0.04	146.9 ± 44.0
G1244-11	18	35	36	30	1.854E+06	1.907E+06	0.972	16.7	0.02	236.4 ± 56.5
G1244-11	19	58	59	28	3.292E+06	3.348E+06	0.983	29.3	0.01	238.9 ± 44.6
G1244-11	20	75	85	35	3.405E+06	3.859E+06	0.882	33.8	0.09	214.9 ± 34.5
G1244-11	21	22	33	12	2.913E+06	4.370E+06	0.667	38.3	0.03	163.0 ± 45.1
G1244-11	22	51	54	36	2.251E+06	2.384E+06	0.944	20.9	0.03	229.7 ± 45.3
G1244-11	23	23	41	15	2.437E+06	4.343E+06	0.561	38.0	0.00	137.4 ± 36.0
		628	881		2.169E+06	3.043E+06		26.6		

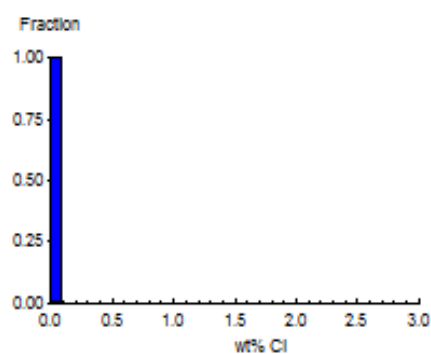
Area of basic unit = 6.293E-07 cm²
 $\chi^2 = 22.185$ with 19 degrees of freedom
 $P(\chi^2) = 27.5\%$
 Age Dispersion = 8.740% (did not converge)
 N_s / N_i = 0.713 ± 0.037
 Mean Ratio = 0.690 ± 0.041

Ages calculated using a zeta of 380.4 ± 5.7 for CN5 glass
 $\rho = 1.302E+06\text{cm}^{-2}$ ND=2048
 ρ_D interpolated between top of can; $\rho = 1.299E+06\text{cm}^{-2}$ ND=1022
 bottom of can; $\rho = 1.304E+06\text{cm}^{-2}$ ND=1026
POOLED AGE = 174.1 ± 10.2 Ma
CENTRAL AGE = 172.8 ± 10.8 Ma

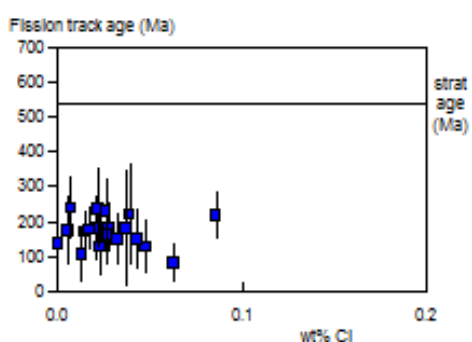
A:



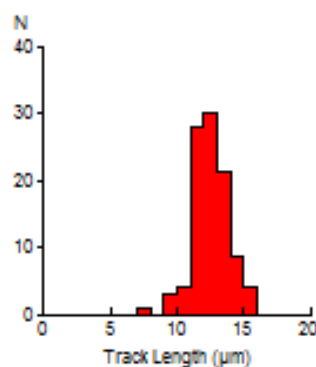
B:



C:



D:



Mean track length 12.51 ± 0.13 μm Std. Dev. 1.34 μm 103 tracks



GC970-84 Apatite
Counted by: COB

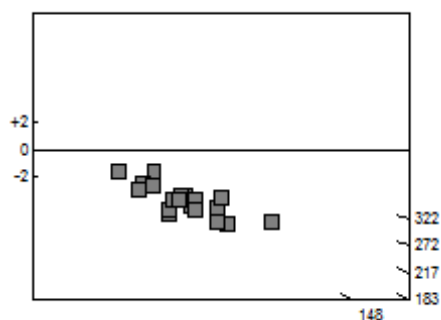
NOFT13-14

Slide ref	Current grain no	N _s	N _i	N _a	ρ _s	ρ _i	RATIO	U (ppm)	Cl (wt%)	F.T. AGE (Ma)
G1244-12	3	11	10	6	2.913E+06	2.648E+06	1.100	23.2	1.85	266.8 ± 116.8
G1244-12	4	24	18	9	4.238E+06	3.178E+06	1.333	27.8	1.80	322.0 ± 100.8
G1244-12	5	33	39	12	4.370E+06	5.164E+06	0.846	45.2	1.74	206.2 ± 49.1
G1244-12	6	32	34	12	4.238E+06	4.502E+06	0.941	39.4	1.69	229.0 ± 56.7
G1244-12	7	17	18	6	4.502E+06	4.767E+06	0.944	41.7	1.87	229.8 ± 77.9
G1244-12	8	30	32	12	3.973E+06	4.238E+06	0.938	37.1	1.45	228.1 ± 58.3
G1244-12	9	14	18	6	3.708E+06	4.767E+06	0.778	41.7	1.75	189.8 ± 67.8
G1244-12	10	20	33	14	2.270E+06	3.746E+06	0.606	32.8	1.59	148.4 ± 42.2
G1244-12	11	47	61	21	3.556E+06	4.616E+06	0.770	40.4	1.89	188.1 ± 36.8
G1244-12	12	21	32	8	4.171E+06	6.356E+06	0.656	55.6	1.88	160.5 ± 45.3
G1244-12	23	25	31	16	2.483E+06	3.079E+06	0.806	27.0	1.71	196.7 ± 53.1
G1244-12	24	41	55	16	4.072E+06	5.462E+06	0.745	47.8	1.69	182.0 ± 37.9
G1244-12	25	46	50	18	4.061E+06	4.414E+06	0.920	38.6	1.79	223.9 ± 46.1
G1244-12	26	34	37	12	4.502E+06	4.900E+06	0.919	42.9	1.69	223.7 ± 53.5
G1244-12	27	37	39	14	4.200E+06	4.427E+06	0.949	38.8	1.64	230.8 ± 53.3
G1244-12	28	20	21	9	3.531E+06	3.708E+06	0.952	32.5	1.88	231.7 ± 72.6
G1244-12	29	34	42	15	3.602E+06	4.449E+06	0.810	39.0	1.59	197.4 ± 45.9
G1244-12	30	80	83	30	4.238E+06	4.396E+06	0.964	38.5	1.81	234.4 ± 37.3
G1244-12	31	28	33	12	3.708E+06	4.370E+06	0.848	38.3	1.80	206.8 ± 53.4
G1244-12	32	53	48	25	3.369E+06	3.051E+06	1.104	26.7	1.70	267.8 ± 53.8
		647	734		3.766E+06	4.272E+06		37.4		

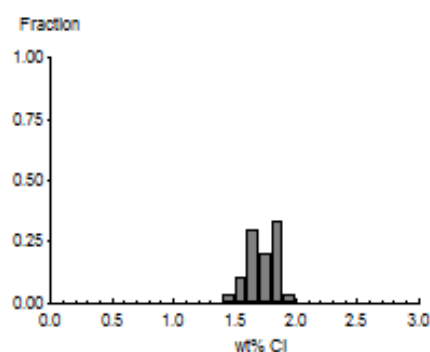
Area of basic unit = 6.293E-07 cm²
 $\chi^2 = 8.508$ with 19 degrees of freedom
 $P(\chi^2) = 98.1\%$
 Age Dispersion = 0.003% (did not converge)
 N_s / N_i = 0.881 ± 0.048
 Mean Ratio = 0.897 ± 0.037

Ages calculated using a zeta of 380.4 ± 5.7 for CN5 glass
 $\rho = 1.302E+06\text{cm}^{-2}$ ND=2048
 ρ_D interpolated between top of can; $\rho = 1.299E+06\text{cm}^{-2}$ ND=1022
 bottom of can; $\rho = 1.304E+06\text{cm}^{-2}$ ND=1026
POOLED AGE = 214.7 ± 12.9 Ma
CENTRAL AGE = 214.7 ± 12.9 Ma

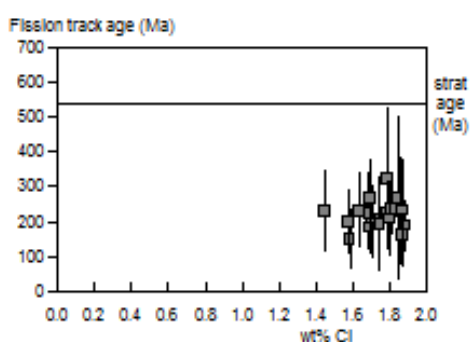
A:



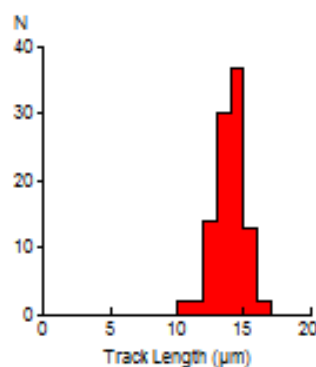
B:



C:



D:



Mean track length 13.99 ± 0.10 μm Std. Dev. 1.05 μm 100 tracks

APPENDIX C

Thermal History interpretation of AFTA data: basic principles and practical application

C.1 Historical background and physical basis

Naturally occurring fission tracks are radiation damage trails produced by the spontaneous fission of ^{238}U atoms, in which a uranium atom splits into two highly energetic fragments, stripped of electrons. Due to electrostatic repulsion between the fragments, they travel rapidly in opposite directions creating a linear zone of intense disruption through the crystal lattice, known as a fission track. Apatite grains typically contain around 10 ppm Uranium (range 1-100 ppm), so over geological time fission tracks accumulate in the crystal lattice. If a collection of apatite grains are mounted and polished, tracks can be revealed where they intersect the polished surface by a simple etching treatment (Fig. C.1). Since spontaneous fission is a form of radioactive decay, in principle the number of tracks in the surface is controlled by uranium content and time, through standard decay laws, so by counting the number of tracks and measuring the uranium content, a “fission track age” can be measured which, in the absence of other factors, should indicate the time over which tracks have accumulated. Reviews of the basics of fission track dating are provided by e.g. Fleischer et al. (1975), Wagner and Van den Haute (1992) and Galbraith (2006).



Fig. C.1: Spontaneous fission tracks in a detrital apatite grain ~ 0.25 mm in length. Fission tracks were revealed by etching in 5M HNO₃ for 20 seconds at 20°C. The majority of linear features in the image are fission tracks. They are randomly orientated in 3 dimensions and the number of tracks revealed in the surface is controlled by the uranium content of the grain, the time over which tracks have accumulated, and the distribution of track lengths, which in turn is a function of the thermal history

Early insights into the thermal sensitivity of fission tracks in apatite

Early applications of fission track dating to accessory apatites from crystalline basement rocks revealed that the technique was extremely thermally sensitive, suggesting that fission track ages could be reset at relatively low temperatures around 100°C over geological timescales (e.g. Wagner and Reimer, 1972). This was supported by early laboratory annealing studies (Wagner, 1968; Naeser and Faul, 1969), and subsequently confirmed by direct measurement of fission track ages in sub-surface samples (Naeser and Forbes, 1976). Integration of fission track ages with confined track length measurements (Fig. C.2), first reported by Bhandari et al. (1971), led to deeper understanding of the method. Early measurements showed that even in volcanic rocks which have experienced only very low temperatures after initial post-eruption cooling, mean confined track lengths (around 14 to 15 μm) were shorter than induced tracks (~16 μm) in the same apatites. Green (1980) showed that this can be understood in terms of thermal annealing of these tracks at low temperatures (<50°C) over geological timescales, highlighting the sensitivity of the technique.



Fig. C.2: Confined fission track lengths in apatite. In order to determine the distribution of track lengths, measurements are made of the full length of horizontal tracks which are totally enclosed within the body of the crystal, which have been etched via fractures or other tracks which intersect the surface of the grain. Note that difference in width of the tracks is due to a difference in etch rate with crystallographic orientation, with a higher etch rate parallel to the C-axis

Results from boreholes in the Otway Basin of SE Australia (Gleadow and Duddy, 1981) provided the first quantitative insights into the thermal stability of tracks in geological conditions, revealing the progressive reduction in fission track age with depth



and temperature, and showing that this was complemented by a corresponding decrease in track length (Fig. C.3). Compilation of confined track length data in a large number of apatite samples showed that the form of the track length distribution was a sensitive indicator of the style of thermal history (Gleadow et al. 1986). Laboratory studies (Green et al. 1985, 1986; Green 1988), together with detailed mathematical analysis (Laslett et al. 1982; Galbraith and Laslett 1988, 1990), established that the reduction in track length (which is, in turn, a manifestation of the reduction in the degree of damage within the track region) causes the reduction in fission track age, by reducing the proportion of tracks that can intersect a polished grain surface. This realization underpins all subsequent studies involving quantitative prediction of apatite fission track (AFT) parameters and extraction of thermal history information from such data.

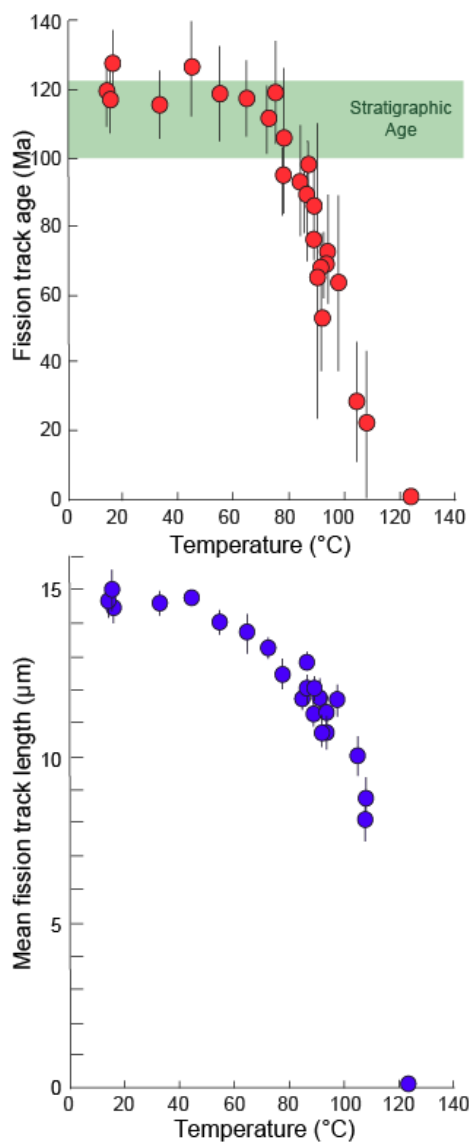


Fig. C.3: Variation of measured fission track age and mean track length with present-day temperature in samples from Otway Basin (Australia) exploration wells which are at maximum temperatures at the present-day. With increasing maximum temperature there is a progressive reduction in fission track age to zero at ~125°C which is the result of the progressive reduction in mean confined track length. These observations provide a direct expression of the thermal stability of fission tracks in geological conditions (after Gleadow and Duddy, 1981).

The Laslett et al. (1987) model

Early laboratory annealing studies, based on measurement of track density as an indicator of the degree of annealing, in accessory apatites of varying character, led to a wide variety of kinetic models of conflicting styles (as reviewed by Green et al. 1986; Green et al. 1988). Based on the recognition of the key role of track length in the annealing process, coupled with the fact that track lengths can be measured with greater precision than track densities, Green et al. (1986) carried out a series of detailed annealing experiments on a well-characterised apatite of uniform composition (Durango apatite, Young et al, 1969), in which mean track length was used to indicate the degree of annealing. This study demonstrated that as a result of heating, the mean track length is progressively reduced and the tracks effectively “shrink” from each end, until in the final stages individual tracks may break up into several segments. This behaviour can be understood in terms of a progressive reduction in the degree of radiation damage within the track region, as displaced atoms return to their original lattice sites by thermally activated diffusion, until in the final stages, discrete zones of etchability are separated by regions which are fully “healed”. Laslett et al. (1987) subsequently showed that the variation of mean track length with temperature and time was well described by a “fanning Arrhenius plot” model, in which contours of equal track length reduction form straight lines in a plot of time against inverse absolute temperature, with the slope of these lines (reflecting an “activation energy”) increasing as the degree of annealing increases (Fig. C.4).

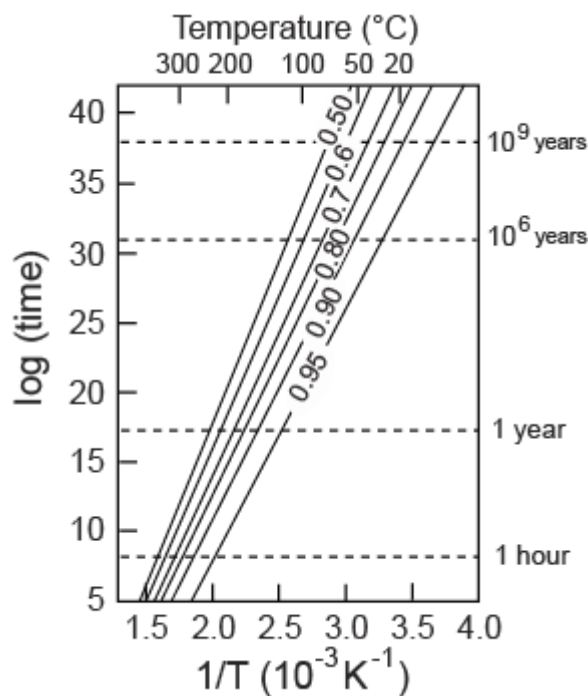


Fig. C.4: “Fanning Arrhenius plot” adopted by Laslett et al. (1987) to describe the variation of mean track length with temperature and time for Durango apatite. In this plot, contours of equal track length reduction form straight lines in a plot of log(time) against inverse absolute temperature (contoured values are the ratio of predicted length to initial length, L/L₀).

Variable temperature behaviour

The improved definition of the kinetics of fission track annealing provided by using mean confined track length as the fundamental parameter (Laslett et al. 1987), combined with a detailed understanding of the way in which reduction in track length is manifested in the fission track age (Green, 1988), provided the basis for making realistic predictions of apatite fission track parameters in geological situations. A key step in this process is the transition from isothermal annealing models to variable temperature behaviour as encountered in geological settings. Duddy et al. (1988) provided a way forward by adopting the principle of ‘equivalent time’ (originally postulated by Goswami et al., 1984), by which the rate of annealing of a track at any given time depends only on the length to which the track has already been reduced, and the prevailing temperature, and not on the history of how the track reached that length. The validity of this assumption is by no means straightforward, and Duddy et al. (1988) provided experimental verification through a series of variable temperature annealing experiments, laying the basis for the successful extension of isothermal annealing models to variable temperature geological histories.

Quantitative modelling of AFTA parameters

Green et al. (1989) built on the advances described above to develop methods for quantitatively modelling the response of fission tracks in apatite to various styles of thermal history. The basis of the approach is the recognition that track length reduction is the controlling process in determining the AFTA parameters that result from any particular history. New fission tracks are continually generated as time passes, such that different tracks sample different proportions of the whole history. If a specified thermal history is broken down into discrete intervals, the pattern of track length reduction with time for populations of tracks formed at different times through the history can be calculated by applying the principle of equivalent time (above) to the thermal history appropriate to each population, resulting in a predicted mean length for each population of tracks at the present day (Fig. C.5).

Fission tracks show an inherent spread in track length, reflecting the range of energies and masses of the fission fragments produced by spontaneous fission. This spread, measured by the standard deviation of the length distribution, increases as the mean length is reduced, largely as a result of an increasing anisotropy of the annealing process (Green et al., 1986). So to calculate the final distribution of track lengths predicted for a sample at the present day, the component distributions of track length resulting from populations of tracks produced at different times throughout the history must be

summed, employing the appropriate spread of lengths for each population. The component populations must also be added in the appropriate proportions, allowing for the biases involved in revelation of tracks of different length (Laslett et al., 1982). By summing components of fission track age appropriate to the length of each time interval, moderated by the effect of length reduction on the reduction of age (Green, 1988), the final fission track age for the sample can also be predicted.

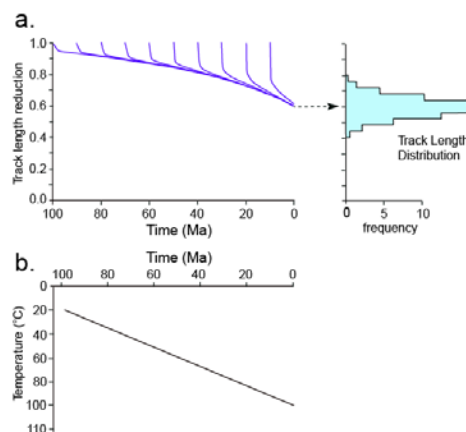


Fig. 5: a). Predicted pattern of track length reduction with time (left) and final track length distribution (right) for populations of tracks formed at different times through the notional thermal history shown in b.), involving progressive heating from 20 to 100°C over 100 Myr. The final track length distribution is calculated by applying the principle of equivalent time to each population of tracks using the Fanning Arrhenius model of Laslett et al. (1987), and summing the track lengths distributions for all populations of tracks in the appropriate length-biased proportions (Laslett et al., 1982). After Green et al. (1989).

Influence of apatite composition on annealing rates

Studies of apatite fission track parameters in subsurface samples from the Otway Basin (Gleadow and Duddy, 1981; Green et al., 1985, 1986) showed that chlorine content exerts a systematic influence on annealing rates (Fig. C.6). This has subsequently been confirmed in laboratory studies by Carlson et al. (1999) and Barbarand et al. (2003a). In both these studies, the authors tend to downplay the influence of chlorine in favour of other factors. But results from both studies clearly illustrate the first-order control exerted by chlorine (Fig. C.7), while also suggesting that other possibly more exotic factors may exert second-order control in some cases. The importance of differential annealing within individual samples related to wt% Cl has now been demonstrated in a number of geological studies (e.g. Argent et al., 2002; Crowhurst et al., 2002; Green et al., 2002; Green, 2005).

A number of studies have suggested that etch pit diameters can be used as an indicator of differential annealing rates between various apatite species (Burtner et al. 1994; Ketcham et al. 1999; Barbarand et al. 2003a). However, Green et al. (2005) demonstrated that annealing rates in the Barbarand et al. (2003a) dataset show a much stronger correlation with wt% Cl than to etch pit size (Fig. C.8).

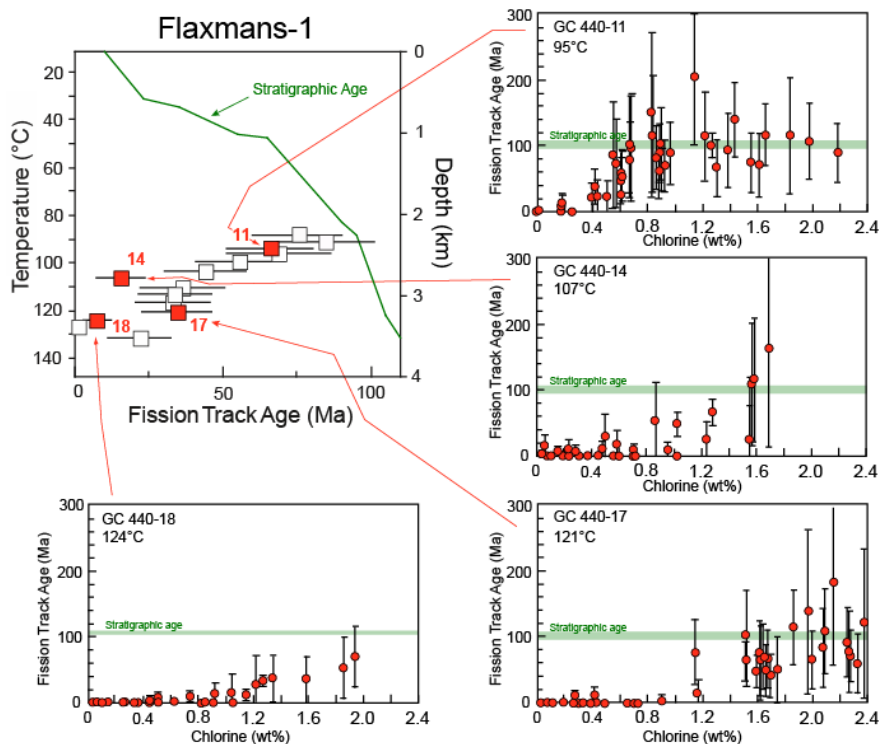


Fig. C.6: Variation of central fission track age with depth for samples from the Flaxmans-1 well, Otway Basin, SE Australia, together with the variation of fission track age with chlorine content for individual apatite grains from four selected samples. In each of these samples the most sensitive (i.e. low wt% chlorine) grains are totally annealed (i.e. zero FT age) while grains with more retentive (higher Cl) grains giving ages up to the depositional age and above. With increasing present-day down-hole temperature (the maximum post-depositional temperature in these samples), the transition to total annealing shifts to progressively higher Cl contents, demonstrating the systematic influence of chlorine content on annealing (Gleadow and Duddy, 1981; Green et al., 1985, 1986). Note that while most of the central fission track ages define a generally smooth decrease with increasing temperature, the age for sample GC440-14 is off trend. This is due to the absence of grains with chlorine >1.6 wt% Cl compared to adjacent samples, which are dominated by more retentive grains and therefore give higher central ages. This major effect of chlorine on apatite fission track age must be taken into account in order to extract meaningful geological constraints from apatite fission track data.

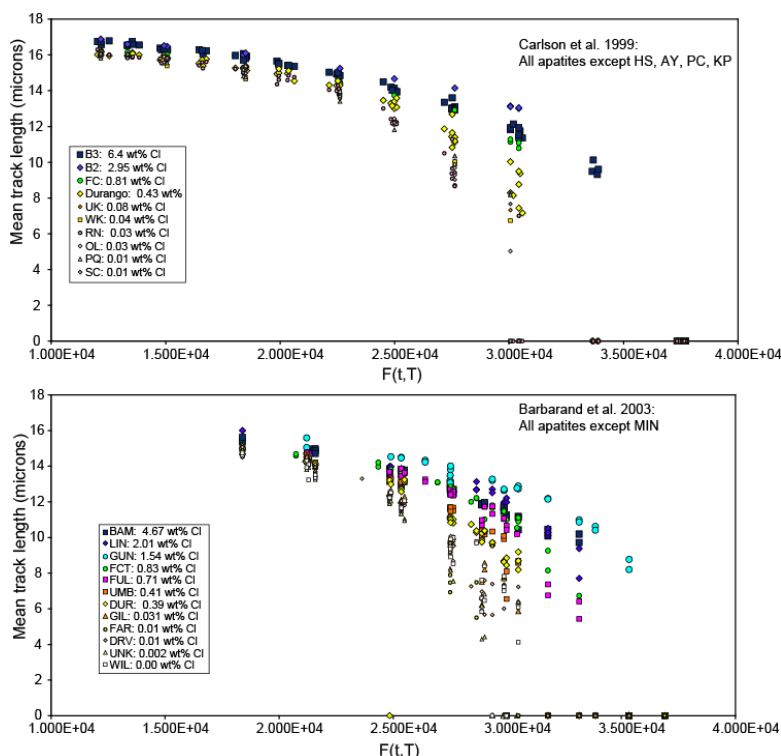


Fig. C.7: Mean track lengths from laboratory annealing experiments reported by Carlson et al. (1999) and Barbarand et al. (2003a), plotted against a unifying function of temperature and time, which reduces all data to a common scale. This function is of the form $F(t,T) = \left[\log t - \log t_0 \right] / \left[(1/T) - (1/T_0) \right]$, where $\log t_0 = -10$ and $1/T_0 = 0.001$. Apatites of different Cl content are coded to illustrate this variation, with high Cl contents (>1 wt% Cl) shown in blue colours and large symbols, apatites low in Cl (<0.1 wt% Cl) shown in pale colours and small symbols, and intermediate compositions shown in yellow, red and green colours. The Durango apatite (yellow diamonds) and Fish Canyon Tuff apatite (green circles) are common to both datasets. These results clearly illustrate the first order control on annealing rates exerted by Cl content, with apatites high in chlorine giving longer lengths for any given heat treatment than those low in Cl. While the first order control from chlorine is clear, other elements produce additional variation, and several apatites have been omitted from these plots as they are not consistent with the main body of data.

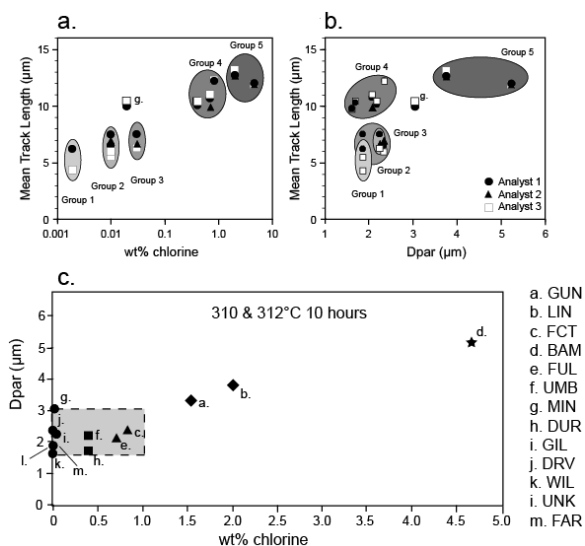


Fig. C.8: Comparison of the variation in mean track length with chlorine content (a.) and with the width of track openings parallel to the c-axis (Dpar) (b.) from the laboratory annealing experiments of Barbarand et al. (2003a). Track size shows only a poor correlation with mean fission track length, whereas chlorine contents shows a very strong correlation, illustrating that Dpar is only a poor proxy for fission track annealing rates. Similar behaviour is seen in results from other annealing conditions reported by Barbarand et al. (2003a) data set, as discussed in detail by Green et al (2005a). The track-size parameter Dpar shows only a poor correlation with chlorine contents between 0. and 1 wt% (c.), and it should therefore be expected that Dpar would provide only a limited indication of differential annealing sensitivities between different apatite species.

Evidence for systematic differences in annealing rates in natural geological samples due to any element other than Cl has yet to be demonstrated. In practical application of AFTA, variation in fission track age and track length with wt% Cl allows identification of any anomalous grains that might represent unusual annealing properties (e.g. Crowhurst et al. 2002). This approach also allows detection of contaminant grains, which can be important in working with ditch cuttings in sub-surface samples, where “caving” of material from shallower levels can be recognised in this way (Japsen et al., 2005; Green et al., 2011). Such anomalous grains can be eliminated from the dataset prior to extraction of thermal history solutions.

In geological conditions, differential annealing effects within individual samples are maximised in rocks which have been heated into the critical temperature range (typically 90-120°C) where the most sensitive (i.e. low Cl) apatites are totally annealed while more resistant apatites (high Cl) are unaffected (Fig. C.6). In such cases, the systematic dispersion in fission track age, correlating with wt% Cl, provides added precision to a thermal history solution (Crowhurst et al., 2002) (Fig. C.9).

Numerous examples exist in the literature of apparently anomalous observations that can probably be simply explained in terms of differences in wt% Cl. One example is the apparent difference in resistance to erosion attributed to adjacent Gneissic and Charnockitic terrains in India reported by Gunnell (2000), which is more likely to be due to a difference in annealing rates in apatites from the two rock types (with Charnockitic apatites likely to be richer in Cl, and hence giving older ages). In such cases,

measurement of Cl contents in the analysed grains can easily resolve such effects.

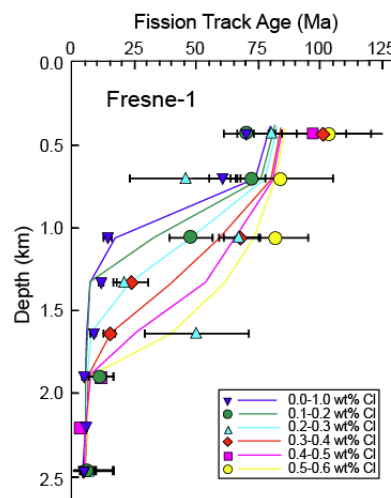


Fig. C.9: Variation of fission track age with depth for apatites of different chlorine content in samples from the Fresne-1 well, Taranaki Basin, New Zealand (after Crowhurst et al., 2002). Apatites with lower chlorine content achieve a given degree of annealing (as expressed by the reduction in fission track age) at shallower levels, corresponding to lower maximum paleotemperatures, compared to apatites with higher chlorine. In particular, note the progressive shift in the transition from partial to total annealing (defined by the inflection in the age-depth trend), with apatites containing 0.5-0.6 wt% Cl becoming totally annealed almost 1 km deeper than samples containing between 0.0 and 0.1 wt% Cl. Curves show the variation of fission track age for each compositional group predicted from the final reconstructed history for the Fresne-1 well, as reported in Crowhurst et al. (2002).

Later kinetic models

Subsequent to publication of the Laslett et al. (1987) kinetic model of fission track annealing, various refinements or alternative forms of the basic fanning Arrhenius plot model have been published. Carlson (1990) suggested a model based on the laboratory annealing data from Green et al. (1986) and other (then unpublished) data, and claimed that because this model was “based on explicit physical mechanisms, extrapolations of annealing rates to the lower temperatures and longer timescales required for the interpretation of natural fission track length distributions can be made with greater confidence than is the case for purely empirical relationships fitted to the experimental annealing data”. However, as explained by Green et al. (1993), all aspects of Carlson's model are in fact purely empirical, and this model is inherently no more reliable than any other model. In addition, as reported by Crowley (1993), detailed inspection shows that Carlson's model does not fit the laboratory data set at all well.

Crowley et al. (1991) published new annealing data in three apatites of different composition, including the Durango apatite for which the Laslett et al. (1987) model was derived, and fitted kinetic models which are similar to the Laslett et al., (1987) model, except for the use of a non-zero inverse temperature intercept ($1/T_0$). It should be noted that Laslett et al. (1987) considered such models but showed that the best estimate of $1/T_0$ in their analysis was not significantly different from zero, and because the assumption of $1/T_0 = 0$ simplifies the mathematical description, they preferred the simpler model.



Despite an apparently superior experimental design compared to the Green et al. (1986) study, the kinetic models offered by Crowley et al. (1991), as well as that of Carlson (1990) give predictions in geological conditions that are not consistent with observations (as reviewed in more detail later), and these models have not achieved widespread use. Crowley et al. (1991) investigated Arrhenius plot models in which contours of equal annealing are curved, although linear models were favoured. Crowley et al. (1991) also fitted a revised model to the annealing data for Durango apatite published by Green et al. (1986). Predictions of the revised model are not very much different to those from the Laslett et al. (1987) model (below) and this model has also not found widespread use.

Subsequently, Laslett and Galbraith (1996) showed that rather than using the reduced track length L/L_0 (where L_0 is the mean length of unannealed tracks) as the controlling parameter, improved models could be achieved by fitting to the measured mean track lengths, L , instead of L/L_0 , while L_0 becomes simply an additional empirical parameter to be estimated. This is of particular importance because Donelick et al. (1990) showed that tracks produced by thermal neutron irradiation begin to anneal (shorten) over very short timescales (minute to hours) even at room temperature. For this reason, mean lengths of unannealed induced confined tracks which are measured weeks to months after irradiation have already undergone some degree of length reduction, and therefore have no fundamental significance.

In our own work, we use a series of Fanning Arrhenius Plot models of the form advocated by Laslett and Galbraith (1996) with finite $1/T_0$ intercept and fitted to measured track lengths, employing coefficients which vary smoothly with wt% Cl, such that the overall annealing rate decreases as wt% Cl increases. This model is based on a combination of laboratory annealing data and geological constraints, using data from a series of exploration wells in which the thermal histories can be reconstructed with confidence. This avoids uncertainties associated with extrapolation of models from laboratory to geological timescales (discussed below). Effectively the relative behaviour of different apatite species in laboratory conditions (similar to that shown in Fig. C.7) is mapped on to the variation within the geological dataset, as there is insufficient overlap over the full range of apatite compositions in the geological data to provide a satisfactory basis for model fitting based on these data alone.

In similar fashion, Ketcham et al. (1999) fitted a number of models to laboratory annealing data (Fig. C.7) in a variety of apatite species reported by Carlson et al. (1999), and showed how these could be combined into a multi-kinetic model which predicts parameters in samples where a range of kinetic species are present. While their laboratory data favour linear fanning Arrhenius plot models,

Ketcham et al. (1999) found that the predictions of curvilinear models provide a closer match to their chosen geological constraints than the linear models.

Precision and accuracy of model predictions in geological conditions

Application of any empirically-constructed kinetic model based on laboratory data to derive meaningful constraints from measured data in geological conditions depends critically on the accuracy and precision involved in the extrapolation of the model over many orders of magnitude in time, and validation of such models is an important step in reliable practical application.

Green et al. (1989) quantitatively assessed the precision associated with extrapolation of the Laslett et al. (1987) model from laboratory to geological timescales, suggesting typical uncertainties of $\sim 0.5 \mu\text{m}$ for mean lengths around $10 \mu\text{m}$ or less, and $\sim 0.3 \mu\text{m}$ for mean lengths longer than $10 \mu\text{m}$. These figures are equivalent to an overall uncertainty in estimates of maximum paleotemperature derived using this approach of around $\pm 5^\circ\text{C}$ (95% c.l.).

Accuracy in this context means the degree to which model predictions reproduce the behaviour of the natural system. This was also assessed in detail by Green et al. (1989), who showed that predictions based on the Laslett et al. (1987) model agree well with observed AFTA parameters in samples from temperatures less than about 70°C from a series of reference wells in the Otway Basin of south-east Australia (Fig. C.10). A systematic mismatch above 70°C (Fig. C.10) can be explained by the difference between the composition of the Durango apatite used in the Laslett et al. (1987) model and the apatites in samples from the Otway Basin, which contain a much broader range of Cl contents (see Fig. C.6 which shows chlorine data in samples from the same data set). As also shown in Fig. C.10, other mono-compositional models provide predictions which differ widely from those of the Laslett et al. (1987) model, and are clearly not as accurate in geological conditions. Corrigan (1993) reached somewhat different conclusions from a similar analysis based on data from the US Gulf Coast, but the most important factor is that different laboratory models give different predictions in geological conditions. Any mismatch between predicted and observed geological behaviour inevitably implies that use of such models to extract thermal history information will inevitably result in unreliable results.

In comparing model predictions with measured data from geological samples, it is vital to ensure that the models used are appropriate to the apatite compositions present in the sample. Fig. C.10 also shows predictions from our own multi-compositional model, together with those from the model of Ketcham et al. (1999). Both these approaches take explicit account of the distribution of wt% Cl in the

sample and the systematic change in annealing properties with increasing Cl content, and both provide a close match to the measured data, with the main difference being a greater dispersion of data in apatites from different Cl contents using the Ketcham et al. (1999) model. Both approaches are also calibrated by a combination of laboratory and geological annealing constraints, so the improved match for the multi-compositional models in Fig. C.10 should perhaps not be too surprising. But the improved accuracy of these models compared to the mono-compositional models reflects the inherent limitations of models based on laboratory data alone, and illustrates the benefits of incorporating geological constraints into model calibration.

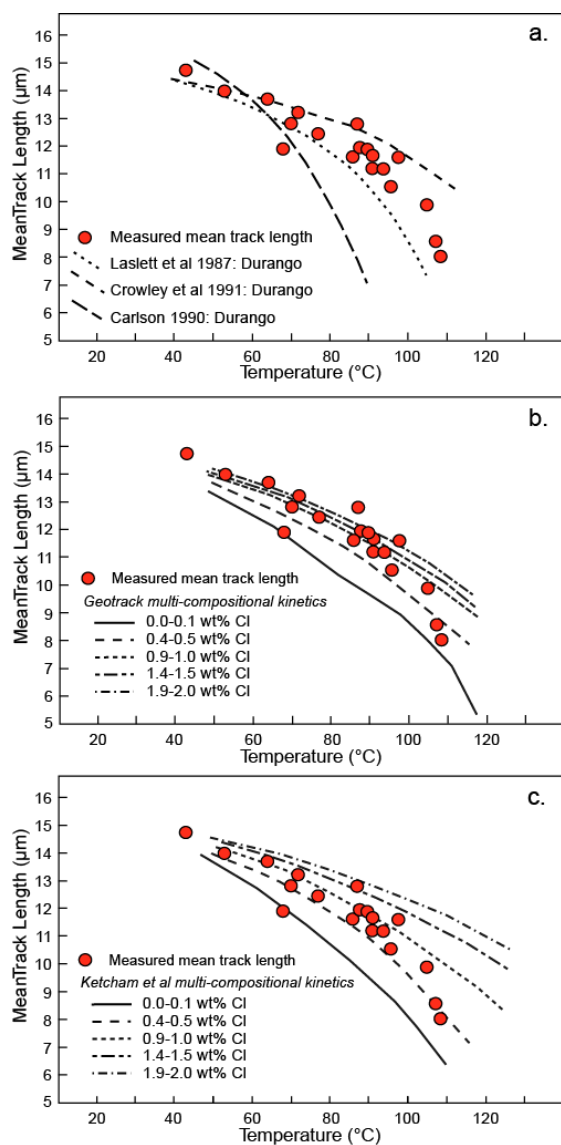


Fig. C.10: Measured mean track lengths in samples from a series of reference wells in the Otway Basin of southeast Australia, compared with values predicted from various annealing models. In a., three mono-compositional annealing models, all based on laboratory annealing in Durango apatite, show various degrees of mismatch to the measured data, emphasising the need for geological calibration in order to make reliable predictions. The Laslett et al. (1987) model provides a reasonable match to the data, while those of Crowley et al (1991) and Carlson (1990) depart significantly from the measured values. In contrast, predictions from Geotrack's multi-compositional model (b.) show a good match to the measured values (which should not be surprising, as data similar to these were employed in construction of the model). Predictions from the model of Ketcham et al (1999), using chlorine as the kinetic parameter (c.) also show a reasonable fit to the data, but show a greater dispersion over the range from 0.0 to 2.0 wt% Cl compared to the Geotrack model.

Accuracy of model predictions at low temperatures

Application of the Laslett et al. (1987) kinetic model to extract thermal history information from AFT data in outcrop samples (using approaches discussed in a later Section) has in many cases resulted in histories involving Late Cenozoic cooling from temperatures around 60°C. This is widely considered to represent an artefact, reflecting the inaccuracy of the model at low temperatures (e.g. Hendriks and Andriessen, 2002; Stephenson et al. 2006).

Vrolijk et al. (1992) studied low temperature annealing in detail, using data in apatites from samples of core from Ocean Drilling Program sites in the Western Pacific, which they suggested can confidently be shown to have never experienced temperatures in excess of 25°C at any time after deposition. In their key sample, MB-7, Vrolijk et al. (1992) reported a mean track length of $14.6 \pm 0.1 \mu\text{m}$, which is considerably shorter than the value of $\sim 15.3 \mu\text{m}$ predicted from the Laslett et al. (1987) model for the reconstructed thermal history of these samples. Thus, they concluded that the Laslett et al. (1987) overestimated the observed track length, suggesting that the model is over-retentive at low temperatures. Predicted values using a number of other models were also longer than the observed mean track length.

However, the comparison of predicted and measured values in the Vrolijk et al. (1992) study is compromised by several issues. For example, the Laslett et al. (1987) model strictly relates only to data generated in exactly the same manner as the data from which the model was originally derived (Green et al., 1986). Inter-laboratory differences, and even within-laboratory differences between different analysts, can easily account for differences in mean track length of the order of 0.5 μm (Barbarand et al., 2003a,b). In addition, the confined track length measurements reported by Vrolijk et al. (1992) were produced using collimated ^{252}Cf fission fragment tracks as hosts for "Tracks-IN-Track" (TINTS). As Barbarand et al. (2003b) reported that measurements on TINTS tend to produce rather shorter mean lengths compared to measurements of "Track-IN-CLeavageS" (TINCLES), some of the reported difference between measured and predicted mean length reported by Vrolijk et al. (1992) could have arisen from this source.

But perhaps the most important factor that could explain at least some of the reported difference is apatite composition. Vrolijk et al. (1992) report a mean Cl content of 0.13 wt% for the MB-7 apatite, as compared with 0.43 wt% in Durango apatite on which the Laslett et al. (1987) model is based. On the basis of evidence discussed earlier, the MB-7 apatite should thus be more easily annealed, and therefore should give a shorter mean track length, than predicted from the Laslett et al. (1987) model, exactly as observed. In fact, since most common apatites tend to contain less than 0.1 wt% Cl, it



should be expected that the apatites analysed in most published studies might be more sensitive than Durango apatite. Thus, it is possible that much of the so-called anomalous Late Cenozoic cooling reported in many studies could be due to such compositional effects, rather than any innate deficiencies in the model (Green, 2004).

In addition to the factors discussed above, it seems far from clear that the thermal histories employed by Vrolijk et al. (1992) are as well controlled as they suggest, and changing the maximum temperature of a sample by as little as 10°C could have a major impact on the expected mean track length.

Spiegel et al. (2007) developed and extended the concept of analysing samples from ODP cores, making explicit allowance for compositional influences on annealing. They compared measured mean track lengths in shallowly buried volcanic apatites with values predicted from reconstructed thermal histories based on the Laslett et al. (1987) model and the Ketcham et al. (1999) model, finding that each model successfully predicted some values and performed less well with others, with differences related to apatite composition. In Fig. C.11, we compare the measured mean track lengths with the predicted values from these two models and also with values predicted using the Geotrack multi-compositional model. For the Geotrack and Ketcham et al. (1999) models, kinetics appropriate to the Cl content of each sample have been used. We note that in three of the samples reported by Spiegel et al. (2007) (samples 43-10, 47-3 and 47-7) the measured mean track lengths appear to be anomalously low compared to those in adjacent samples with similar compositions. This is most likely due to the presence of shorter track lengths from grains derived from older sources, which is supported by the larger than usual standard deviations reported for these three samples compared to the rest of the dataset (Spiegel et al. 2007, Table 4). Results from these three samples have therefore been omitted from Fig. C.11.

Values predicted using the three models give rather different results in Fig. C.11. Values predicted using the Geotrack model are up to ~0.25 μm less than the measured values at the highest and lowest mean Cl contents, although the agreement is excellent for compositions between 0.2 and 0.8 wt% Cl. Values predicted using the Ketcham et al. (1999) model are more consistently around 0.5 μm less than measured values over the entire compositional range. In contrast, values predicted using the Laslett et al. (1987) model for apatites containing 0.0-0.2 wt% Cl are around 0.5 μm longer than the measured values (as expected from the above discussion), and this difference first increases and then decreases with increasing wt% Cl, such that for Cl contents around 0.8 wt% Cl the agreement is excellent. While mean track lengths for apatites of similar composition to Durango apatite (~0.4 wt% Cl) are shorter than predicted, the general level of agreement of values

predicted from the Laslett et al. (1987) model in Fig. C.11 should be regarded as impressive, since this model is based purely on extrapolation of laboratory data, with no geological control, yet the agreement is almost as good as for models which directly incorporate geological constraints. It should be clear from Fig. C.11 that any failure of this model at low temperatures is relatively minor, and in particular, the prediction from this model of significant length reduction even at temperatures as low as 10°C over geological timescales closely reproduces the natural system behaviour, as discussed further below. We should also note that the comparisons by Spiegel et al. (2007) are subject to the same issues with respect to possible analytical differences as discussed in relation to the Vrolijk et al. (1992) study, above.

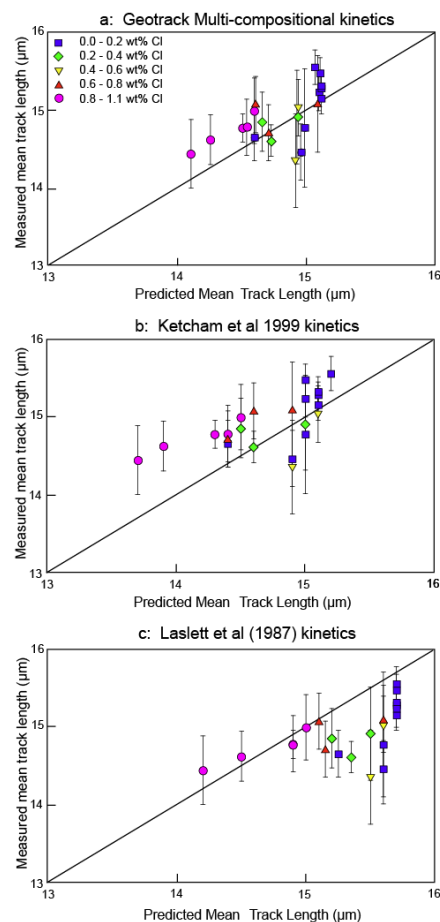


Fig. C.11: Measured mean track lengths in a series of samples designed to provide constraints on low temperature annealing behaviour in geological conditions (from Spiegel et al., 2007), plotted against the values predicted from various annealing models. Apatite compositions are shown, and kinetics appropriate to each composition have been used for the two multi-compositional models in a. and b.. Values predicted using the Geotrack model (a.) show generally excellent agreement overall, while being up to ~0.25 μm less than the measured values at the highest and lowest mean Cl contents. Values predicted using the Ketcham et al. (1999) model (b.) are more consistently around 0.5 μm less than measured values over the entire compositional range, while values predicted using the Laslett et al. (1987) model (c.) are around 0.5 μm longer than the measured values for apatites containing 0.0-0.2 wt% Cl, with the disparity increasing to slightly over 0.5 μm for compositions similar to Durango apatite (~0.4 wt% Cl) and then decreasing at higher Cl contents, such that around 0.8 wt% Cl the agreement is excellent. While it is clear that multi-compositional models provide better matches to the low temperature constraints, the general level of agreement of values predicted from the Laslett et al. (1987) model should be regarded as impressive, since this model is based purely on extrapolation of laboratory data, with no geological control, yet the agreement is almost as good as for models which directly incorporate geological constraints. This disproves the common misconception that the Laslett et al. (1987) model is too sensitive at low temperatures, as discussed in the text.



C.2 Extracting thermal history information from AFTA data

Basic system response

Understanding the thermal history response of fission tracks in detrital apatites to heating and cooling is fundamental to appreciating how the technique can

be applied in practice. The basic system response within a typical sedimentary basin framework, based on principles outlined in Fig. C.5, is illustrated in Fig. C.12. The nature of this response is common to all forms of kinetic models discussed earlier, and is a fundamental property of the AFT system.

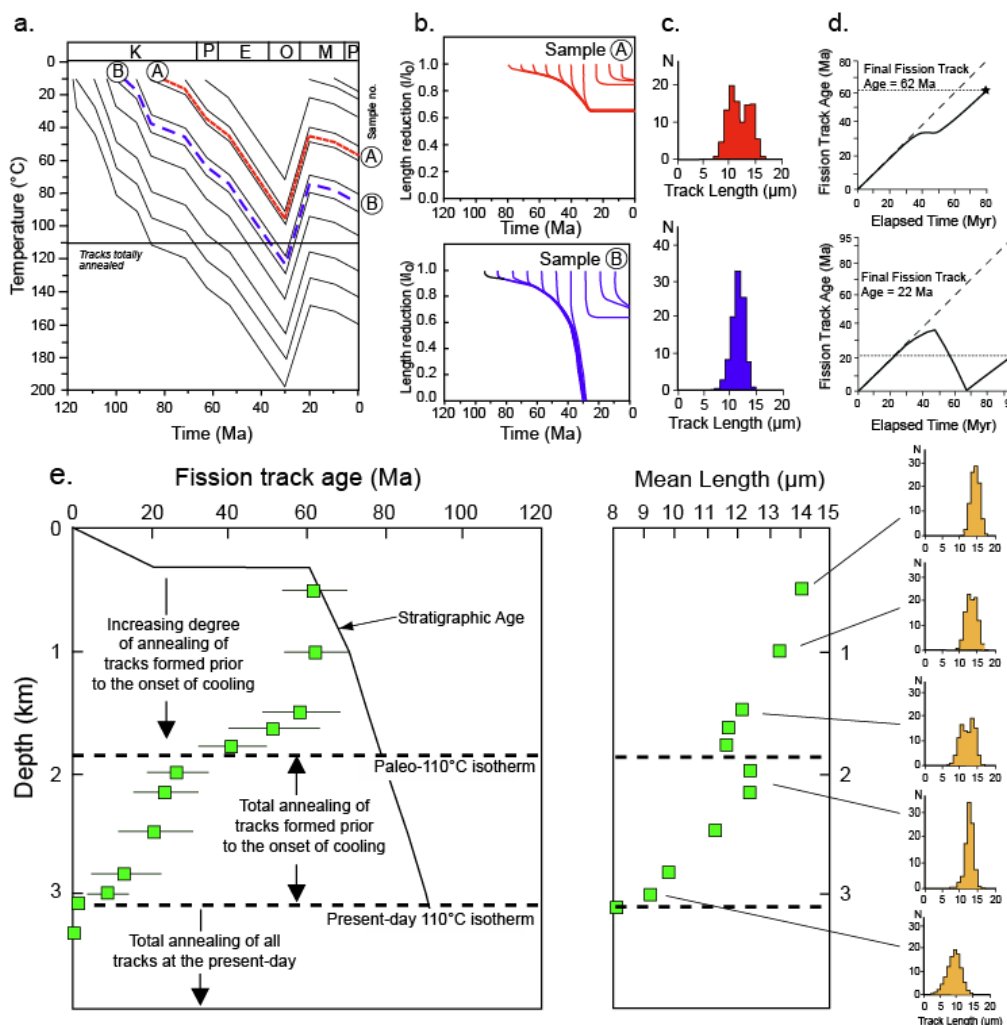


Fig. C.12: Thermal history response of fission tracks in apatite under geological conditions. While this is based on a mono-compositional apatite of Durango composition using the Laslett et al. (1987) model, the nature of this response is common to all forms of kinetic models, and is a fundamental property of the AFT system governed by a fanning Arrhenius plot. **a.** Notional thermal history for a sedimentary sequence that underwent progressive burial through the Cretaceous to middle Cenozoic, followed by cooling due to uplift and erosion commencing at 30 Ma and completed by 20 Ma, with minor reburial from 20 Ma to the present-day. The thermal histories of two samples A. and B. are shown. **b.** Track length shortening trajectories for tracks produced at different times in Samples A and B. As temperature increases, the length of all tracks is progressively reduced, and because temperature dominates over time in the kinetics of annealing, at any time during this phase of the history all but the most recently formed tracks at any given time have the same mean length (although each population of tracks has a finite spread in length). At the point when the maximum temperature is reached and the history changes from heating to cooling, all tracks formed up to that point in time are effectively “frozen” at the length to which they have been reduced. They do not undergo further shortening because annealing rates are much slower at the reduced temperatures now prevailing, and they do not get longer because the annealing process is irreversible. Those tracks formed after the onset of cooling remain longer because of the lower annealing rates at the prevailing lower temperatures. Sample B reached a maximum temperature sufficient to reduce the length of all tracks produced up to that time to zero. At the present day, this sample contains only one track population, formed after the sample cooled to temperatures at which tracks could be retained (~110°C for typical apatite compositions). **c.** Track length distributions for sample A and B resulting from the thermal histories shown in **a.** For sample A, two populations of tracks are present in this sample at the present-day: a shorter population representing tracks formed up until the onset of cooling from the paleo-thermal maximum, and a longer population formed after the onset of cooling. For sample B, the measured track length distribution will reflect the thermal history in the post-cooling period only. **d.** Evolution of fission track age with time resulting from the thermal histories shown in **a.** For sample A, the final measured fission track age will represent the summed contributions from the shorter population of tracks which will contribute a reduced component to the fission track age compared to the time interval over which tracks have been retained, while the contribution to the fission track age of the longer population will be much closer to the time elapsed since the onset of cooling. For sample B, the final fission track age will be determined by the time when the sample began to retain tracks, but moderated by the degree of length reduction of tracks formed during the cooling history. **e.** Predicted variation of fission track parameters with depth for a well section which has undergone a thermal history of the style shown in **a.** Fission track age declines rapidly with increasing depth through the shallower section, as the mean length of the shorter population of tracks (formed up to the onset of cooling) is progressively shortened and the proportion of these tracks that can reach the polished grain surface and be revealed decreases. Similarly, the mean track length reduces due to the decreasing mean length of the shorter population. But as the depth (and temperature of ~110°C) corresponding to total annealing of all tracks formed prior to the onset of cooling is approached, the mean track length begins to increase again, as the shorter population of tracks becomes increasingly difficult to reveal and therefore contributes less to the overall mean for the sample which is increasingly dominated by the longer population of tracks formed after cooling. As the transition from partial to total annealing of tracks formed prior to cooling is crossed at the paleo-isotherm of ~110°C, the mean track length increases abruptly as the sample is now dominated only by longer tracks formed after the onset of cooling. And the fission track age reduction shows a characteristic “break in slope”, below which only a single component of tracks is present, with parameters controlled by the history after the onset of cooling. With further increase in depth, both the fission track age and mean track length show progressive reduction to zero at a present-day ~110°C, although in detail this temperature is controlled by apatite composition and the timescale of heating/burial.



For Sample A in Fig. C.12a, as temperature increases (representing increased burial depth in this example) the length of all tracks is progressively reduced, and because temperature dominates over time in the kinetics of annealing, at any time during this phase of the history all but the most recently formed tracks at any given time have the same mean length (Fig. C.12b) (but remember that each population of tracks has a finite spread in length). At the point when the maximum temperature is reached and the history changes from heating to cooling, all tracks formed up to that point in time are effectively “frozen” at the length to which they have been reduced. They do not undergo further shortening because annealing rates are much slower at the reduced temperatures now prevailing, and they do not get longer because the annealing process is irreversible. Those tracks formed after the onset of cooling remain longer because of the much lower annealing rates at the prevailing lower temperatures.

At the end of the history (i.e. the present day), two populations of tracks are present in Sample A; a shorter population representing tracks formed up until the onset of cooling from the paleo-thermal maximum, and a longer population formed after the onset of cooling, resulting in a bimodal track length distribution (Fig. C.12c). The shorter population of tracks will contribute a reduced component to the fission track age, compared to the time interval over which tracks have been retained, while the contribution to the fission track age of the longer population will be much closer to the time elapsed since the onset of cooling. The final measured fission track age will represent the summed contributions of both components (Fig. C.12d).

Sample B in Fig. C.12a reached a maximum temperature sufficient to reduce the length of all tracks produced up to that time to zero (Fig. C.12b) (i.e. all the radiation damage has been repaired and no etchable tracks remain). At the present day, this sample contains only one track population (Fig. C.12c), formed after the sample cooled to temperatures at which tracks could be retained (~110°C for typical apatite compositions). The track length distribution in this sample will reflect the thermal history in the post-cooling period, while the fission track age will be determined by the time when the sample began to retain tracks, but moderated by the degree of length reduction of tracks formed during the cooling history (Fig. C.12d).

Extending these basic principles through the vertical section results in the variation of fission track age and mean track length with depth shown in Fig. C.12e, which is characteristic of a section which has cooled from higher temperatures. Fission track age declines rapidly with increasing depth through the shallower section, as the mean length of the shorter population of tracks (formed up to the onset of cooling) is progressively shortened and the proportion of these tracks that can reach the polished grain surface to be

revealed decreases. Similarly, the mean track length reduces due to the decreasing mean length of the shorter population. But as the depth (and temperature) corresponding to total annealing of all tracks formed prior to the onset of cooling is approached, the mean track length begins to increase again, as the shorter population of tracks becomes increasingly difficult to reveal and therefore contributes less to the overall mean for the sample, which is increasingly dominated by the longer population of tracks formed after cooling. As the transition from partial to total annealing of tracks formed prior to cooling is crossed, the mean track length increases abruptly as the sample is now dominated only by longer tracks formed after the onset of cooling. And the fission track age reduction shows a characteristic “break in slope”, below which only a single component of tracks is present, with parameters controlled by the history after the onset of cooling. With further increase in depth, both the fission track age and mean track length show progressive reduction to zero at a temperature controlled by apatite composition and the timescale of heating/burial, similar to the simple situations illustrated in Fig. C.3.

What information is contained in fission track age and length data?

Fig. C.12 illustrates how samples at different depths through a vertical section contain different types of information regarding the underlying thermal history. In samples shallower than the transition from partial to total annealing, which we will refer to as the “paleo-110°C isotherm” (although we stress that in detail this temperature will depend on apatite composition and timescale of heating), the length of the shorter component of the track length distribution is determined by the maximum temperature to which each sample was heated. And the proportion of short to long tracks at any given horizon is determined by the ratio of the time prior to cooling and the time after cooling (moderated by the geometric biases in revealing tracks of different length as described by Laslett et al. 1982). The fission track age is determined by a combination of these factors, and has no fundamental significance in its own right (i.e. the fission track age does not denote a time at which some specific event occurred). In contrast, samples from below the paleo-110°C isotherm contain only tracks formed after cooling, and therefore only provide a minimum estimate of the maximum temperature. But the fission track age in such samples is controlled by the time at which the samples cooled through the paleo-110°C isotherm, again moderated by the track length reduction as a result of the history after the onset of cooling.

To summarise, for the style of history illustrated in Fig. C.12, which is typical of exhumed sedimentary basins, AFTA can provide the following information:

In samples shallower than the paleo-110°C isotherm:

- maximum paleotemperature from the mean length of the shorter component
- onset of cooling from the proportion of short to long tracks
- additional refinement of the above from the degree of fission track age reduction

In samples deeper than the paleo-110°C isotherm:

- minimum estimate of the maximum paleotemperature
- onset of cooling from the combination of fission track age and track lengths

Thus, we obtain different types of thermal history information from different facets of the data at different positions within the section in Fig. C.12. The practical consequence of this is that in order to obtain the maximum amount of information from AFTA it is necessary to analyse a sequence of samples spanning a range of vertical horizons. As a corollary of this, the amount of information that can be obtained from a single sample may be limited.

What information is NOT contained in AFTA data?

Also implicit in Fig. C.12 is the fact that there is a definite limit to the amount of information that can be obtained from AFTA data in such situations. In any sample from a depth shallower than the paleo-110°C isotherm, when the paleo-thermal maximum is reached track populations formed at different times through the history are reduced to more or less the same mean track length (but note that a finite spread in length will be present because of the inherent distribution of track lengths). For this reason, all information on the prior history of such samples has been lost (except for the total duration over which tracks have been retained, and this can be very difficult to reconstruct, as discussed below. Fig. C.13 illustrates how successive heating episodes overprint the effects of earlier episodes, leaving only evidence of the maximum temperature episode and the subsequent history after cooling from the paleo-thermal maximum. Thus **AFTA data are sensitive only to the magnitude of the maximum temperature and the timing of the onset of cooling (in relation to the overall time over which tracks have been retained), and preserve no information on the prior history (except that temperatures must have been lower than at the paleo-thermal maximum).**

Similar considerations apply to scenarios involving continuous cooling histories, as shown in Fig. C.14, which illustrates the insensitivity of such histories to the detailed variation of temperature with time. Perhaps most importantly, the final AFTA parameters are particularly insensitive to the earliest history, which provides such a minor degree of information to the fission track age and track length distribution that

huge differences in time produce insignificant changes in the expected parameters which are beyond practical resolution. Thus, in monotonic cooling histories, the data are insensitive to the early history and specifically to the time at which the sample began to retain tracks.

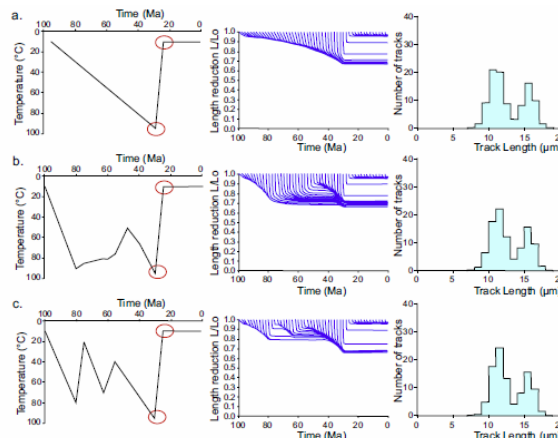


Fig. C 13: Shortening trajectories (centre) for tracks produced at different times through three thermal history scenarios (left) representing increasing levels of complexity from a. through c. The resulting track length distributions are also shown (right). Despite the obvious differences in the thermal histories, the resulting track length distributions are effectively identical because the time and magnitude of maximum temperatures are the same for each history (circled points on the thermal histories). This outcome reflects the fundamental kinetics of the AFT system such that the data are sensitive only to the magnitude of the maximum temperature and the timing of the onset of cooling (in relation to the overall time over which tracks have been retained), and preserve no information on the prior history (except that temperatures must have been lower than at the paleo-thermal maximum). Thus, successive heating episodes overprint the effects of earlier episodes, leaving only evidence of the maximum temperature episode and the subsequent history after cooling from the paleo-thermal maximum... by the evolution of track lengths with time for history. It is therefore not possible to discriminate between these three scenarios from apatite fission track data.

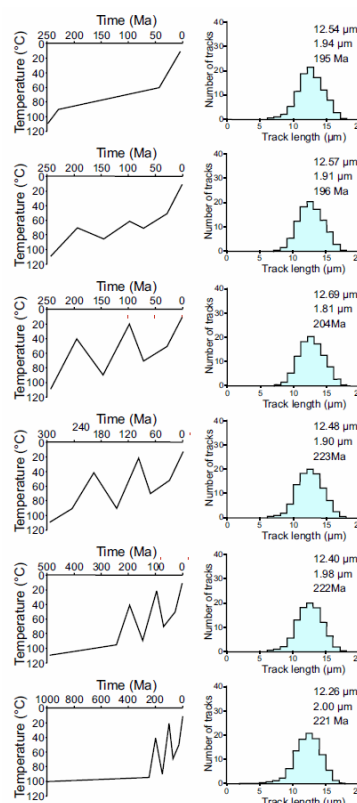


Fig. C.14: Predicted track length distributions (also listing the predicted mean track length, standard deviation of the length distribution and apatite fission track age) for a series of cooling histories of increasing complexity. The fission track parameters resulting from these histories are indistinguishable, despite the time of cooling below 110°C varying from 250 Ma to 1000 Ma, and for histories

ranging from progressive cooling to various more complex heating and cooling histories. The final AFTA parameters are particularly insensitive to the earliest history, which provides such a minor degree of information to the fission track age and track length distribution that huge differences in time produce insignificant changes in the expected parameters which are beyond practical resolution. Predictions based on a mono-compositional apatite of Durango composition using the Laslett et al. (1987) model.

Note that Figs. C.12, C.13 and C.14 are constructed for mono-compositional apatites, but the principles involved are equally applicable to apatites containing a range of annealing properties (due to differing Cl contents). As illustrated in Fig. C.9, AFTA data from the Fresne-1 well in the Taranaki Basin of New Zealand (Crowhurst et al. 2002) provides a multi-compositional counterpart involving real data for comparison with the notional mono-compositional data in Fig. C.10.

Practical implementation

Because of the high degree of redundancy in the data (i.e. many histories result in the same measured age and length parameters, Figs. C.13, C.14), extraction of explicit thermal history solutions directly from apatite fission track data is not possible. Instead, the problem is approached by forward modelling the parameters expected from a range of specified thermal histories and defining the range of conditions that provide predictions that are consistent with the measured data.

Our approach is designed primarily for application to sedimentary basins, and takes account of the fact that sedimentary horizons are deposited at the surface and then buried/heated to some maximum depth/temperature, after which they may be exhumed and cooled. By modelling expected AFTA parameters resulting from a range of possible thermal histories, we can define the range of values of maximum paleotemperature and the onset of cooling giving predictions which match the measured data within 95% confidence limits, using likelihood theory similar to that described by Gallagher (1995). The basic principles involved are illustrated in Fig. C.15 for a mono-compositional apatite, while Fig. C.16 illustrates the extension of these principles to multi-compositional data.

It is important to stress that no attempt is made to define the whole thermal history, because the post-depositional history prior to the onset of cooling is overprinted by the paleo-thermal maximum (Fig. C.12). For this reason we focus on determining those aspects of the thermal history that directly control the measured AFTA parameters, viz. the maximum paleotemperature and the time at which cooling from the paleo-thermal maximum began. Additional episodes of heating and cooling following the onset of cooling from the paleo-thermal maximum can often be resolved, as discussed in more detail in Section C.3.

The episodic heating and cooling approach is designed specifically for application to sedimentary basins, but we also believe that it is relevant to many (if not all) basement terrains, and such an approach is

essential in basement regions where sedimentary outliers occur, revealing earlier cycles of exhumation, burial and re-exhumation (e.g. Green and Duddy, 2006; 2007).

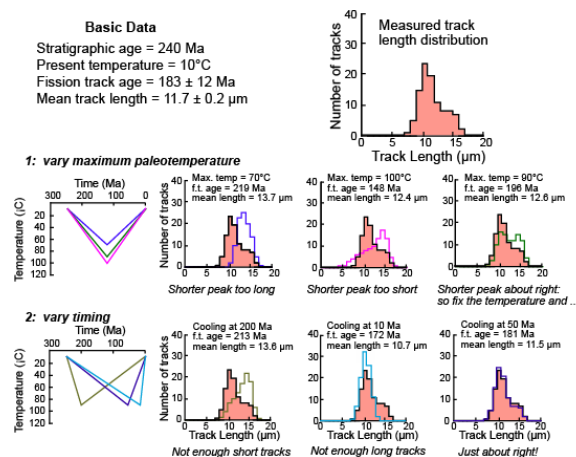


Fig. C.15: Principles of AFTA interpretation illustrated for a mono-compositional apatite, showing how a thermal history solution can be extracted from measured AFTA parameters (fission track age, mean track length and track length distribution). For samples of sedimentary rock it is necessary to know the stratigraphic age and present temperature of the sample. In principle, the surface temperature at the time of deposition is also required, but because the maximum temperature is the major control on track length (e.g. Figs. C.12 to C.14), the influence of the depositional temperature is minimised once the sediment is heated above -50°C . By predicting the AFTA parameters for various thermal history scenarios we can define the best-fit thermal history. As a first step, we assume that cooling from the maximum paleotemperature occurred at the midpoint of the history (120 Ma in this case). By varying the maximum temperature and comparing measured and predicted parameters, we find a good match with the shorter population of tracks in the measured track length distribution at a maximum paleotemperature of 90°C . But the predicted track length distribution contains too many long tracks. A good match between the predicted and measured track length distributions, as well as the fission track age, is achieved with cooling commencing at 50 Ma, while keeping the maximum temperature constant at 90°C . Note that no attempt is made to define the whole thermal history, because the history prior to the onset of cooling is overprinted by the thermal maximum. Note also that by itself, the measured fission track age of 183 ± 12 Ma provides no information on the time of cooling, which only comes from kinetic modelling of the details of the track length distribution together with the fission track age. Predictions based on a mono-compositional apatite of Durango composition using the Laslett et al. (1987) model.

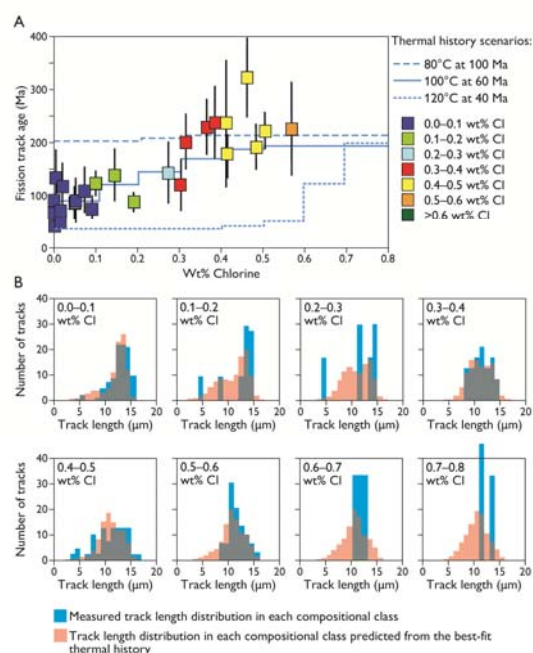


Fig. C.16: AFTA interpretation methodology for a multi-compositional apatite. The same basic information and interpretation strategy as described in Fig. C.15 is used for samples which contain apatite of different compositions, but supplemented by the wt% chlorine of each apatite grain (measured by electron microprobe) in which a fission track age or track length is measured. Fission track ages and track lengths are grouped according to the chlorine content into 0.1 wt% Cl intervals and a multi-compositional annealing model is used which takes specific account of the influence of wt% Cl on annealing rates. The



matching procedure is the same as for a single composition, but now involves the simultaneous matching of fission track age and the details of the track length distribution in all compositional groups present in the sample. In the example, 8 groups are present containing between 0 and 0.8 wt% Cl, and the best-fit match to the data is achieved for cooling from a maximum temperature of 100°C beginning at 60 Ma (real data in a Permian sandstone outcrop sample from NE England).

A multi-compositional annealing model is used which takes specific account of the influence of wt% Cl on annealing rates. This model consists of a series of parallel kinetic equations, each taking the form of a linear fanning Arrhenius plot with non-zero intercept (Laslett et al., 1987; Crowley et al., 1991; Ketcham et al., 1999), with coefficients which vary systematically with wt% Cl. In many respects the Geotrack multi-compositional annealing model is similar to that of Ketcham et al. (1999), and gives similar predictions (cf Fig. C.10).

Wherever possible, AFTA data are integrated with data from other paleo-thermal indicators such as vitrinite reflectance, and/or indicators of burial such as sonic velocity (discussed later). Such data provide an independent check on the interpretation of the AFTA data, and ensure that the resulting thermal histories and the information derived from them are not affected by artefacts of any individual technique.

One of the advantages of this approach is that determination of maximum paleotemperatures from AFTA data in a series of samples over a range of depths or elevations allows definition of the variation of paleotemperatures with depth, which in turn provides unique insights into the underlying mechanisms of heating and cooling, as described in a later section.

Summary comments.-

In all approaches which involve extracting quantitative thermal history constraints from apatite fission track data, it should be appreciated that the resulting thermal history solution will only ever be an approximation to the true underlying history. Whether monotonic cooling histories or episodic heating and cooling is employed, for any but the simplest of histories, factors such as the natural spread in the track length distribution, which increases as tracks are progressively shortened (Green et al., 1986), plus the high level of redundancy in the data resulting from the basic nature of the system response, as discussed earlier, impose fundamental limits to the detail that can be resolved.

These factors must be borne in mind in considering information derived from AFT data in individual samples. We suggest that failure to fully appreciate the limitations of the method lies behind many perceived problems with published AFT studies (e.g. Gunnel, 2000), and in many cases too much is expected from the technique. We suggest that it is when attention is focussed on the unique information that can be obtained that the power of the technique becomes apparent.

C.3 Practical issues in interpreting and understanding AFTA data

The meaning of a fission track age

Fission track ages from crustal sections are often discussed in terms of a zonation of ages (e.g. Naeser et al., 1989) with ages being unaffected at shallow depths (“Zone of No Annealing”, <70°C), while at depths greater than ~3 - 4 km (temperatures in excess of ~125°C), no tracks are retained (“Total Annealing Zone”). Between these two extremes, fission track ages are progressively reduced to zero through a “Partial Annealing Zone” or “PAZ”. While this zonation provided a simple conceptual basis for early studies based on ages alone, the combination of borehole data (Gleadow and Duddy, 1981) and laboratory experiments (Green, 1988) showed that fission track age and length reduction proceed even at temperatures below 70°C, albeit more slowly than at higher temperatures. This can be seen most easily in confined track length data due to the higher precision of these measurements compared to fission track ages (Fig. C.3).

For this reason, a measured fission track age only rarely indicates the time over which tracks have been retained in an apatite grain. In the same way, a fission track age rarely reflects a “cooling age”, and we recommend that this term should not be used in any circumstances. In slowly cooled terrains, radiometric ages are often referenced to a “closure temperature”, below which the daughter product (in our case, a fission track) is effectively retained. However, given the lack of stability of fission tracks in apatite even at low temperatures, this concept is of dubious validity for fission track ages in apatite, and it is not possible to literally relate a fission track age to a specific point on a cooling path. Instead, **an apatite fission track age should be regarded as an integrated measure of the balance between the production of tracks by spontaneous fission and the reduction in track density due to the reduction in track length which results from the thermal history.**

Only in samples which have cooled extremely rapidly to temperatures less than 50°C and subsequently remained at such temperatures will the fission track age be close to the time over which the sample has been cool enough to retain tracks. Experience has shown that such situations are rare. More commonly, the fission track age and length data must be assessed in tandem, using the quantitative modelling approach described earlier in order to extract information on the timing (and magnitude) of cooling events from the data.

Long term residence in the Partial Annealing Zone vs heating and cooling

It is a common fallacy that the presence of an exhumed partial annealing zone, as identified for

example by a break in slope in the variation of fission track age with depth (cf. Figs. C.3, C.9) represents a prolonged period of residence in the Partial Annealing Zone prior to exhumation. Consideration of Fig. C.12 shows that this is not necessary, as this type of data is easily produced by heating (e.g. by burial) of the sequence to temperatures characterising the PAZ followed immediately by rapid subsequent cooling/exhumation. This misunderstanding arises, in part, because of the common adoption of monotonic cooling histories for explaining apatite fission track data, which is discussed in more detail below.

“Boomerang plots”

Green (1986) showed that in a sequence of rocks from the NW of England that have undergone a single dominant episode of heating and subsequent cooling, with individual samples reaching different maximum temperatures prior to the onset of cooling, the relationship between mean confined track length and fission track age showed a systematic variation defining a “boomerang-shaped” trend (Fig. C.17). Samples that have undergone only minor thermal disturbance have old ages with relatively long mean track lengths, while samples in which all fission tracks were totally annealed prior to the onset of cooling give much younger fission track ages (“reset ages”), also characterised by long (~14 μm) mean lengths. Between these two extremes, as the fission track age decreases (representing increasing maximum paleotemperatures prior to the onset of cooling) the mean track length decreases as the partially annealed tracks are progressively shortened. This continues until the final stages of age reduction, when the partially annealed tracks become so short that their contribution to the mean length is diminished and the mean length increase with further reduction in fission track age, trending upwards towards the long mean length characterising the reset ages. The variation in Fig. C.17 is analogous to that illustrated in Fig. C.10, except that samples from different depths/temperatures return to the surface at low temperature after the onset of cooling, and thus each sample contains a similar population of long tracks, in addition to the shorter population which has been annealed to differing degrees in different samples reflecting different maximum paleotemperatures prior to the onset of cooling.

Returning to the question of the meaning of a fission track age, from above, Fig. C.17 illustrates the way in which partially reset fission track ages reflect the degree of shortening of those tracks formed prior to the onset of cooling. Only those samples in which all tracks were totally annealed give fission track ages around 60 Ma, but ALL samples underwent cooling at this time. The measured fission track age in any other sample provides no direct indication of the timing of any event in its own right.

Gallagher and Brown (1997) emphasised the usefulness of this type of plot in considering the implications of regional AFT datasets, albeit in the context of monotonic cooling. But in many regions, age vs. length data show a very different type of trend to the simple pattern reported by Green (1986). For example, results from Norway (Rohrman et al. 1995) show an almost opposite relationship to the classic “boomerang” trend, while data from Africa and Brazil (Gallagher and Brown. 1999a, 1999b) show wide dispersion with only a slight tendency towards longest lengths associated with the youngest ages. Compared to the simple situation in NW England where a single dominant heating/cooling episode has produced a well-defined trend, non-boomerang style relationships imply a much more complex history, most likely involving a series of paleo-thermal episodes, each of which may vary in magnitude across the region. Therefore, such plots should be interpreted with care, and should always be considered together with the systematic change in the form of the track length distribution through the plot, which was central to the original description by Green (1986).

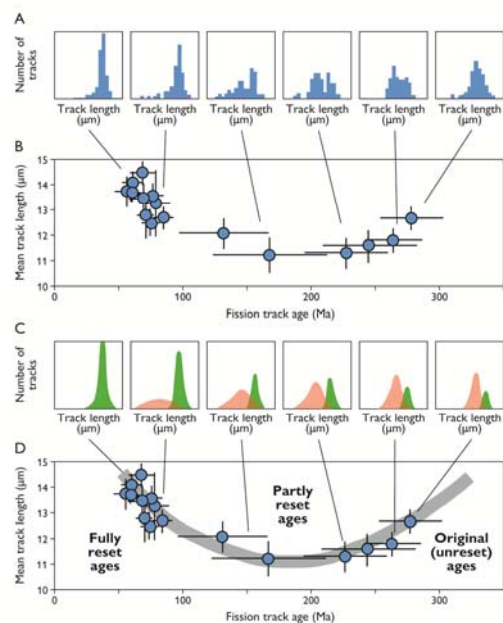


Fig. C.17: Boomerang plot: relationship between mean track length and fission track age for a suite of outcrop samples which have undergone cooling from different maximum paleotemperature at the same time (Green 1986). Samples that have experienced low maximum temperatures have old ages with relatively long mean track lengths, while samples in which all fission tracks were totally annealed prior to the onset of cooling give much younger fission track ages (“reset ages”), also characterised by long (~14 μm) mean lengths. Between these two extremes, as the fission track age decreases (representing increasing maximum paleotemperatures prior to the onset of cooling) the mean track length decreases as the partially annealed tracks are progressively shortened. This continues until the final stages of age reduction, when the partially annealed tracks become so short that their contribution to the mean length is diminished and the mean length increase with further reduction in fission track age, trending upwards towards the long mean length characterising the reset ages. This dataset can be considered analogous to the situation illustrated in Fig. C.12, but with all samples cooling to low (near surface) temperatures, such that each contains a population of long tracks formed after cooling.

Monotonic cooling vs episodic heating and cooling

While clearly not applicable to sedimentary basins, many thermochronological studies are carried out

within a framework involving monotonic cooling from above $\sim 110^\circ\text{C}$ to surface temperatures. Such approaches are routinely applied to basement terrains but even in such regions the presence of the merest veneer of sedimentary cover means that the underlying basement was at the surface when that cover was deposited. Failure to understand this issue can result in quite erroneous interpretations (e.g. Persano et al., 2006; Brown, 2007; Gibson, 2007; Green and Duddy, 2007). While episodic heating and cooling is clearly more realistic in sedimentary basins, as witnessed by the common occurrence of unconformities in sedimentary sequences, we suggest that such histories may also be quite reasonable for many basement terrains. This is clearly appropriate where sedimentary outliers are present, but we see no reason why it should not also be true in areas devoid of present-day cover, which could simply indicate that the former cover has been totally stripped.

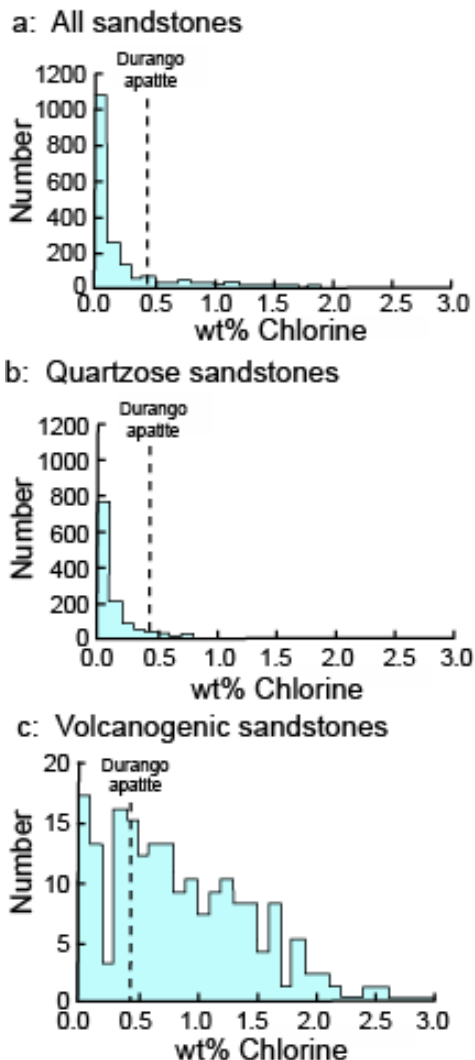


Fig. C.18: Typical distributions of wt% Cl in apatites from different sources. **a:** Histogram of Cl contents (wt%) in over 1750 apatite grains from over 100 samples of various sedimentary and igneous rocks. Most samples give Cl contents below ~ 0.5 wt%, while those apatites giving higher Cl contents are characteristic of volcanogenic sandstones and basic igneous sources. **b:** Histogram of Cl contents (wt%) in 1168 apatite grains from 61 samples which can loosely be characterised as "normal quartzo-feldspathic sandstone". The distribution is similar to that in the upper figure, except for a lower number of grains with Cl contents greater than $\sim 1\%$. **c:** Histogram of Cl contents (wt%) in 188 apatite grains from 15 samples of volcanogenic sandstone. The distribution is much flatter than the other two, with a much higher proportion of Cl-rich grains.

The impact of composition on thermal history interpretation of AFTA data

Natural apatites essentially have the composition $\text{Ca}_5(\text{PO}_4)_3(\text{F},\text{OH},\text{Cl})$. Most common detrital and accessory apatites are predominantly fluor-apatites, but come contain appreciable amounts of chlorine (Fig. C.18). In most quartzo-feldspathic sandstones, the majority of grains contain between 0 and 0.1 wt% Cl, while a smaller number of grains give values up to ~ 0.5 wt% Cl and occasional grains contain up to 1 wt% Cl and above (Fig. C.18a). In contrast, volcanogenic sandstones typically contain apatites showing a much broader spread of Cl contents up to 2 or even 3 wt% and beyond (Fig. C.18b). Cl contents in granitic basement samples and silicic high-level intrusives are typically much more dominated by compositions close to end-member Fluorapatite (Fig. C.18c) while apatites from Gabbroic and other basic intrusive rock types may contain appreciable amounts of Cl, although many exceptions occur to these general rules.

As discussed earlier, the amount of chlorine in the apatite lattice exerts a subtle control on fission track annealing rates, which is typically most pronounced in the temperature range 90 to 120°C (Figs. C.9, C.10). In samples heated to such temperatures, individual apatite grains may show a significant spread in the degree of annealing (i.e. length reduction and fission track age reduction). Such within-sample variation can be very useful in identifying samples exposed to paleotemperatures in this range.

Ignoring the effects of compositional variation can lead to major errors in interpretation, particularly if analytical procedures are not designed to take such effects into account. To illustrate the potential problems that can arise, Fig. C.19a shows a dataset in which grains were selected in a continuous transect across the grain mount, with a thermal history solution extracted by making due allowance for the variation of fission track age and length with wt% Cl. Fig. C.19b illustrates the result of a biased analysis in which fission track ages were measured only in high wt% Cl grains which contain high track densities and which could represent a favourable "target" for counting, while track lengths have been measured in the more common (and more sensitive) apatites containing lower amounts of chlorine. In this case, the thermal history solution extracted from the biased data results in a wildly inaccurate interpretation (Fig. C.19b).

Some workers prefer to use the size of etch pits as a kinetic parameter for resolving differences in annealing within samples (Burtner et al. 1994). But as discussed earlier, etch pit dimensions provide only a very poor indicator of annealing sensitivity (Fig. C.8), and due to the relatively small range of etch pit sizes for most common apatites this approach lacks the resolution that is possible using chlorine content.

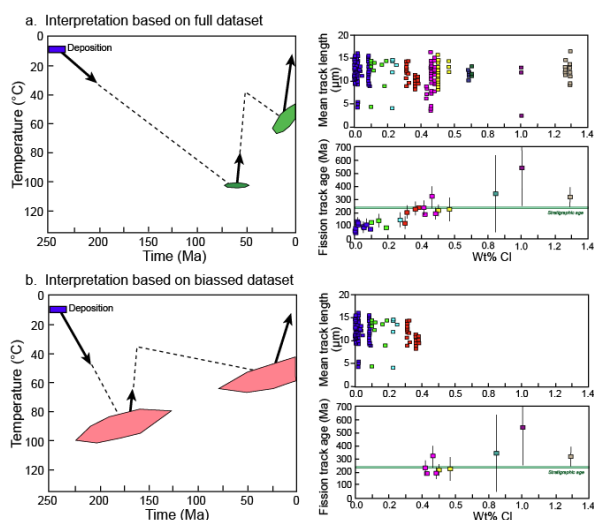


Fig. C.19: Thermal history solutions extracted from AFTA data from the same Triassic outcrop sample. In **a.**, complete allowance made for the variation of fission track age and track length with apatite chlorine content. In **b.**, the solution is based on track length data from only the most abundant (low wt% Cl) grains while fission track ages are measured only in the higher wt% Cl grains. Such a situation could easily arise if ages are only measured in grains containing high track densities, without making due allowance for the influence of wt% Cl. The solution in this case is very different from the correct solution (**a.**), illustrating the problems that can arise if compositional effects are not correctly taken into account.

In addition, use of etch pit sizes is extremely demanding of etching procedures, which must be reproducible to the standards employed in the original calibration experiments (Carlson et al. 1999). And in borehole studies involving conditions where fission tracks in some apatites are totally annealed, measurement of etch-pit sizes in these grains is clearly not possible.

Therefore, to ensure accurate thermal history interpretations from AFTA it is an essential step in data collection that grains should be analysed without reference to track density, Cl content should be measured in every grain for which either fission track age or track length measurements are made, and the data should be assessed in terms of their variation with wt% Cl, as illustrated in Fig. C.16.

Influence of tracks inherited from sediment source terrains

An apatite in which the fission track age is older than the depositional age of the host sedimentary rock clearly retains tracks that were formed in the sediment provenance terrain, prior to deposition. The effect of such tracks is often posed as a potential problem for AFTA. However, this rarely poses practical problems, and can sometimes prove advantageous.

The contribution to the measured fission track age and the length distribution made by these "inherited tracks" will be characteristic of the thermal history of the sediment provenance terrains. The influence of such tracks on the ability to extract information on the post-depositional thermal history of a sedimentary rock from AFTA data will depend essentially on the relative duration and severity of heating during the pre-depositional and post-

depositional history. For example, in apatites derived from an ancient basement terrain and deposited in Neogene sedimentary rocks, in which only a small proportion of tracks may have formed after deposition of the host sediment, AFTA data will be dominated by tracks formed prior to deposition. In samples of this nature which have been heated to only moderate temperatures after deposition (say $<60^{\circ}\text{C}$), it may not be possible to resolve the effects of this heating from the influence of the pre-depositional history. But as the severity of post-depositional annealing increases (i.e. with increasing maximum post-depositional temperature), the effects of the pre-depositional history are progressively "overprinted", and the AFTA parameters become dominated by the post-depositional history.

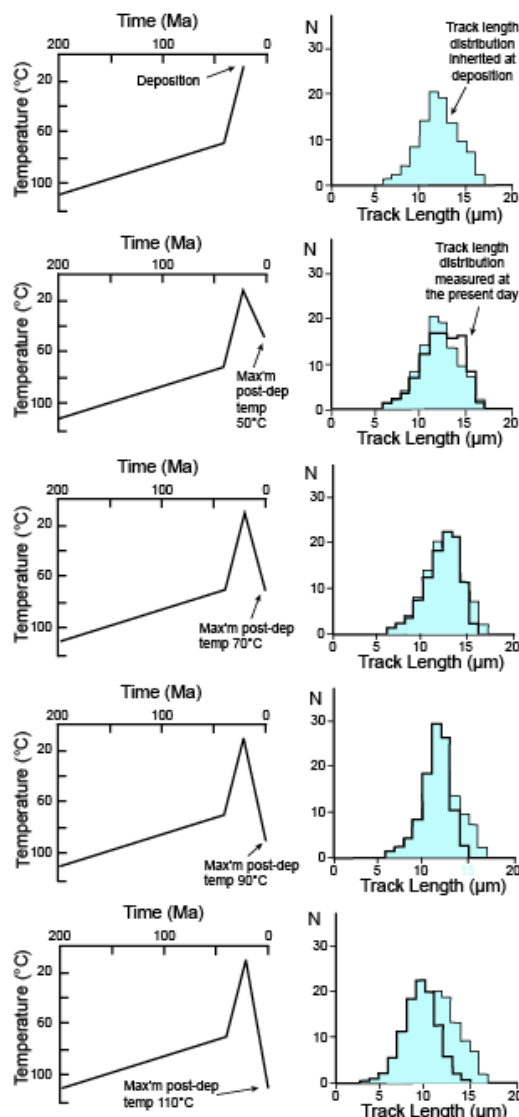


Fig. C.20: Progressive overprinting of inherited tracks by post-depositional heating. For samples containing a mixture of tracks formed pre- and post-deposition, only the shortest tracks retain a provenance signature. In the Figure, as the post-depositional temperature increases, the pre-depositional track length distribution (in outline) is progressively overprinted from longer lengths to shorter lengths, as the latter have experienced higher pre-depositional temperatures, and require even higher post-depositional temperatures to be further shortened. Once the effects of post-depositional annealing begin to dominate over the pre-depositional history at temperatures above about 90°C in the example, the resulting AFTA data can provide reliable constraints on the post-depositional history.

Fig. C.20 illustrates how in samples containing a mixture of tracks formed pre- and post-deposition, only the shortest tracks retain a provenance signature. The pre-depositional track length distribution is progressively overprinted from longer lengths to shorter lengths, as the latter have experienced higher pre-depositional temperatures, and require even higher post-depositional temperatures to be further shortened. This is a direct consequence of the principle of “equivalent time”, discussed earlier. Once the effects of post-depositional annealing begin to dominate over the pre-depositional history, the resulting AFTA data can provide reliable constraints on the post-depositional history. As heating becomes sufficiently severe, the fission track age will be reduced to a value less than the depositional age, and the age data will also become dominated by the effects of the post-depositional history.

In general, inherited tracks pose practical problems in extracting information on the post-depositional thermal history only for samples in which the majority of tracks were formed prior to deposition, perhaps in a Neogene sediment in which apatites were derived from a stable Paleozoic shield with fission track ages of ~400 Myr or more, or in samples that have experienced only very minor post-depositional heating (say 50°C). In such cases, often the only information on the post-depositional thermal history that can be obtained from AFTA might be that the sample has not been heated above say 90°C at any time after deposition.

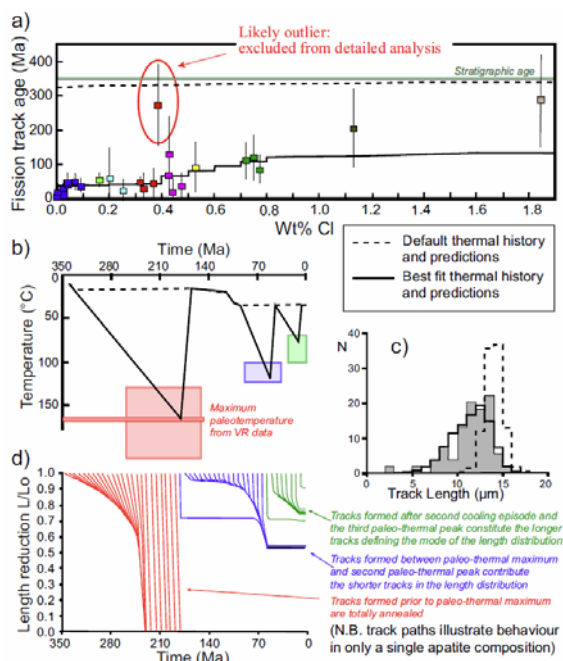


Fig. C.21: Resolution of multiple episodes from AFTA data in a single sample is possible where the events are sufficiently separated in temperature and time. In this example, based on AFTA data (a.) in combination with vitrinite reflectance results in a sample from the Dodo Canyon K-03 well in the Mackenzie valley, North West Territories, Canada, three thermal episodes are resolved (b.). Predicted track shortening trajectories for the three-episode history (c.) shows how all tracks are erased in the earliest episode (prior to 180 Ma), a population of shorter tracks are produced at the paleo-thermal peak in the second episode and a longer population of tracks (which constitutes the main mode of the distribution) is produced in the final episode. These tracks are still shorter than expected at surface temperatures, which allows resolution of this final episode (as illustrated by comparing the measured track length distribution in d. with the distribution predicted by the default thermal history).

Resolving multiple paleo-thermal episodes in individual samples

In samples which have undergone two episodes of heating and cooling, AFTA data can often provide constraints on both episodes, provided that the magnitude and timing of the paleo-thermal maximum and subsequent peak are sufficiently separated (Fig. C.21). In rare cases (e.g. Green et al. 2001a; Turner et al. 2008), three discrete episodes can be resolved in data from a single sample. This is most likely when the earliest event involves a maximum paleotemperature sufficient to totally anneal all tracks (typically >math>110^{\circ}\text{C}</math>), followed by a subsequent peak around 90 to 100°C which reduces tracks to a mean length around 10 microns, and then cooling to low temperature is followed by re-heating to around 70°C sufficient to reduce lengths of tracks formed after the second event to around 12-13 microns. In such circumstances, integration of AFTA data with results from other techniques (particularly vitrinite reflectance) can provide corroborative evidence of the earliest, maximum temperature, episode, as discussed in the next section.

C.4 Integration with other methods

Introduction

Significant advantages can be obtained by combining AFTA data with results from other methods. One reason for this is the inherent redundancy in the AFTA method, in the sense that a large number of thermal histories can result in very similar AFTA parameters, due to the dominance of maximum paleotemperatures in the kinetics of annealing (Figs. C.13, C.14). In addition, the natural spread in the length distribution imposes limits on the recognition of low temperature events, and can cause problems in resolving complex histories involving multiple episodes. Integration with independent techniques not only provides corroboration of conclusions derived from AFTA, but can also refine the range of thermal history solutions defined from AFTA alone and provide a coherent thermal history framework. Here we discuss some of the techniques that have been used in tandem with AFTA and discuss the benefits that can be obtained.

Geological data

In order to ensure that the information obtained from AFTA is meaningful, it is essential that interpretation is carried out within the context of the known geological setting. AFTA data in isolation can often be explained by such a wide range of histories that unless the depositional age of a sample is specified (in as much detail as possible), together with the present-day temperature, no meaningful thermal history information can be obtained. By specifying the time at which the apatite was at the surface, and the present temperature, these fundamental constraints on two points of the temperature-time



history provide a framework within which the post-depositional history of the host sedimentary rock can be defined.

To provide the required geological context we define a “Default Thermal History”, which is that part of the history which can be defined on the basis of the available geological evidence (or alternatively - the history that would be appropriate if no paleo-thermal events have affected the sample). This can be particularly important for samples from sedimentary sections containing a number of unconformities separating thin units of different ages, as the presence of the overlying section shows that the deeper units were close to the surface when the shallower units were deposited.

Vitrinite reflectance

Vitrinite reflectance (VR), based on the increase in reflectivity of the organic maceral vitrinite (a key constituent of coal) with temperature, is the standard measure of organic maturity for hydrocarbon exploration (e.g. Tissot and Welte, 1984). The kinetics of this process are well understood (Burnham and Sweeney, 1989), and are very similar to those of fission track annealing in apatite (Duddy et al, 1994, 1998), with VR values of 0.65% to 0.7% corresponding to total annealing of fission tracks in typical apatites (Duddy et al. 1994). These factors make VR an ideal complement to AFTA data applied to sedimentary sequences, as demonstrated in a wide range of studies (e.g. Duddy, 1997; Green et al. 2004; Japsen et al. 2005, 2007a; Turner et al. 2008).

In particular, VR provides independent determination of maximum post-depositional paleotemperatures, which can provide support for those indicated by AFTA. This is important, because data from either technique alone might be viewed with suspicion, but when two independent techniques provide consistent paleotemperatures the conclusions can be regarded as reliable. A classic example is provided by studies of wells on the East Midlands Shelf in the Southern North Sea of the UK, where early VR data were disregarded as indicating amounts of eroded section which were “not consistent with the known geological evolution” (Cope 1986). Subsequent application of AFTA to wells from this region (Green, 1989) confirmed the heating suggested by the VR data, showing that the section in these wells had indeed been more deeply buried and then exhumed.

Integration of VR data from fine grained units with AFTA data from sandstones also allows determination of paleotemperatures over a wider range of depths than possible from AFTA alone. The combination of both techniques can provide much tighter control on paleogeothermal gradients and amounts of removed section than would be possible from either technique on its own. In addition, integration of VR with AFTA data can be of great assistance in confirming earlier events soon after

deposition, which may not be confidently defined from AFTA alone (e.g. Green et al. 2004).

Despite the importance of VR data to the oil exploration industry and its widespread routine application, in recent years it has become apparent that VR data generated by different analysts are not equivalent (see discussion in Green et al. 2002). We find a high degree of consistency between thermal history interpretations from AFTA and VR data generated using an approach involving measurement of maximum reflectance under oil ($R_{o,max}$) in polished thick sections (Cook, 1982). In this approach, which is recommended by the International Commission on Organic and Coal Petrography (www.iccop.org), identification of the indigenous vitrinite population is made on textural grounds. This allows independent assessment of the possible presence of reworked vitrinite populations from petrographic evidence, as well as allowing identification of caved material in sub-surface samples. Alternation between reflectance and fluorescence modes allows checking for associated fluorescing liptinite, bitumen impregnation, or the presence, intensity, and source of oil-cut which may affect the reading. An alternative approach, often encountered in hydrocarbon industry reports, involves measurements of random reflectance ($R_{o,rand}$) in strewn slides of organic concentrates, with the indigenous vitrinite population often identified only after the analysis is complete by inspection of histograms of measurements and separation into perceived sub-populations. In our experience, this approach can lead to serious errors in determining maturity levels (usually resulting in underestimation). Integration of AFTA with VR data allows such cases to be readily identified.

A key factor in interpreting VR data is the possible suppression of reflectance levels, as often observed for example in H-rich source-rock horizons (e.g. Wilkins et al., 1992). Suppression can often be recognised by local departures from an overall trend, but where few data are available this is less straightforward. This can be particularly problematical where VR data (and other organic maturity indicators) are only measured in source rock horizons. Again, integration with AFTA allows detection of anomalous vitrinite reflectance values.

Data from a range of additional organic-based methods for assessing maturity levels, such as biomarker reactions (e.g. MacKenzie and McKenzie, 1983), Spore Colour Index (Fisher et al. 1980) or Rock Eval Tmax (Tissot and Welte, 1978), can be converted to equivalent VR values which can also be integrated with AFTA data. While biomarker reactions show promise as quantitative thermal indicators, expense and difficulties with elucidating the true kinetic descriptions have so far limited their usefulness, while SCI values are less commonly available and Rock Eval Tmax values are subject to variability as a result of variation in organic facies.



While these methods and others have some practical limitations all may be used, where available, to complement VR and AFTA data.

Fluid inclusions

Fluid inclusions are micron-sized vacuoles of liquid or gas which have been trapped within crystal imperfections during mineral growth. Univariant phase transitions observed during heating and freezing of fluid inclusions in the laboratory can yield valuable information concerning the composition and density of the fluids trapped within the inclusions and the temperature and pressure conditions at which the mineral precipitated. Taking advantage of the independent constraint on maximum paleotemperature provided from fluid inclusions, AFTA has been used to estimate the duration of heating related to diagenesis (Duddy et al., 1998; O'Brien et al., 1996; Parnell et al. 2005) and impact events (Parnell et al. 2007). Integration of AFTA data with information from fluid inclusions has also defined the timing of episodes of hot fluid circulation (Parnell et al. 1999) and has clarified issues related to the timing of hydrocarbon generation (Mark et al. 2008) in the UK West of Shetland region.

Sonic velocities

The progressive compaction of sediments with increasing burial has been widely used as the basis for estimating former burial depths in exhumed basins (e.g. Marie, 1975; Bulat and Stoker, 1987; Hillis, 1995; Japsen, 2000). Comparison of compaction proxies such as sonic velocity in an exhumed formation with a reference curve defining the expected variation with depth in sequences at maximum burial depth provides an indication of the amount of net exhumation. Selection of appropriate reference curves has been problematical in some areas, leading to erroneous conclusions regarding the extent and magnitude of exhumation (Cope, 1986; Green et al. 2001b). More rigorous definition of the necessary reference curves in recent years (Japsen et al. 2007b) allows more reliable estimation of former burial depths, and integration of such data with constraints from AFTA and VR data has provided highly consistent reconstructions of eroded section in Denmark (Japsen et al. 2007a) and Cardigan Bay, Western UK (Holford et al., 2005).

Since these compaction-based methods are controlled primarily by maximum burial depths, in situations where they provide consistent indications of former burial depths with those derived from paleo-thermal methods such as AFTA and VR, the results can be regarded with confidence. In addition, while results from AFTA and VR can often be explained by a range of paleogeothermal gradients and amounts of removed section, additional constraints from compaction-based methods can significantly reduce the range of viable solutions, as illustrated for

example by results from the Hans-1 well, Offshore Denmark (Japsen et al. 2007a).

Zircon fission track analysis (ZFTA)

Zircon is another common uranium-bearing detrital mineral amenable to fission track analysis. From both laboratory annealing studies and geological evidence (Hurford, 1986; Tagami et al, 1996), fission tracks in zircon are known to be more resistant to annealing than fission tracks in apatite. Investigation of zircon data in samples with different levels of vitrinite reflectance suggests that no significant fission track age reduction occurs in zircon at VR levels below ~4% (Geotrack unpublished results). VR values in excess of 5% (equivalent to maximum paleotemperatures in excess of 300°C) are required in order to produce any significant age reduction. Some evidence suggests that the rock needs to reach the stage of Greenschist facies metamorphism in order to produce observable effects in zircon. Therefore in most sedimentary basin settings, ZFTA can provide little or no information on post-depositional heating, except where intrusions are present or in cases of extremely high heat flow (e.g. Logan and Duddy, 1998). However, the relative stability of tracks in zircon makes ZFTA a useful tool for investigating sediment provenance. ZFTA data can also provide useful constraints on depositional ages (e.g. Morais Neto et al., 2008), since in the absence of post-depositional resetting, a zircon fission track age must represent cooling of sediment source regions, thereby providing an upper limit on the depositional age.

C.5 Application of AFTA to Thermal History Reconstruction in sedimentary basins

AFTA data in individual samples can provide constraints on the paleo-thermal maximum as well as one or possibly two subsequent paleo-thermal peaks. But the amount of information that can be obtained from a single sample is limited, and the real strength of the technique emerges from application to sequences of samples over a range of depths in boreholes, or over a range of elevations in an outcrop section. In such cases, integrated AFTA and VR analyses can provide a well-defined thermal history framework, involving quantitative definition of the timing and magnitude of major paleo-thermal events as well as determination of paleogeothermal gradients, allowing unique insights into mechanisms of heating and cooling. This information allows reconstruction of the thermal and burial/uplift histories of the sedimentary section, as explained below.

Default Thermal Histories

As discussed earlier, AFTA and VR data must be investigated within a context in order to provide

meaningful information on the magnitude of possible paleo-thermal effects (i.e events in which a rock sample was hotter in the past than it is today, due to either deeper burial, elevated basal heat flow, local igneous intrusion or hot fluid movements). In sedimentary sections, this context is provided by a Default Thermal History, which represents the history that can be constructed in the absence of any paleo-thermal effects. For sub-surface samples, this is calculated by combining the burial history derived from the preserved sedimentary section with the present-day geothermal gradient and surface temperature. Because both AFTA and VR data are dominated by the maximum temperatures experienced, this provides a basic point of reference for the expected degree of fission track annealing and the organic maturity. If measured AFTA and/or VR data are consistent with the values predicted from the Default Thermal History, then the sample is presently at or close to its maximum post-depositional temperature, and the data retain little or no information on any palaeo-thermal effects (because the data are dominated by maximum temperature, as explained earlier). But if AFTA data show a greater degree of fission track annealing or VR data show higher maturity than expected on the basis of the Default Thermal History, then the sampled horizon must have been hotter in the past. In this case, AFTA allows determination of the time at which cooling began, and both AFTA and VR can define the magnitude of the maximum palaeotemperature reached by individual samples.

A key factor in defining Default Thermal Histories for sub-surface samples is definition of the present-day thermal regime. Information on present-day temperatures in hydrocarbon exploration wells usually comes in the form of bottom-hole temperatures (BHTs) from logging runs, or in less common circumstances from Drill Stem Tests (DSTs) which sample formation fluids directly. A key problem in using such information to reconstruct present-day temperatures is the disturbance to the thermal field imposed by drilling of a well due to the introduction of drilling fluids which produce significant cooling. BHT values, which are normally recorded within a short time after drilling must be “corrected” to estimate the true formation temperature. Conversely, DST temperatures are generally thought to more closely reflect true ambient temperatures and can be used directly.

The most common BHT correction method is the “Horner correction”, based on an exponential increase towards the true temperature with time, but this requires repeated temperature measurements from multiple logging runs, as well as the time between runs. This information is not always available, so a number of simpler methods have been suggested. In our own work, we use a simple method based on observations of borehole temperatures over timescales of years (Andrews-Speed et al, 1984). In this approach, quoted BHT values are corrected by

increasing the difference between the surface or seabed temperature and the uncorrected BHT by 20% for uncorrected temperatures below 150°F (66°C), and by 25% above 150°F. In wells where multiple temperature measurements are available at a given depth, the earliest recorded BHT value was used. If no circulation times are available, the lowest temperature value at each depth is used. Whilst simplistic, this procedure has the advantage of allowing a common approach in all cases, and results in present-day temperatures which are consistent with the kinetic descriptions of AFTA and VR employed to extract information on paleo-thermal histories. Thus, a self-consistent framework is achieved, which is essential in any approach to this subject.

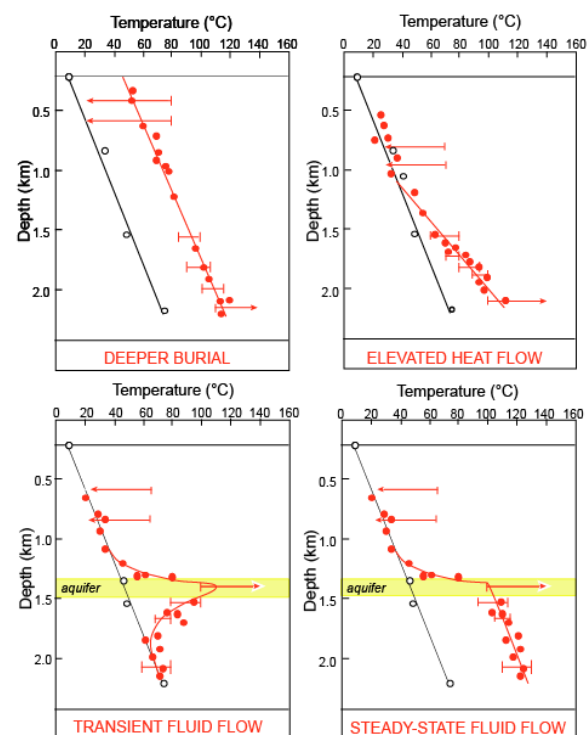


Fig. C.22: The way in which paleotemperatures characterising a particular paleo-thermal episode vary through a vertical sequence of rocks (the “paleotemperature profile”) provides key information on the mechanisms of heating and cooling. Deeper burial followed by exhumation, with no change in basal heat flow, will result in paleotemperatures defining a linear profile parallel to the present-day thermal profile but offset to higher temperatures. Elevated heat flow results in a linear paleotemperature profile with a higher slope compared to the present-day profile. In contrast, transient hot fluid flow through a localised aquifer results in a markedly non-linear profile with a maximum centred on the aquifer, while prolonged fluid flow can result in a linear profile below the aquifer as the deeper section reaches a “steady-state” situation. Combinations of these four simple cases are possible.

Paleotemperature profiles

The variation of paleotemperatures with depth, or the “paleotemperature profile”, provides key information on likely mechanisms of heating and cooling (Bray et al., 1992; Duddy et al., 1994; Green et al., 2002) (Fig. C.22). Provided that heterogeneities in lithology through the section are sufficient to smooth out any potential large-scale variations in thermal conductivity, heating due solely to deeper burial should produce a more or less linear paleotemperature profile with a similar gradient to the present temperature profile. In contrast, heating

due primarily to increased basal heat flow (perhaps also with some component of deeper burial) should produce a more or less linear paleotemperature profile with a higher gradient than the present temperature profile. Non-linear profiles may be produced by contact heating around intrusive bodies, or in the absence of intrusions are diagnostic of lateral introduction of heat, most likely due to passage of hot fluids within confined aquifer horizons.

Estimating additional burial (removed section)

Where heating can be attributed to some degree of deeper burial, possibly combined with elevated heat flow, fitting a linear profile to paleotemperatures as a function of depth allows the palaeogeothermal gradient at the paleo-thermal maximum to be determined and extrapolation of the palaeogeothermal gradient from the depth of the appropriate unconformity to an assumed palaeo-surface temperature (Fig. C.23) provides an estimate of the amount of additional section that was once present and was removed during cooling (see Bray et al., 1992; Duddy et al., 1994; Green et al., 2002, 2004). The inverse correlation between these two parameters results in a hyperbolic ellipsoid region of allowed values as shown in Fig. C.23. If a preferred value of paleogeothermal gradient is available (e.g. if the present-day gradient if heat flow has not changed through time) or if amounts of additional burial can be independently constrained (e.g. from sonic velocity data), then the complementary parameter can be defined with greater confidence from such plots.

It should be stressed that estimating amounts of removed section by extrapolating a linear paleotemperature profile assumes that the additional section had the same average thermal conductivity as the preserved section. If independent evidence suggests that this assumption is not appropriate, then a more detailed analysis using suitable thermal conductivities is required in order to provide a more accurate solution. But we submit that this approach is inherently more reliable than extrapolation of VR profiles to values of 0.2% to estimate amounts of removed section, since the underlying principles are more explicit, and problems such as those highlighted by Dow (1977) and Katz et al (1988) are more easily avoided.

This method also requires use of a preferred value for the paleo-surface temperature, which can be obtained from paleo-climate studies (e.g. Zachos et al. 2001). The influence of this factor can be assessed by dividing the change in temperature by the appropriate paleogeothermal gradient. For instance, for a paleogeothermal gradient of 30°C/km, a 10°C increase in paleo-surface temperature is equivalent to a reduction of 333 metres of removed section. Thus, subtle changes in surface temperature may be equivalent to major changes in amounts of removed

section. This, combined with discussion of possible non-linear paleotemperature profiles above, emphasises that estimation of removed section in this way is not a precise method, and the results can only ever be regarded as providing a general indication of the true amount.

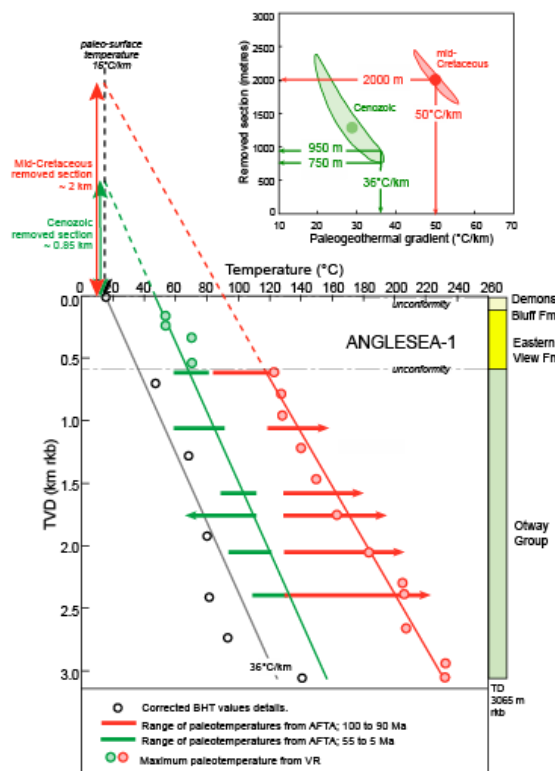


Fig. C.23: Extrapolation of paleotemperature profiles to estimate eroded section in the Anglesea-1 well, Otway Basin (after Green et al., 2004). AFTA and VR results define linear paleotemperature profiles for two thermal episodes: Mid-Cretaceous (cooling beginning between 100 and 90 Ma) associated with the unconformity between the Otway Group and the Eastern View Formation and Tertiary (cooling beginning between 55 and 5 Ma) associated with the unconformity at the top of the Demons Bluff Formation at the ground surface. Fitting of linear profiles using maximum likelihood methods defines the range of paleogeothermal gradients consistent with the observed paleotemperatures. Linear extrapolation of these paleo-gradients to an appropriate paleo-surface temperature (in this case 15°C) defines the magnitude of additional section required to explain the paleotemperatures in each episode (subsequently removed by erosion). A cross-plot of allowed values paleogeothermal gradient and removed section shows the allowed ranges ($\pm 95\%$ confidence limits) for the Mid-Cretaceous and Tertiary thermal episodes. The paleogeothermal gradient for the mid-Cretaceous episode was between 45 and 55°C/km, significantly higher than the present-day gradient of 36°C/km, and was associated with 2000 \pm 300 m of additional burial. The results allow a wider range of paleogeothermal gradient for the Tertiary episode (~ 20 to 37°C/km), encompassing the present-day gradient of 36°C/km, for which 750-950 m of additional burial is required to explain the Tertiary paleotemperature constraints. Note that this analysis assumes that the thermal conductivity of the eroded sequences was the same as that of the preserved sequences.

Thermal History Reconstruction

By integrating the information on the timing and magnitude of the main paleo-thermal events that have affected the sedimentary section with information provided by the preserved section (i.e. the Default Thermal History), a more complete thermal and burial/uplift history can be reconstructed (e.g. Green et al., 2004).

It should be evident from the above discussion that rigorous control on paleogeothermal gradients and therefore on amounts of additional burial is usually possible only at limited times in the history (i.e. the main paleo-thermal maxima and possibly one or two subsequent paleo-thermal peaks). It is not possible to



define the complete burial or thermal history, and instead we focus on defining the key paleo-thermal events in as much detail as possible. In doing so, it is important to realise that processes other than burial may play key roles in controlling the thermal history. Elevated basal heat flow may produce a paleo-thermal maximum which does not correlate with the time of maximum burial and may in fact occur within a period of continuing burial, while heating as a result of hot fluid movement can occur at any time (Duddy et al., 1994; 1998). In addition, variation in surface temperature may cause significant cooling of a sedimentary section during progressive burial, as illustrated by Japsen et al. (2007a) in the Eastern North Sea during the Cenozoic.

Precision and accuracy in thermal history reconstruction

In discussing precision and accuracy in thermal history reconstruction it is important to distinguish between the degree to which thermal history constraints can be defined, on the one hand, and how this translates to uncertainty in the corresponding burial history. Green et al. (2002) discussed these issues at some length, and only the basic points are reproduced here. Precision in this context describes the narrowness of the 95% confidence intervals on maximum paleotemperatures, corresponding amounts of additional burial and the onset of cooling, while accuracy deals with how close to the true values the estimates might be.

Accuracy of the thermal history constraints derived from AFTA is determined by how well the kinetic model used to define those constraints describes the natural system. As discussed earlier and as illustrated in Figs. C.7 and C.11, multi-compositional models provide reasonably accurate predictions when compared to data from geologically well-controlled situations. Obtaining consistent indications of maximum paleotemperatures from multiple techniques provides an additional check on accuracy. The precision of paleotemperatures determined from AFTA depends critically on the paleotemperature itself. Below around 60°C, mean track length varies only slowly with temperature, and it is often only possible to place an upper limit on the maximum paleotemperature. At higher temperatures, track length changes more rapidly with increasing temperature and the fission track age reduction becomes increasingly pronounced (Fig. C.2), and maximum paleotemperatures in this range becomes more precise, such that maximum paleotemperatures around 100°C can be defined within an overall uncertainty (95% confidence limits) of ~5°C. In other words, it is possible to define that a sample reached a paleotemperature between 100 and 105°C. But as the paleotemperature increases further, and tracks become totally annealed, the only constraint that is possible is a minimum estimate of the maximum paleotemperature.

Translating paleotemperatures defined from AFTA to estimates of former burial depth is much less precise, and also potentially a lot less accurate. Precise estimation requires control on paleogeothermal gradient that can only be obtained by paleotemperature constraints over a range of depth, ideally from both AFTA and VR data. Even with high quality datasets with consistent constraints from AFTA and VR over a depth interval of ~3 km, a 95% confidence interval of around 10°C/km around a best-fit paleogeothermal gradient of ~50°C/km is the best that can be achieved (i.e. 50±5°C/km). This translates to a confidence interval of around 600 m or more for best-fit values of removed section around 2 km (i.e. 2.0±0.3 km). So even for the most tightly-constrained datasets, estimating amounts of removed section in this way is not a precise method, and for less-well defined datasets, uncertainties can be much higher. This is exacerbated by considering the accuracy of predicting amounts of removed section by extrapolation of paleotemperature profiles, since assumptions regarding such factors as the paleo-surface temperature and the linearity of the profile through the removed section play a key role in the process (see Green et al., 2002 for a thorough review of these factors).

In terms of the timing information that can be obtained from AFTA, the numbers of fission tracks that can be counted for the fission track age determination and the numbers of track lengths that can be measured play a major role in determining precision. In any given sample, these are determined by the apatite abundance, the quality of the grains and the thermal history of the sample. In a best-case scenario, the onset of cooling from paleotemperatures sufficiently high to totally anneal all tracks may be defined with an uncertainty of around ±5% (e.g. 200±10 Ma). So this technique does not provide the sort of high precision analyses that can be obtained from mass spectrometer-based techniques. But AFTA does provide information that cannot be obtained from any other approach, and since the systematics of the method are extremely well understood, the information is highly reliable, provided that appropriate procedures are employed at every step of the process. But as we have tried to highlight in the foregoing discussion, failure to correctly implement any step of the process can result in highly misleading information.

Sample requirements for AFTA and sampling strategies

Apatite is a common accessory phase in many crystalline rocks, and being among the most resistant of detrital minerals (Morton, 1984) forms a common detrital constituent of most sandstones and other coarse sedimentary rocks, which can readily be extracted using standard heavy mineral separation methods. AFTA[®] can be applied either to outcrop samples or to ditch cuttings or core for sub-surface samples, and in both situations similar considerations



apply regarding sampling. In sedimentary sequences, medium grained sandstones are the most suitable lithologies for analysis, although coarse grits to or coarse silts can be used. It is advisable to collect around 1 kg of material from the most mineralogically immature units available. In general, experience shows that 80 to 90% of sandstone samples collected on this basis contain sufficient apatite for analysis.

Note that since a high quality analysis can be derived from as few as 20 grains of apatite, the overall abundance of apatite required is very low. Inspection of thin sections or even heavy mineral separates may not reveal apatite in samples which contain sufficient for analysis, so the ultimate test is to refine the apatite fraction as far as possible and then to prepare, polish and etch a grain mount. Since apatite is the only mineral that can be etched by dilute nitric acid, the etched apatite grains can easily be identified within a mass of other grains (multi-mineral composites, carbonates, sulphides) with similar density. The presence of these additional grains on the grain mount has no effect on the resulting analysis.

In downhole studies, samples of cuttings can be composited over a depth interval representing a range in downhole temperature of up to $\sim 5^{\circ}\text{C}$, corresponding to a depth range of about 150m for a typical geothermal gradient of $30^{\circ}\text{C}/\text{km}$. Sample should not be composited across an unconformity or major stratigraphic boundary. Where core samples are available, an integral solid piece of core, since the sample will be crushed anyway. Offcuts, rubble or scraps remaining from previous sampling can all be used, and again compositing over a range of depths is possible.

The most appropriate sampling strategy depends to some extent on the problems to be addressed, but in general, in order to obtain as much information as possible on key aspects of the paleo-thermal history such as paleogeothermal gradients, removed section etc, a vertical sequence of samples is required, spanning as wide a range of depths as possible from near surface to a depth where present downhole temperatures exceed about 110°C (corresponding to around 3 to 3.5 km for a typical geothermal gradient of $30^{\circ}\text{C}/\text{km}$), where tracks are totally annealed in the present day thermal regime. Integration with VR data is recommended as routine practice, for reasons discussed earlier. VR samples should be distributed more or less evenly through a well section, including the temperature realm above 110°C , and integrating information from this depth range with AFTA data provides a more complete reconstruction that would otherwise be available.

References

- Andrews-Speed, C.P., Oxburgh, E.R., and Cooper, B.A., 1984. Temperatures and depth-dependent heat flow in Western North Sea: AAPG Bulletin, v. 11, p. 1764 - 1784.
- Argent, J.D., Stewart, S.A., Green, P.F. and Underhill, J.R., 2002, Heterogeneous exhumation in the Inner Moray Firth, UK North Sea: constraints from new AFTA[®] and seismic data: Journal of the Geological Society of London, v. 159, p. 715-729.
- Barbarand, J., Carter, A., Wood, I. and Hurford, A.J., 2003a, Compositional and structural control of fission track annealing in apatite: Chemical Geology, v. 198, p. 107-137.
- Barbarand, J., Hurford, A.J. and Carter, A., 2003b, Variation in apatite fission-track length measurement: implications for thermal history modelling: Chemical Geology, v. 198, p. 77-106.
- Bhandari, N., Bhat, S.G., Lal, D., Rajagopalan, G., Tamhane, A.S. and Venkatavaradan, V.S., 1971, Fission fragment tracks in apatite: recordable track lengths: Earth and Planetary Science Letters, v.13, p. 191-199.
- Bray, R.J., Green, P.F. and Duddy, I.R., 1992. Thermal History Reconstruction using apatite fission track analysis and vitrinite reflectance: a case study from the UK East Midlands and the Southern North Sea: *in* Hardman, R.F.P., ed., Exploration Britain: Into the next decade, Geological Society Special Publication, v. 67, p. 3-25.
- Brown, M.C., 2007, Discussion on 'Apatite (U – Th)/He age constraints on the Mesozoic and Cenozoic evolution of the Bathurst Region, New South Wales: evidence for antiquity of the continental drainage divide along a passive margin': Australian Journal of Earth Science, v. 54, p. 1011–1012.
- Bulat, J. and Stoker, S.J., 1987, Uplift determination from interval velocity studies, UK, southern North Sea: *in* J. Brooks & K.W. Glennie, eds., Petroleum Geology of North West Europe, Graham & Trotman, pp. 293–305.
- Burnham, A.K. and Sweeney, J.J., 1989, A chemical kinetic model of vitrinite reflectance maturation: Geochimica et Cosmochimica Acta, v. 53, p. 2649-2657.
- Burtner, R.L., Nigrini, A. and Donelick, R.A., 1994, Thermochronology of lower Cretaceous source rocks in the Idaho-Wyoming thrust belt: AAPG Bulletin, v. 78, p. 1613-1636.
- Carlson, W.D., 1990, Mechanisms and kinetics of apatite fission-track annealing: American Mineralogist, v. 75, p. 1120 – 1139.
- Carlson, W.D., Donelick, R.A. & Ketcham, R.A., 1999, Variability of apatite fission-track annealing kinetics: I. Experimental results. American Mineralogist, v. 84, p. 1213-1223.



- Cook, A., ed. 1982, The origin and petrology of organic matter in coals, oil shales and petroleum source rocks: The University of Wollongong, Wollongong, N.S.W., 106 pp.
- Cope, M. J., 1986, An interpretation of vitrinite reflectance data from the Southern North Sea Basin: *in* Brooks, J. Goff, J.C. & Van Hoon, B.. eds) Habitat of Palaeozoic gas in northwest Europe: Geological Society, London, Special Publications, v. 23, p. 85-98.
- Corrigan, J.D., 1993, Apatite fission-track analysis of Oligocene strata in South Texas, U.S.A.: Testing annealing models: *Chemical Geology*, v. 10, p. 227-249.
- Crowley, K.D., Cameron, M. and Schaeffer, R.L., 1991, Experimental studies of annealing of etched fission tracks in fluorapatite: *Geochimica et Cosmochimica Acta*, v. 55, p. 1449-1465.
- Crowley, K.D. 1993, Mechanisms and kinetics of apatite fission-track annealing – Discussion: *American Mineralogist*, v. 78, p. 210 – 212.
- Crowhurst, P.V., Green, P.F. & Kamp, P.J.J., 2002, Appraisal of (U-Th)/He apatite thermochronology as a thermal history tool for hydrocarbon exploration: an example from the Taranaki Basin, New Zealand: *AAPG Bulletin*, v. 86, p. 1801-1819.
- Donelick, R.A., Roden, M.K., Mooers, J.D., Carpenter, B.S. and Miller, D.S., 1990, Etchable length reduction of induced fission tracks in apatite at room temperature (~23C): crystallographic orientation effects and “initial” mean lengths: *Nuclear Tracks and Radiation Measurements*, v. 17, p. 261-265.
- Dow, W. 1977. Kerogen studies and geological interpretations. *Journal of Geochemical Exploration*, v. 7, p. 79-99.
- Duddy, I.R., 1997, Focussing exploration in the Otway Basin: understanding timing of source rock maturation, *APPEA Journal*, v. 37, p. 178-191.
- Duddy, I.R., Green, P.F. & Laslett G.M., 1988, Thermal annealing of fission tracks in apatite 3. Variable temperature behaviour: *Chemical Geology (Isotope Geoscience Section)*, v. 73, p. 25-38.
- Duddy, I.R., Green, P.F., Bray, R.J. and Hegarty, K.A., 1994, Recognition of the Thermal Effects of Fluid Flow in Sedimentary Basins: *in* Parnell, J. ed., 1994, *Geofluids: Origin, Migration and Evolution of Fluids in Sedimentary Basins*, Geological Society, London, Special Publications, v. 78, p. 325-345.
- Duddy, I.R., Green, P.F., Hegarty, K.A, Bray, R.J. and O’Brien, G.W., 1998, Dating and duration of hot fluid flow events determined using AFTA[®] and vitrinite reflectance-based thermal history reconstruction: *in* Parnell, J., ed., 1998, *Dating and duration of hot fluid flow and fluid-rock interaction*. Geological Society, London, Special Publications, v. 144, p. 41-51.
- Fisher, M.J., Barnard, P.C. and Cooper, B.S. 1980. Organic maturation and hydrocarbon generation in the Mesozoic sediments of the Sverdrup Basin, Arctic Canada. IV Int. Palynol. Conf. Lucknow (1976-77). v.2, p. 581-588.
- Fleischer, R.L., Price, P.B. and Walker, R.M., 1975, Nuclear tracks in solids. University of California Press, Berkeley.
- Galbraith, R.F., 2006, Statistics for fission track analysis. Chapman and Hall/CRC.
- Galbraith, R.F. and Laslett, G.M., 1988, Some calculations relevant to the thermal annealing of fission tracks in apatite: *Proceedings of the Royal Society, London*. v. A419, p. 305-321.
- Galbraith, R.F. and Laslett, G.M., 1990, Apatite fission track analysis: geological thermal history analysis based on a three-dimensional random process of linear radiation damage: *Philosophical Transactions of the Royal Society of London*, v. 332, p. 419-438.
- Gallagher, K., 1995, Evolving temperature histories from apatite fission-track data: *Earth and Planetary Science Letters*, v. 136, p. 421-435.
- Gallagher, K. and Brown, R., 1997 The onshore record of passive margin evolution: *Journal of the Geological Society, London*, v. 154, p.451-457.
- Gallagher, K. and Brown, R., 1999a, Denudation and uplift at passive margins: the record on the Atlantic Margin of Southern Africa: *Philosophical Transactions of the Royal Society of London*, v. 357, p. 835–859.
- Gallagher, K and Brown, R., 1999b, The Mesozoic denudation history of the Atlantic margins of southern Africa and southeast Brazil and the relationship to offshore sedimentation: *in* Cameron, N.R., Bate, R.H. and Clure, V.S., eds., *The oil and gas habitats of the South Atlantic*, Geological Society Special Publications, v. 153, p. 41-53.
- Gibson, D.L., 2007, Discussion on ‘Apatite (U – Th)/He age constraints on the Mesozoic and Cenozoic evolution of the Bathurst Region, New South Wales: evidence for antiquity of the continental drainage divide along a passive margin’: *Australian Journal of Earth Science*, v. 54, p. 1012–1015.
- Gleadow, A.J.W. and Duddy, I.R., 1981, Fission track analysis: a new tool for the evaluation of thermal histories and hydrocarbon potential: *APEA Journal*, v. 23, p. 93-102.
- Gleadow, A.J.W., Duddy, I.R., Green, P.F. and Lovering, J.F., 1986, Confined fission track lengths in apatite – a diagnostic tool for thermal history analysis: *Contributions to Mineralogy and Petrology*, v. 94, p. 405-415.
- Goswami, J.N., Jha, R. and Lal, D., 1984, Quantitative treatment of annealing of charged particle tracks in common rock minerals: *Earth and Planetary Science Letters*, v. 71, p. 120-128.



- Green, P.F., 1980, On the cause of the shortening of spontaneous fission tracks in certain minerals: *Nuclear Tracks*, v. 4, p. 91-100.
- Green, P.F., 1986, On the thermo-tectonic evolution of Northern England: evidence from fission track analysis: *Geological Magazine*, v. 123, p. 493-506.
- Green, P.F., 1988, The relationship between track shortening and fission track age reduction in apatite: combined influences of inherent instability, annealing anisotropy, length bias and system calibration: *Earth and Planetary Science Letters*, v. 89, p. 335 – 352.
- Green, P.F., 1989, Thermal and tectonic history of the East Midlands shelf (onshore UK) and surrounding regions assessed by apatite fission track analysis: *Journal of the Geological Society of London*, v. 146, p. 755-773.
- Green P., 2004, The importance of validating annealing models: 10th International Conference on Fission Track Dating and Thermochronology, Amsterdam, The Netherlands (abstract), p.53.
- Green, P.F., 2005, Post-Carboniferous burial and exhumation histories of Carboniferous rocks of the Southern North Sea and adjacent Onshore UK. *In*: Collinson, J.D., Evans, D.J., Holliday, D.W. and Jones, N.S. (eds), Carboniferous hydrocarbon geology: the Southern North Sea and surrounding Onshore areas. *Occasional Publications, Yorkshire Geological Society*, v. 7, p. 25-34.
- Green, P.F. and Duddy, I.R., 2006, Interpretation of apatite (U-Th)/He ages and fission track ages from cratons: *Earth and Planetary Science Letters*, v. 244, p. 541-547.
- Green, P.F. and Duddy, I.R., 2007, Discussion on ‘Apatite (U – Th)/He age constraints on the Mesozoic and Cenozoic evolution of the Bathurst Region, New South Wales: evidence for antiquity of the continental drainage divide along a passive margin’: *Australian Journal of Earth Science*, v. 54, p. 1009-1011.
- Green, P.F., Duddy, I.R., Gleadow, A.J.W., Tingate, P.R. and Laslett, G.M., 1985, Fission-track annealing in apatite: track length measurements and the form of the Arrhenius plot: *Nuclear Tracks*, v. 10, p. 323-328.
- Green, P.F., Duddy, I.R., Gleadow, A.J.W., Tingate, P.R. and Laslett, G.M., 1986, Thermal annealing of fission tracks in apatite 1. A qualitative description: *Chemical Geology (Isotope Geoscience Section)*, v. 59, p. 237-253.
- Green, P.F., Duddy, I.R. and Laslett, G.M., 1988, Can fission track annealing be described by first-order kinetics? *Earth and Planetary Science Letters*, v. 87, p. 216 – 228.
- Green, P.F., Duddy, I.R., Laslett, G.M., Hegarty, K.A., Gleadow, A.J.W. and Lovering, J.F., 1989, Thermal annealing of fission tracks in apatite 4. Quantitative modelling techniques and extension to geological timescales: *Chemical Geology (Isotope Geoscience Section)*, v. 79, p. 155-182.
- Green, P.F., Laslett, G.M. and Duddy, I.R., 1993, Mechanisms and kinetics of fission-track annealing, *American Mineralogist*, v. 78, p. 441 – 445.
- Green, P.F., Duddy, I.R., Bray, R.J., Duncan, W.I. and Corcoran, D.V., 2001a, The influence of thermal history on hydrocarbon prospectivity in the Central Irish Sea Basin: *in* Shannon, P.M., Haughton, P.D.W. and Corcoran, D.V., eds., *The Petroleum Exploration of Ireland’s Offshore Basins*, Geological Society, London, Special Publications, v. 188, p. 171-188.
- Green, P.F., Thompson, K. and Hudson, J.D., 2001b, Recognising tectonic events in undeformed regions: contrasting results from the Midland Platform and East Midlands Shelf, Central England: *Journal of the Geological Society, London*, v. 158, p. 59-73.
- Green, P.F., I.R. Duddy, and K.A. Hegarty, 2002, Quantifying exhumation from apatite fission-track analysis and vitrinite reflectance data: precision, accuracy and latest results from the Atlantic margin of NW Europe: *in* Doré, A.G., Cartwright, J., Stoker, M.S., Turner, J.P. and White, N., Exhumation of the North Atlantic Margin: Timing, mechanisms and Implications for Petroleum Exploration, Geological Society Special Publication, v. 196, p. 331-354.
- Green P.F., Crowhurst P.V., Duddy I.R., 2004, Integration of AFTA and (U-Th)/He thermochronology to enhance the resolution and precision of thermal history reconstruction in the Anglesea-1 well, Otway Basin, SE Australia: *in* Eastern Australian Basins Symposium II, Boulton, P.J., Johns, D.R., Lang, S.C., eds., Petroleum Exploration Society of Australia, Special Publication, p. 117–131.
- Green, P.F., Duddy, I.R. and Hegarty, K.A., 2005, Comment on “Compositional and structural control of fission track annealing in apatite” by J. Barbarand, A. Carter, I. Wood and A.J. Hurford, *Chemical Geology*, 198 (2003) 107-137: *Chemical Geology*, v. 214, p. 351-358.
- Green, P.F., Japsen, P.J., Chalmers, J.A. & Bonow, J.M. 2011: Erosion surfaces and missing section in West Greenland. *Journal of the Geological Society (London)* **168**, 817-829.
- Gunnell, Y., 2000, Apatite fission-track thermochronology: an overview of its potential and limitations in geomorphology: *Basin Research*, v. 12, p. 115 – 132.
- Hendriks, B. W. H. and Andriessen, P., 2002, Pattern and timing of the post-Caledonian denudation of northern Scandinavia constrained by apatite fission-track thermochronology: *in* Doré, A. G., Cartwright, J., Stoker, M. S., Turner, J. P. and White, N., eds., Exhumation of the North Atlantic Margin: Timing, Mechanisms and Implications for Petroleum Exploration, Geological Society of London Special Publication, v. 196, p. 117–137.



- Hillis, R.R., 1995, Quantification of Tertiary exhumation in the United Kingdom southern North Sea using sonic velocity data: AAPG Bulletin, v. 79, p. 130–152.
- Holford, S.P., Green, P.F., and Turner, J.P., 2005, Palaeothermal and compaction studies in the Mochras borehole (NW Wales) reveal early Cretaceous and Neogene exhumation and argue against regional Paleogene uplift in the southern Irish Sea: Journal of the Geological Society, London, v. 162, p. 829-840.
- Hurford, A.J., 1986, Cooling and uplift patterns in the Lepontine Alps, South Central Switzerland and an age of vertical movement on the Insubric fault line: Contributions to Mineralogy and Petrology, v. 92, p. 413-427.
- Japsen, P. 2000. Investigation of multi-phase erosion using reconstructed shale trends based on sonic data. Sole Pit axis, North Sea: Global and Planetary Change, v.24, p. 189-210.
- Japsen, P., Green, P.F. and Chalmers, J.A., 2005, Separation of Palaeogene and Neogene uplift on Nuussuaq, West Greenland, Journal of the Geological Society, London, v. 162, p. 299-314.
- Japsen, P., Green, P.F., Nielsen, L.H., Rasmussen, E.S. and Bidstrup, T., 2007a, Mesozoic-Cenozoic exhumation in the eastern North Sea Basin: a multi-disciplinary study based on palaeo-thermal, palaeo-burial, stratigraphic and seismic data: Basin Research, v. 19, p. 451-490.
- Japsen, P., Mukerji, T. and Mavko, G., 2007b, Constraints on velocity-depth trends from rock physics models: Geophysical Prospecting, v. 55, p. 135-154.
- Katz, B.J., Pfeifer, R.N. and Schunk, D.J., 1988, Interpretation of discontinuous vitrinite reflectance profiles: AAPG Bulletin, v. 73. p. 926-931.
- Ketcham, R.A., Donelick, R.A. and Carlson, W.D., 1999, Variability of apatite fission-track annealing kinetics: III. Extrapolation to geological timescales: American Mineralogist, v. 84, p. 1235 – 1255.
- Laslett, G.M. and Galbraith, R.F., 1996, Statistical modelling of thermal annealing of fission tracks in apatite: Geochimica et Cosmochimica Acta, v. 24, p. 5117-5131.
- Laslett, G.M., Kendall, W.S., Gleadow, A.J.W. and Duddy, I.R., 1982 Bias in measurement of fission track length distributions: Nuclear Tracks, v. 6, p. 79-85.
- Laslett, G.M., Green, P.F., Duddy, I.R. and Gleadow, A.J.W., 1987, Thermal annealing of fission tracks in apatite 2. A quantitative analysis: Chemical Geology (Isotope Geoscience Section), v. 65, p. 1-13.
- Logan, P. and Duddy, I.R., 1998, An investigation of the thermal history of the Ahnet and Reggane Basins, Central Algeria, and the consequences for hydrocarbon generation and accumulation: in MacGregor, D.S., Moody, R.T. and Clark-Lowes, D.D., eds., Petroleum Geology of North Africa, Geological Society, London, Special Publications, v. 132, p 131-155.
- MacKenzie, A.S. and McKenzie, D. 1983. Isomerization and aromatization of hydrocarbons in sedimentary basins formed by extension. Geological Magazine, v. 120, p. 417-528.
- Marie, J.P.P., 1975, Rotliegendes stratigraphy and diagenesis: in Woodland, A.W., ed., Petroleum and the continental shelf of north-west Europe, Applied Science, London, p. 205–211.
- Mark, D., Green, P.F., Parnell, J., Kelly, S.P., Lee, M.R. and Sherlock, S.C., 2008, Late Palaeozoic hydrocarbon migration through the Clair field, West of Shetland, UK Atlantic margin: Geochimica et Cosmochimica Acta, v. 72, p. 2510-2533.
- Morais Neto, J.M., Green, P.F., Karner, G.D. and Alkmim, F.F. 2008: Age of the Serra do Martins Formation, Borborema Plateau, northeastern Brazil: Constraints from apatite and zircon fission track analysis. Boletim Geociencias Petrobras v.16, p. 23-52.
- Morton, A.C. 1984. Stability of detrital heavy minerals in Tertiary sandstones from the North Sea Basin. Clay Minerals, v. 19, p. 287-308.
- Naeser, C.W. and Faul, H., 1969, Fission track annealing in apatite and sphene: Journal of Geophysical Research, v. 74, p. 705-710.
- Naeser C.W. and Forbes R.B., 1976, Variation of fission track ages with depth in two deep drill holes: EOS (abstract), v. 57, p. 363.
- Naeser, C.W., Naeser N.D. and McCulloh T.H., 1989, The application of fission track dating to the depositional and thermal history of rocks in sedimentary basins: in Naeser N.D. and McCulloh T.H., eds., 1989, Thermal history of sedimentary basins – methods and case histories: Springer-Verlag, New York, p. 157-180.
- O'Brien, G.W., Lisk, M., Duddy, I., Eadington, Cadman, S. and Fellows, M., 1996, Late Tertiary fluid migration in the Timor Sea: A key control on thermal and diagenetic histories? APEA Journal, v. 36, p. 399-426.
- Parnell, J., Carey, P. F., Green, P. and Duncan, W., 1999, Hydrocarbon migration history, West of Shetland: integrated fluid inclusion and fission track studies: in Fleet, A.J. and Boldy, S.A.R., eds., Petroleum Geology of Northwest Europe, Proceedings of the 5th Conference, Geological Society, London, p. 613-625.
- Parnell, J., Green, P.F., Watt, G. and Middleton, D., 2005, Thermal history and oil charge on the UK Atlantic Margin: Petroleum Geoscience, v. 11, p. 99-112.
- Parnell, J., Bowden, S.A., Osinski, G.R., Lee, P., Green, P.F., Taylor, C. and Baron, M., 2007, Organic geochemistry of impactites from the Houghton impact structure, Devon Island, Nunavut,



- Canada: *Geochimica et Cosmochimica Acta*, v. 71, p. 1800-1819.
- Persano, C., Bishop, P. and Stuart, F.M., 2006, Apatite (U – Th)/He age constraints on the Mesozoic and Cenozoic evolution of the Bathurst Region, New South Wales: evidence for antiquity of the continental drainage divide along a passive margin: *Australian Journal of Earth Science*, v. 53, p. 1041–1050.
- Rohrman, M., van der Beek, P., Andriessen, P. and Cloetingh, S., 1995, Meso-Cenozoic morphotectonic evolution of southern Norway: Neogene domal uplift inferred from apatite fission track thermochronology: *Tectonics*, v. 14, p. 704–718.
- Spiegel, C., Kohn, B.P., Raza, A., Raiuner, T. and Gleadow, A.J.W., 2007, The effect of low-temperature exposure on apatite fission track stability: A natural annealing experiment in the deep ocean: *Geochimica et Cosmochimica Acta*, v. 71, p. 4512-4537.
- Stephenson, J., Gallagher, K. and Holmes, C., 2006, A Bayesian approach to calibrating apatite fission track annealing models for laboratory and geological timescales: *Geochimica et Cosmochimica Acta*, v. 70, p. 5183-5200.
- Tagami, T., Carter, A. and Hurford, A.J., 1996, Natural long term annealing of the zircon fission-track system in Vienna Basin deep borehole samples: constraints upon the partial annealing zone and closure temperature: *Chemical Geology*, v. 130, p. 147–157.
- Tissot, B.P. and Welte, D.H., 1984, *Petroleum formation and occurrence*: Springer-Verlag.
- Turner, J.P., Green, P.F., Holford, S.P. and Lawrence, S.R., 2008, Thermal history of the Rio-Muni (West Africa) – NE Brazil margins during continental breakup: *Earth and Planetary Science Letters*, v. 270, p. 354–367.
- Vrolijk, P., Donelick, R., Queng, J. and Cloos, M., 1992, Testing models of fission track annealing in apatite in a simple thermal setting; Site 800, Leg129: *in* Larson, R. and Lancelot, Y., eds., *Proceedings of the Ocean Drilling Program, Science Results*, v. 129 p.169–178.
- Wagner, G.A., 1968, Fission track dating of apatites, *Earth and Planetary Science Letters*, v. 4, p. 411-415.
- Wagner, G.A. and Reimer, G.M., 1972. Fission track tectonics: the tectonic interpretation of fission track ages: *Earth and Planetary Science Letters*, v. 14, p. 263-268.
- Wagner, G.A. and Van den Haute, P., 1992, *Fission-track dating*: Kluwer Academic Publishers, 285pp.
- Wilkins, R.W.T., Wilmshurst, J.R., Russell, N.J., Hladky, G., Ellacott, M.V. and Buckingham, C. 1992. Fluorescence alteration and the suppression of vitrinite reflectance. *Organic Geochemistry*, v. 18, p. 629-640.
- Young, D., Myers, A.T., Munson, E.L. and Conklin, N.M., 1969, *Mineralogy and geochemistry of fluorapatite from Cerro de Mercado, Durango, Mexico*: US Geological Survey Professional Papers, v. 650-D, p.D84-D93.
- Zachos, J.C., Pagani, M., Sloan, L.C., Thomas, E. and Billups, K. (2001) Trends, rhythms, and aberrations in global climate 65 Ma to present. *Science*, v. 292, p. 686–693.



APPENDIX D

Vitrinite Reflectance Measurements

D.1 New vitrinite reflectance determinations

New vitrinite reflectance data were collected as part of this study, with details of determinations described in sections D.1 and D.2 below.

Samples

Samples were submitted for vitrinite reflectance determination to Keiraville Konsultants, Australia. Results and sample details are summarised in Table D.2, while supporting data, including maceral descriptions and raw data sheets, are presented in the following pages.

Equipment

Leitz MPV1.1 photometer equipped with separate fluorescence illuminator, Swift point counter. Reflectance standards: spinel 0.42%, YAG 0.91%, GGG 1.72%, SiC standard for cokes and masked uranyl glass for measurement of intensity (I) in fluorescence mode. With the Keiraville Konsultants equipment, it is possible to alternate from reflectance to fluorescence mode to check for associated fluorescing liptinite, or importantly with some samples, to check for bitumen impregnation, or the presence, intensity, and source of oil-cut.

Sample preparation

Samples are normally mounted in cold setting polyester resin and polished using Cr₂O₃ and MgO polishing powders. Epoxy resins or araldite can be used if required. "Whole rock" samples are normally used but demineralisation can be undertaken. Large samples of coals and cokes can be mounted and examined.

Vitrinite Reflectance measurement

The procedure used generally follows Australian Standard (AS) 2486, but has been slightly modified for use with dispersed organic matter (DOM). For each sample, a minimum of 25 fields is measured (the number may be less if vitrinite is rare or if a



limited number of particles of vitrinite is supplied, as may be the case with hand-picked samples). If wide dispersal of vitrinite reflectances is found, the number of readings (N) is increased until a stable mean is obtained.

Vitrinite identification is made primarily on textural grounds, and this allows an independent assessment to be made of cavings and re-worked vitrinite populations. Histograms are only used for population definition when a cavings population significantly overlaps the range of the indigenous population. Where such data provides additional information, the mean maximum reflectance of inertinite and/or the mean maximum reflectance of liptinite (exinite) is reported. For each field, the maximum reflectance position is located and the reading recorded. The stage is then rotated by 180° which should give the same reading. In practice, the readings are seldom identical because of stage run-out and slight surface irregularities. If the readings are within $\pm 5\%$ relative, they are accepted. If not, the cause of the difference is sought and the results rejected. The usual source of differences is surface relief. The measurement of both maxima results in a total of 50 measurements being taken for the 25 fields reported. Thus, the 50 readings consist of 25 pairs of closely spaced readings which provide a check on the levelling of the surface and hence additional precision.

As the vitrinite reflectance measurements are being made, the various features of the samples are noted on a check sheet to allow a sample description to be compiled. When the reflectance measurements are complete, a thorough check is made of liptinite fluorescence characteristics. At the same time, organic matter abundance is estimated using a global estimate, a grain count method or point count method as required.

Data presentation

Individual sample results are reported in the following format:

KK No.	Depth (ft)	R_{Vmax}^*1	Range*2	N*3
x10324	3106	0.79	0.64 - 0.91	25

*1 Mean of all the maximum reflectance readings obtained.

*2 Lowest Rmax and highest Rmax of the population considered to represent the first generation vitrinite population.

*3 Number of fields measured (Number of measurements = 2N because 2 maximum values are recorded for each field)



Methods - Organic matter abundance and type.

After completion of vitrinite reflectance readings, the microscope is switched to fluorescence-mode and an estimate made of the abundance of each liptinite maceral. Fluorescence colours are also noted (BG 3 long UV excitation, TK400 dichroic mirror and a K490 barrier filter). The abundances are estimated using comparison charts. The categories used for liptinite (and other components) are:

Descriptor	%	Source potential
Absent	0	None
Rare	<0.1	Very poor
Sparse	$0.1 < x < 0.5$	Poor to fair
Common	$0.5 < x < 2.0$	Fair to good
Abundant	$2.0 < x < 10.0$	Good to very good
Major	$10.0 < x < 40.0$	Very good (excellent if algal)
Dominant	>40.0	Excellent

Dispersed Organic Matter (DOM) composition

At the same time as liptinite abundances are estimated, total DOM, vitrinite and inertinite abundances are estimated and reported in the categories listed above. Liptinite (exinite) fluorescence intensity and colour, lithology and a brief description of organic matter type and abundance are also recorded in a further column. Coal is described separately from dispersed organic matter (DOM). These data can be used to estimate the specific yield of the DOM and form a valuable adjunct to TOC data.

Lithological composition

The lithological abundances are ranked. For cuttings, these data can be useful in conjunction with geophysical logs in assessing the abundance and nature of cavings. For cores, it provides a record of the lithology examined and of the lithological associations of the organic matter.

Coal abundance and composition

Where coals are present, their abundance is recorded and their composition is reported as microlithotypes thus:

Coal major, Vitrinite>Inertinite>Exinite, Clarodurite>vitrite>clarite>inertite.



These data give an approximate maceral composition and information about the organic facies of the coal. Where coal is a major or dominant component, and more precise maceral composition data are required, point count analyses should be requested. However, the precision of the original sampling is commonly a limiting factor in obtaining better quality data.

Abundance factor analysis

Especially where cuttings samples are used, abundance factor analyses are used to obtain an assessment of the maceral assemblages in the various lithologies. This can be done by a combination analysis using a point counter, but a large number of categories is required, and the precision is low if DOM is less than about 10%. For an abundance factor analysis (for core, 50 microscope fields of view) we assess the abundance of DOM, coal and shaly coal in 50 grains. The data can be used to plot DOM and coal abundance profiles.

Analyst/Advisor: Professor A.C. Cook

Prior to transmittal of final results, all samples are examined and checked by A.C. Cook who has more than 30 years' experience of work on coals, cokes, source rocks and source rock maturation.

D.2 Integration of vitrinite reflectance data with AFTA

Vitrinite reflectance is a time-temperature indicator governed by a kinetic response in a similar manner to the annealing of fission tracks in apatite as described in Appendix C. In this study, vitrinite reflectance data are interpreted on the basis of the distributed activation energy model describing the evolution of VR with temperature and time described by Burnham and Sweeney (1989), as implemented in the BasinMod™ software package of Platte River Associates. In a considerable number of wells from around the world, in which AFTA has been used to constrain the thermal history, we have found that the Burnham and Sweeney (1989) model gives good agreement between predicted and observed VR data, in a variety of settings.

As in the case of fission track annealing, it is clear from the chemical kinetic description embodied in equation 2 of Burham and Sweeney (1989) that temperature is more important than time in controlling the increase of vitrinite reflectance. If the Burham and Sweeney (1989) distributed activation energy model is expressed in the form of an Arrhenius plot (a plot of the logarithm of time versus inverse absolute temperature),



then the slopes of lines defining contours of equal vitrinite reflectance in such a plot are very similar to those describing the kinetic description of annealing of fission tracks in Durango apatite developed by Laslett et al. (1987), which is used to interpret the AFTA data in this report. This feature of the two quite independent approaches to thermal history analysis means that for a particular sample, a given degree of fission track annealing in apatite of Durango composition will be associated with the same value of vitrinite reflectance regardless of the heating rate experienced by a sample. Thus paleotemperature estimates based on either AFTA or VR data sets should be equivalent, regardless of the duration of heating. As a guide, Table D.1 gives paleotemperature estimates for various values of VR for two different heating times.

One practical consequence of this relationship between AFTA and VR is, for example, that a VR value of 0.7% is associated with total annealing of all fission tracks in apatite of Durango composition, and that total annealing of all fission tracks in apatites of more Chlorine-rich composition is accomplished between VR values of 0.7 and ~0.9%.

Furthermore, because vitrinite reflectance continues to increase progressively with increasing temperature, VR data allow direct estimation of maximum paleotemperatures in the range where fission tracks in apatite are totally annealed (generally above ~110°C) and where therefore AFTA only provides minimum estimates. Maximum paleotemperature estimates based on vitrinite reflectance data from a well in which most AFTA samples were totally annealed will allow constraints on the paleogeothermal gradient that would not be possible from AFTA alone. In such cases the AFTA data should allow tight constraints to be placed on the time of cooling and also the cooling history, since AFTA parameters will be dominated by the effects of tracks formed after cooling from maximum paleotemperatures. Even in situations where AFTA samples were not totally annealed, integration of AFTA and VR can allow paleotemperature control over a greater range of depth, e.g. by combining AFTA from sand-dominated units with VR from other parts of the section, thereby providing tighter constraint on the paleogeothermal gradient.

References

- Burnham, A.K. and Sweeney, J.J. (1989) A chemical kinetic model of vitrinite reflectance maturation. *Geochim. et Cosmochim. Acta*, 53, 2649-2657.
- Laslett, G.M., Green, P.F., Duddy, I.R. and Gleadow, A.J.W. (1987) Thermal annealing of fission tracks in apatite 2. A quantitative analysis. *Chem. Geol. (Isot. Geosci.Sect.)*, 65, 1-13.



Table D.1: Paleotemperature - vitrinite reflectance nomogram based on Equation 2 of Burnham and Sweeney (1989)

Paleotemperature (°C / °F)	Vitrinite Reflectance (%)	
	1 Ma Duration of heating	10 Ma Duration of heating
40 / 104	0.29	0.32
50 / 122	0.31	0.35
60 / 140	0.35	0.40
70 / 158	0.39	0.45
80 / 176	0.43	0.52
90 / 194	0.49	0.58
100 / 212	0.55	0.64
110 / 230	0.61	0.70
120 / 248	0.66	0.78
130 / 266	0.72	0.89
140 / 284	0.81	1.04
150 / 302	0.92	1.20
160 / 320	1.07	1.35
170 / 338	1.23	1.55
180 / 356	1.42	1.80
190 / 374	1.63	2.05
200 / 392	1.86	2.33
210 / 410	2.13	2.65
220 / 428	2.40	2.94
230 / 446	2.70	3.23



Table D.2: Vitrinite reflectance sample details and results - outcrop samples from southernmost Norway (Geotrack Report #970A)

Sample number	Source #	Location Digital Lat/Long Elevation (m)	Stratigraphic Subdivision	Stratigraphic age (Ma)	VR (Range) %	N
Norwegian outcrop						
GC970-63.1	468887	Bjoroja Tunnel, 10Km SW Bergen			0.38 (0.33-0.41)	25

Note: Some samples may contain both vitrinite and inertinite. Only vitrinite data is shown.

*1 See Appendix A for discussion of present temperature data.

**GC970**

KK #	Depth (m)	$\bar{R}_{v\max}$	Range	SD	N	Sample description including liptinite fluorescence, maceral abundances, mineral fluorescence
L5044	-	0.38	0.33-0.41	0.023	25	Fluorescing liptinite absent. (Coal, V vitrite. The sample
-63.1	\bar{R}_I	-	-	-	-	Comprises exclusively of coal and vitrinite is the only maceral type present. Relict cellular texture is preserved in some coals. Pyrite sparse.)
O/C						

SOUTHERN NORWAY REGION-Outcrops**Early – Middle Oxford an**

-63.1 shows some of the features of jet and so its low reflectance may not be indicative of maturation level.

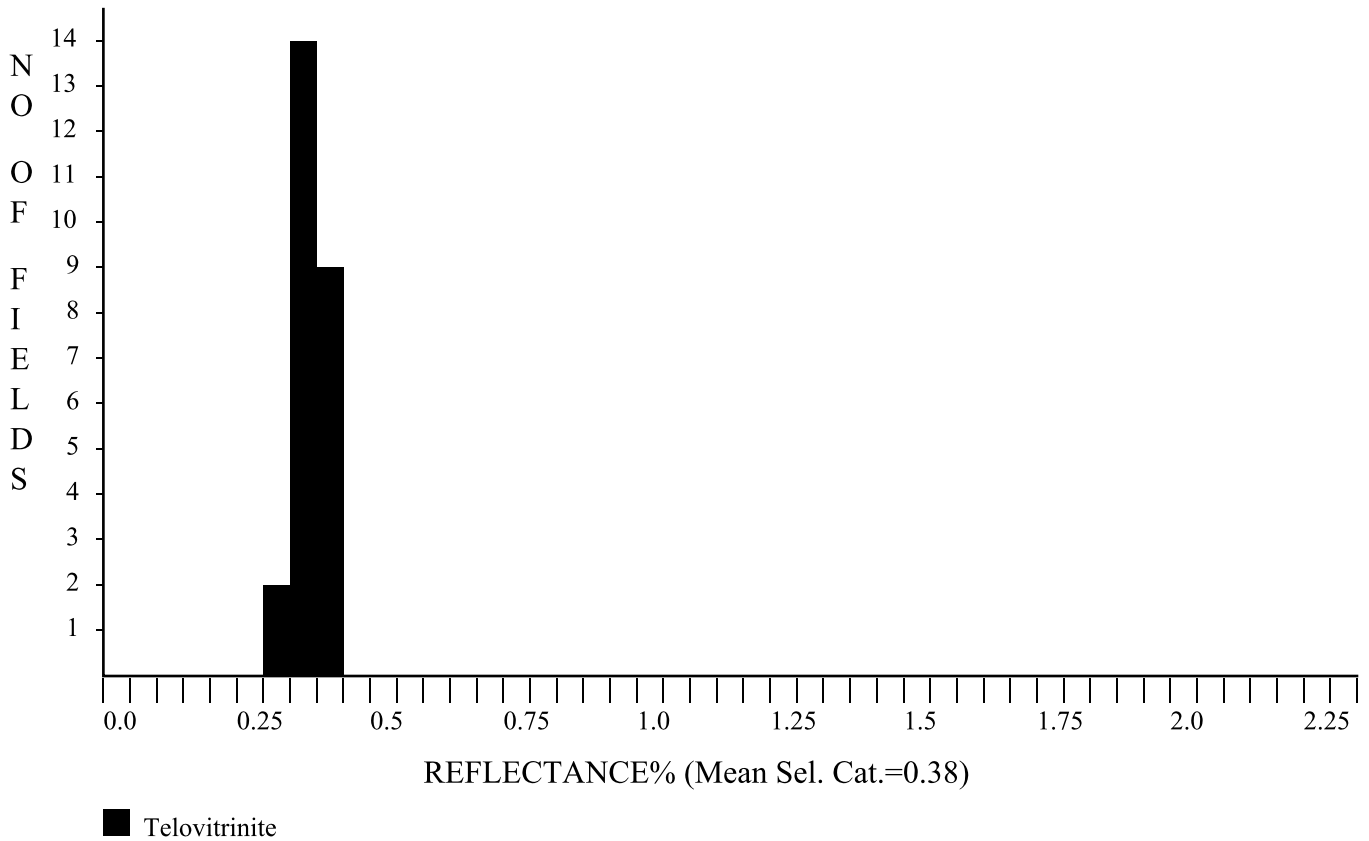
ACC 15 Oct 2011



Keiraville Konsultants Pty Ltd
7 Dallas Street
Keiraville, NSW 2500
Australia

Telephone: (02) 42299843
International: +61-2-42 299843
Fax: +61-(0)2-42 499624
Email: alanccook@ozemail.com.au

GC970-63.1, Southern Norway Region outcrops, E-M Oxfordian, O/C(L5044)



<u>Maceral Category</u>	<u>N</u>	<u>Mean</u>	<u>Standard Deviation</u>
Telovitrinite	25	0.38	0.023
<u>Total</u>	25	0.38	0.023

Selected categories: Telovitrinite:

No. of Readings:	25
Mean of Selected Categories:	0.38
Standard Deviation of Selected categories:	0.023



VITRINITE%		INERTINITE%										LIPTINITE%										OIL DROPS		BITUMEN
TV	DV	Sfus	Scler	Fus	Macr	Id	Micr	Spor	Cut	Sub	Res	Ld	Bituminite	Telalginit	Lamaignite	Oil cut		0.0						
100		0.0	0.0	0.0	0.0	0.0	0.0	0.0	0.0	0.0	0.0	0.0	0.0	0.0	0.0	0.0	0.0	0.0						
0.3	0.6			0.9		1.2				1.5			1.8			2.1		2.4	2.7					
0.31	0.61			0.91		1.21				1.51			1.81			2.11		2.41	2.71					
0.32	0.62			0.92		1.22				1.52			1.82			2.12		2.42	2.72					
0.33	0.63	Telov		0.93		1.23				1.53			1.83			2.13		2.43	2.73					
0.34	0.64			0.94		1.24				1.54			1.84			2.14		2.44	2.74					
0.35	0.65			0.95		1.25				1.55			1.85			2.15		2.45	2.75					
0.36	0.66			0.96		1.26				1.56			1.86			2.16		2.46	2.76					
0.37	0.67			0.97		1.27				1.57			1.87			2.17		2.47	2.77					
0.38	0.68			0.98		1.28				1.58			1.88			2.18		2.48	2.78					
0.39	0.69			0.99		1.29				1.59			1.89			2.19		2.49	2.79					
0.4	0.7			1		1.3				1.6			1.9			2.2		2.5	2.8					
0.41	0.71			1.01		1.31				1.61			1.91			2.21		2.51	2.81					
0.42	0.72			1.02		1.32				1.62			1.92			2.22		2.52	2.82					
0.43	0.73			1.03		1.33				1.63			1.93			2.23		2.53	2.83					
0.44	0.74			1.04		1.34				1.64			1.94			2.24		2.54	2.84					
0.45	0.75			1.05		1.35				1.65			1.95			2.25		2.55	2.85					
0.46	0.76			1.06		1.36				1.66			1.96			2.26		2.56	2.86					
0.47	0.77			1.07		1.37				1.67			1.97			2.27		2.57	2.87					
0.48	0.78			1.08		1.38				1.68			1.98			2.28		2.58	2.88					
0.49	0.79			1.09		1.39				1.69			1.99			2.29		2.59	2.89					
0.5	0.8			1.1		1.4				1.7			2			2.3		2.6	2.9					
0.51	0.81			1.11		1.41				1.71			2.01			2.31		2.61	2.91					
0.52	0.82			1.12		1.42				1.72			2.02			2.32		2.62	2.92					
0.53	0.83			1.13		1.43				1.73			2.03			2.33		2.63	2.93					
0.54	0.84			1.14		1.44				1.74			2.04			2.34		2.64	2.94					
0.55	0.85			1.15		1.45				1.75			2.05			2.35		2.65	2.95					
0.56	0.86			1.16		1.46				1.76			2.06			2.36		2.66	2.96					
0.57	0.87			1.17		1.47				1.77			2.07			2.37		2.67	2.97					
0.58	0.88			1.18		1.48				1.78			2.08			2.38		2.68	2.98					
0.59	0.89			1.19		1.49				1.79			2.09			2.39		2.69	2.99					

Sample Number: L5044 Well Name: GC970-63.1, Norwegian Outcrops
 Date: 2011-10-08 Op: SPR FGV - First Generation Vitrinite, RV - Reworked Vitrinite, BTT - Bituminite, B - Bitumen, Inert - Inertinite, Cav - Cavings, DA - Drilling Mud Additives
 Copyright Keiraville Konsultants Pty Ltd, 2009. Depth: - Sample Type: O_C